EVALUATION OF INFILTRATION, RUN-OFF AND SEDIMENT MOBILISATION USING RAINFALL SIMULATIONS IN THE RIEBEEK-KASTEEL AREA, WESTERN CAPE

By

JOSEPH TWAHIRWA (2219105)

Submitted in fulfilment of the requirements for the degree of "Magister Scientiae" in Environmental Science, in the Department of Earth Sciences, Faculty of Natural Sciences, University of the Western Cape.

Supervisor: Mr A.C.T. Scheepers
Co-supervisor: Dr W.P. de Clercq

January 2010

Table of contents

List of figures

List of tables

Appendix

"Although we are committed to scientific truth, there comes a point where this truth is not enough, where the application of truth to human objectives comes into play, we are no longer considering theoretical forces and ideal substances. We are now obliged to work with materials that are real, impure, and sometimes unpredictable. Our aim is no longer to discern absolute truth, but rather to create a product that will perform a function."
Samuel C. Florman

Keywords

Rainfall
Simulation
Overland flow
Infiltration
Run-off
Sediment
Mobilisation
Particle-size distribution
Soil grain size
A-horizon
Laser
Drag force
Agglomeration
Sediment particles
DigiSizer
Volume frequency
Cumulative value
Goedertrou
Riebeek-Kasteel

Abstract

The project was conducted on a small-scale catchment at Goedertrou in the Riebeek-Kasteel district. The focus of this study was to address some of the hydrological processes active in the research catchment, namely infiltration, run-off and sediment mobilisation on different soil types. It was done to investigate the origin of Berg River pollutants.

To answer the overall question about what influence the natural salt load of the Berg River, a number of subprojects have been identified, one of which is to understand the hydrological processes in the soil mantle and vadose zone.
Hence, the study aimed to answer the research questions mentioned and discussed in section 1.3 of Chapter 1.

Considering the results, it could be suggested that decayed root systems from the rows of plants, soil cracks, small channels and openings created by small animals, as well as slope orientation and, therefore, soil composition, all played a major role in influencing the ability of the soil to absorb the simulated rainfall.
In this study, the factors that influenced run-off are micro topography, soil moisture, root system, animal activities in soil profile, soil crack dimensions and the hydraulic conductivity.

The main factors that played a major role to influence sediments mobilisation are strongly believed to be the micro topography within the ring, slope gradient and length, vegetation cover and rainfall-simulation intensity. After using different techniques, the results show that farmers must be aware that with storm rainfall, particles smaller than 65 µm are subject to mobilisation. It is important to let land-users know that they need proper and appropriate methods for land-use.

Declaration

I declare that **EVALUATION OF INFILTRATION, RUN-OFF AND SEDIMENT MOBILISATION USING RAINFALL SIMULATIONS IN THE RIEBEEK-KASTEEL AREA, WESTERN CAPE** is my own work, that it has not been submitted for any degree or examination at any other tertiary institution, and that all the sources I have used or quoted have been indicated and acknowledged by complete references.

JOSEPH TWAHIRWA

SIGNED**.....**

Acknowledgements

First, I thank God Almighty from whom all blessings flow. I thank the University of the Western Cape for allowing me to register as a tertiary student in 2002, regardless of the fact that I had been out of an academic environment for 15 years.

Second, I would like to extend my appreciation to the University of Stellenbosch for financial support. I also thank the staff of the Department of Soil Science for the invaluable help that they provided me during the laboratory work phase of this research. I thank in particular Ms Botha, for the unmatched role she played in the sediment grain-size analysis.

A sincere gratitude goes to Mr Theo Scheepers and Dr Willem de Clercq, whom I regularly went to for advice when necessary. In the same way, I also give special thanks to Mr Daniel Folefoc, whose help in the field was always appreciated.

I would like to express my gratitude to the Rector of the University of the Western Cape for his personal assistance and his incredible inspiration, which I will always remember.
My thanks also go to Prof Richard Mudsen of the University of Missouri, Prof David K. Kreamer of the University of Nevada Las Vegas, and Prof Robert C. Laudon of the University of Missouri-Rolla for their advice. I also thank Prof Jean Poesen of the Catholic University of Leuven for his major role in advising on the literature review.

The staff members of the Earth Sciences Department, University of the Western Cape, including Prof Nebo Jovanovic, Prof Abraham Thomas, Prof Charles Okojeni, Prof P. Carey, Dr Shafick Adams, Mr Reginald Domoney, Ms Bronwin Honigwachs, Ms Wasielah Davids, Ms Ruth Mary and Ms Haili Jia (all of whom will be remembered for the rest of life) are thanked for their assistance, advice and friendship at all the times.

I would also like to thank my colleagues in or from the Post Graduate Lab (L.60), especially Anthony Duah, Wisemen Chingombe, James Ayuk, Palesa Leuta, Opuari Mimonitu, Vuyolwethu, Gunter Frantz, Yafah Hoosain, Selwyn Adams, Christopher Nkala, Gaathier Mahed Fazy, Amos Ngola and Angelo. Your help is remarkable; you are very special to me.

Finally, a special acknowledgement goes to my courageous wife and all Retreat Seventh Day Adventist Church members and friends. The dedication, encouragement, support and faith that they showed during the past two years kept me focused on my goals.

Joseph Twahirwa
Cape Town, 2009

Chapter 1

1.1 Introduction

The total land area of the earth is approximately 14 billion ha, of that 11% or 1.480 million ha is arable land, 24% is pastureland; 31% or 4.320 million ha is forest or woodland; and 34% is other land (Graaff, 1992). The rate of desertification appears to be accelerating, especially in parts of Sahelo-Sudanian Africa, the Near East and North Africa, South Asia and parts of South America. In 1981, it was estimated that 5–7 million ha of the above mentioned arable land, or approximately 0.3% to 0.5% of the world total, was lost annually through land degradation, and this was expected to increase to 10 million ha per year in 2000 (Graaff, 1992).

In the context of the United Nations Convention to Combat Desertification (UNCCD), land degradation means a reduction or a loss, in arid, semi-arid and dry subhumid areas, of the biological or economic productivity and complexity of rain-fed cropland, irrigated cropland, or range, pasture, forest and woodlands. Degradation therefore results from land-uses or from a process or combination of processes involving human activities and habitation patterns, such as soil erosion caused by wind and/or water, deterioration of the physical, chemical, biological and economic properties of soil, and long-term losses of natural vegetation (Hoffman and Ashwell, 2001).

Land degradation is a worldwide problem from which many third world countries in Africa in particular suffer (Sfeir-Younis, 1985) and which is caused by and counteracted by both natural forces and human intervention. The United Nations Environmental Programme (UNEP) estimates that land degradation affects approximately 70% of all the dry lands, or a quarter of the Earth's land area (Hoffman and Ashwell, 2001). It occurs under different climatic conditions, but is a common phenomenon in areas with Mediterranean climates. The World Conservation Strategy of 1980 advanced the idea of sustainable development, and defined it as "a development which meets the needs of the

present without compromising the ability of future generations to meet their own needs" (Graaff, 1992). In terms of origin and consequences, land degradation processes are defined as chemical, where there is excess accumulation of salt; physical, where there is wind and water erosion; and biological, where there is deforestation and overgrazing (Graaff, 1992).

Three global ecological problems have a bearing on sustainability: (i) the potential climate changes (greenhouse effect); (ii) the loss of genetic resources (biodiversity); and (iii) the use of inappropriate agricultural technologies, affecting soil, vegetation and water resources (Graaff, 1992). However, according to a FAO report (1988), the third category can be subdivided into three types of adverse agricultural effect: (a) pest resistance to biocides; (b) groundwater and surface water contamination; and (c) land degradation because of erosion, soil exhaustion and soil compaction (Graaff, 1992).

A FAO/UNEP study (1983) also recognises the soil-mining problem or cultivation without adding enough chemical or natural fertilisers. This results in a gradual loss of soil fertility (Graaff, 1992).

The salinity that follows on long-term irrigation, where through an accumulation of salts a reverse osmosis process happens, is also a problem (Graaff, 1992), as is leaching or washing away of nutrients needed by crops, from either the groundwater or run-off. Another problem often encountered is toxicities and pollution from waste products of industries and cities, brought in via the atmosphere or via drainage water (Graaff, 1992).

The Berg River catchment in the Mediterranean climatic environment of the Western Cape has a salinisation problem. To address the problem, the overarching question to be answered is whether the natural salt load of the Berg River is being altered by land-use practices. This theme forms the focus of a multidisciplinary project financed by the Water Research Commission. The project is conducted in a small-scale catchment at Goedertrou in the Riebeek-Kasteel district.

To answer the overarching question about the natural salt load of the Berg River, a number of subprojects were identified, one of which is to understand the hydrological processes in the soil mantle and vadose zone. These processes, among others, include infiltration, run-off and sediment mobilisation.

The principal environmental issues associated with run-off are the impacts on surface water, groundwater and the soil through the transport of water pollutants. Ultimately, these consequences translate into human health risks, ecosystem disturbance and visual impact on water resources.

1.2 Rationale and aims of the study

In the introductory paragraphs of this dissertation, the salinisation problem in the Berg River Catchment was mentioned. The importance of the process of infiltration and run-off was stressed. The latter two processes and the grain size distribution of the material mobilised by run-off form the focus of this study. Because the study area has a Mediterranean climate with rainfall mainly in winter, rainfall simulation was used, so that data collection could also take place during summer, when no or very little rainfall occurs.

The observations of De Clercq *et al.* (2005) revealed that in early winter, before wheat had been planted and with an almost bare soil surface, water ran off rapidly and dammed behind the existing contour banks, which eventually channelled it to a nearby dam and on some occasions even out of the catchment. Conversely, after being planted with wheat, lesser amounts of water reached the contour banks. Most of it infiltrated without further run-off.

Field observations of cracks in soil surfaces in some parts of the catchment and multiple instances of termite activity seem to result in the formation of macro pores in the soil. The influence of these pores on the infiltration is not clear (De Clercq *et al.*, 2005) and must be investigated.

Drops destroy the surface soil aggregates and gradually form a continuous crust with a much lower hydraulic conductivity than that of the original soil surface (Morini and Benyamini, 1977).

To understand the hydrological processes active in an area, one must have a good understanding of soil types that occur in the area. During a rainfall event, different soil types will influence the rate of infiltration, the amount of run-off from the surface and the type of material being mobilised. For the study area, a soil map compiled by researchers from Stellenbosch University working under the same umbrella project, was already available.

Hence, the current study aims to answer the following research questions:

1) What factors play a role during the infiltration process on the different soil types and how will this influence the depth of infiltration?

2) How do the different soil types and infiltration rates influence run-off?

3) What grain size material is most easily mobilised during rainfall events under the infiltration and run-off scenarios characteristic of each soil type?

To answer research questions 1 and 2, the main objective was therefore to analyse the vertical and horizontal distribution of moisture in the A-horizon of a particular soil in a fixed area and to determine the run-off from such a soil after a rainfall event.

To answer research question 3, the objective was to analyse the particle-size distribution of solids in the run-off water emanating from the different soil types after a rainfall event.

The methodology employed to satisfy the above objectives are discussed in the next section.

1.3 Research approach and methodology

To do any measurements on the infiltration and run-off as indicated above, rainfall in an area is required to initiate the different processes. Natural rainfall in this Mediterranean-type area happens during winter and this amounts to a very low value of approximately 228.6 mm per annum (Cape West Coast, 2007). Rainfall in arid and semi- arid regions is often unreliable and makes research difficult. For this reason, it was decided to use rainfall simulation, which was available whenever and wherever required. Through rainfall simulation, drop size and rainfall intensity can be controlled and adjusted as closely as possible to a natural rainfall event.

Rainfall simulation is not a new technique and it has been used for almost a hundred years (Loch *et al.,* 2001). The development of rainfall simulators reflects advances in both technology and knowledge of rainfall and certainly in the interaction of rainfall with the soil. There are currently many types of rainfall simulator in use (Loch *et al.,* 2001).

Rainfall simulators have been used abroad for a considerable time to confirm natural run-off plot results and to provide useful data on the various factors that affect soil erosion (Loch *et al.,* 2001). Rainfall simulations were done for the summer of 2006 and 2007 in the smaller catchment of Goedertrou in Riebeek-Kasteel. Each simulation was done close to the position of a soil pit (Figure 9), to allow comparison with soil parameters gained from the soil analyses and measurements.

However, rainfall-simulation studies in South Africa were only initiated in 1980. This was to assess the range of soil loss and run-off on arable land and as an indicator of areas that constitute high priority for increased efforts in combating soil erosion, as well as generating local input data for use in a soil loss equation (Crosby *et al.,* 1983).

Rainfall simulation can moreover be used to study the impacts of a particular management practice on the properties of a particular material, or it can be used to enrich our understanding of processes, such as infiltration, run-off or erosion (Loch, 2000).

Likewise, it is possible to use parameters derived from rainfall simulations as a starting point for modelling the behaviour of landscapes, sometimes under quite long periods of natural rain (Loch, 2000).

Figure 1.1 The rainfall simulator being calibrated at Stellenbosch University (photo courtesy of Andrei Rosanov)

In the study area, rainfall simulations were conducted in the summer of 2006 and 2007. Each simulation was done close to the position of soil pit (see Figure 1.9 for the position of soil pits in the study area). This was done to allow a comparison of the infiltration, size of mobilised sediments and run-off rates on the various soil types in the area.

The simulator used (Figure 1.1) was upgraded and tested before it was used to perform the planned simulations. It consisted of a nozzle mounted at the top of an aluminium frame, allowing the droplets to fall with an intensity of 63.5 mm/h within a metal ring enclosing an area of 0.945 m^2.

A small electric pump and a regulator valve controlled the pressure under which rainfall was simulated. A pressure of 0.5 bars was used for all simulations. This gave a rainfall intensity of approximately 63.5 mm/h, which was the lowest intensity possible with this particular simulator. Lower pressures did not generate any droplets, and higher pressures

caused a spray mist, which was unlike the general rainfall in the area. The intensity of 63.5 mm/h was considerably higher than the natural rainfall intensity for the area, but could not be prevented because of technical shortcomings of the simulator. It nevertheless gave an idea of what could be expected under extreme conditions.

Figure 1.2 shows a metal ring enclosing an area with wheat stubbles. Clay soil was used to seal off the contact between the ring and the ground surface on the outside of the ring, thereby ensuring that no water was lost from the ring.

Figure 1.2 Metal ring-enclosed surface with 75% coverage of wheat stubble (photo courtesy of Willem de Clercq)

When the first run-off happened, it was channelled from the ring outlet through a plastic pipe and collected in a container.

Figure 1.3 Metal container that served to collect the run-off water

The volume of the run-off was measured with a measuring cylinder. Samples taken every 5 min were stored in plastic bottles. These were packed in wooden boxes and taken to the

laboratory of the Soil Science Department at Stellenbosch University to assess the sediment content.

To answer research questions 1 and 2 regarding infiltration and run-off from different soil types, rainfall was simulated on each of the 13 soil types in the study area. As expected, the time to saturate a particular soil type in the ring area differed from place to place (Poesen, 1987). Each simulation lasted until the run-off from the ring area was constant.

The time taken for the first run-off to occur was recorded, as well as the volume of run-off every 5 min. After each simulation, soil samples were taken from the ring area at depths of 10 mm, 20 mm, 40 mm, 60 mm, 80 mm, 100 mm, 150 mm, 200 mm, 250 mm, 300 mm. Lavee *et al.* (1997: 342–343) refer to these depths as "rainfall depths". This was done to determine the position of the wetted front and to analyse the moisture content. Sample sites were selected to include both "in-row" and "between-row" positions, to verify the influence of crop growth on the distribution of the moisture front in the ring area. Figure 1.4 below shows a typical profile from where soil samples were taken.

Figure 1.4 Soil horizon indicating the upper 300 mm from where samples were collected

All samples were placed in specially sealed plastic bags, then weighed and the results recorded. After weighing, the samples were packed and stored in wooden boxes (see Figure 1.5) for further analyses in the laboratory.

Figure 1.5 the wooden box used for storing and transportation of soil samples

The analysis was done using the basic technique for determination of gravimetric soil moisture content, a method often used to calibrate other instruments, such as neutron soil moisture probes (Reynolds, 1970). In the laboratory, the samples were weighed and dried in an oven for 24 h, at a temperature of 100 °C, until a constant weight was achieved. The mass of the initial sample minus the oven-dried mass gave the moisture content in grams. This was then expressed as a percentage, by multiplying the moisture content in grams by 100 and dividing it by the mass of the oven-dried sample.

To answer research question 3 regarding the grain size distribution of mobilised particles from different soil types, samples of the collected run-off from each simulation were evaporated in the laboratory and the residue mounted on microscope slides. These were then photographed (50 × magnification) and analysed for their grain size distribution using “Image J” software.

To compare the solids in the run-off from the ring plots with the grain size distribution of the A-horizons of the different soil types in the study area, samples of the run-off were also analysed with more sophisticated Saturn DigiSizer 5200 V1.10 software to achieve a more complete evaluation of sediment distribution. Sediments were separated from the

water with a vacuum pump connected to a tension meter that sucked water from the specific flasks. The cells of the tension meter were gently cleaned with distilled water to minimize the quantity of sediment that could remain on them. Wet sediments were then placed in an oven at 100 °C for 24 h, in weighed and labelled beakers. After 24 h, the beakers containing the samples were weighed again. The difference between the final and the initial weights gave the sediment content value in grams. From these analyses, grain size distribution curves were constructed. These are presented and discussed in Chapter 4.

1.4 The study area and study site description

The study area, on the farm Goedertrou, is located approximately 3 km to the NE of the town of Riebeek-Wes (33° 18'S; 18° 55'E) and approximately 75 km north of Cape Town, in the Western Cape Province, South Africa (Figure 1.6). It covers an area of approximately 60 ha and forms part of the Berg River catchment.

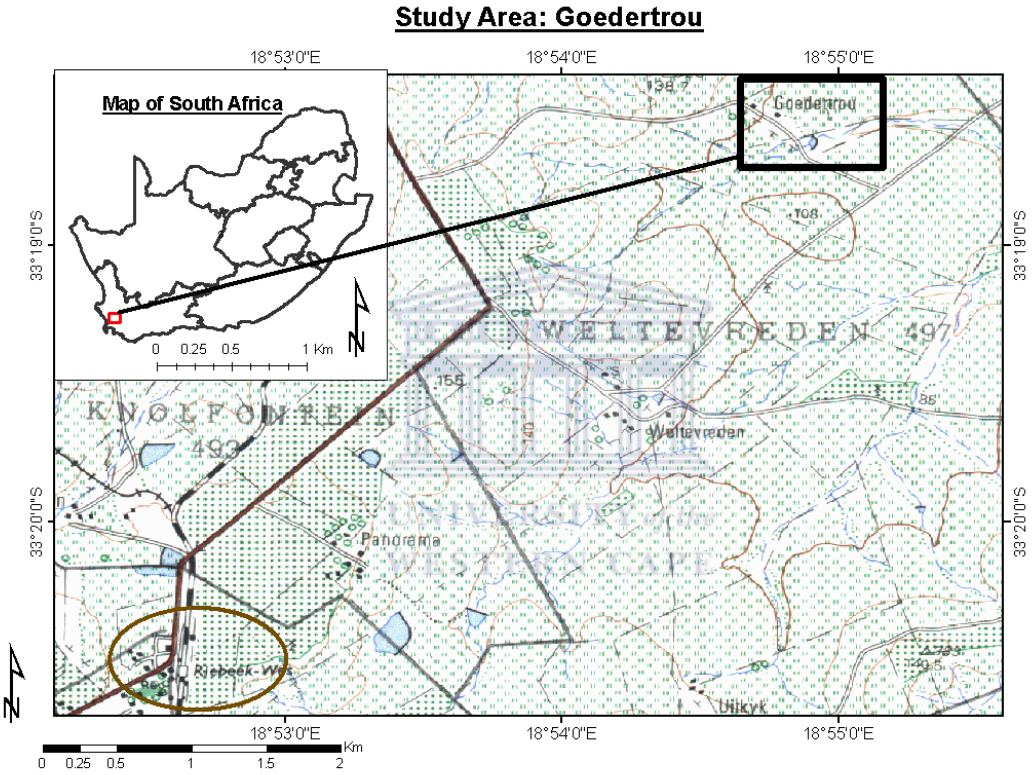

Figure 1.6 Location of the study area on a topographic map

Figure 1.7 Aerial photographic view of the demarcated study area at Goedertrou

Topographically the area can be described as low rolling hills with the Kasteelberg (Figure 1.8) at an elevation of 946 m, the highest peak in the area and situated to the west of the area. The nature of the rocks and their response to erosion determined the drainage pattern that developed on the newly evolved landscape dominated by the Post African Surface (Partridge and Maud, 1987). In terms of the general shape of the landscape, both the steepness of the slopes and the total relief influence the way precipitation reaches the streams in the drainage basin.

The area is mostly underlain by rocks of the Malmesbury Group, the only exception being the Kasteelberg Mountain, consisting of Table Mountain Group sandstones. The Malmesbury Group rocks typically vary from highly weathered at the surface to slightly weathered deeper down. In places, levelled remnants of silcrete (an indication of the Post African Surface) are underlain by clays, varying from highly leached kaolinite clays to mottled clays in the lower parts of the catchment. The distribution and development of the Post African Surface is well covered in a publication by Partridge and Maud (1987). Unconsolidated alluvium overlies this weathered material where the drainage line bisects the catchment, its depth increasing towards the northeast (CSIR, 2005).

Figure 1.8 Kasteelberg Mountain (West Coast Tourism Organisation, 2000)

Soil forms that occur in the study area are known from samples that were taken from soil pits (see Figure 1.9) and analysed by the University of Stellenbosch. In this way, soil physical information for each soil type was obtained (de Clercq *et al.,* 2007).
These soils consist mainly of clays and can be subdivided into the various soil forms. The **Augrabies** (Ag) soil form has an orthic A-horizon. The orthic A-horizon is a surface horizon that does not qualify as organic, humic, vertic or melanic topsoil, although it could have been darkened by organic matter (Soil Classification Working Group, 1991). The Augrabies soil form also has a neocarbonate B-horizon soil family. When it is described as **Ag1**, it means that it has a bleached A-horizon and luvic B1-horizon. It has slight or no subsoil wetness.

The **Cartref** (Cf) soil form also has an orthic A- and an E-horizon, and has a lithocutanic B-horizon. When the A-horizon is bleached and the E-horizon has a yellow colour, it is described as Cf1. This soil form generally has moderate subsoil wetness.

The **Glenrosa** (Gs) soil form has an Orthic A-horizon, as well as a Lithocutanic B-horizon. This soil form is described as Gs1 only when the A-horizon is bleached, when it has soft or hard B-horizons, when B-and C-horizons are non-calcareous, and also when it has slight or no subsurface wetness. The Glenrosa form is referred to as Gs2 when it has a bleached A-horizon, a soft or hard B-horizon and when wetness is present in the B1-horizon. The Glenrosa soil form is referred to as Gs3 when it has a bleached A-horizon, a soft B-horizon, and slight or no wetness in the B1-horizon. In addition, it must have non-calcareous B- and B-horizons, and a slight wetness of the subsoil.

The Gs4 category is referred to as a Glenrosa soil form when the A-horizon is bleached, the B-horizon is soft, and there is no wetness in the B1-horizon. The B- and C-horizons must be non-calcareous, with slight or no subsoil wetness. The fifth Glenrosa soil form is referred to as Gs5 when there is a bleached A-horizon, a hard B-horizon, and no wetness is present in the B1-horizon. In addition, the B- and C-horizons must be non-calcareous and no or only slight subsoil wetness is present. In the last category, Gs6, the A-horizon

is bleached and there is a hard B-horizon. Wetness is present in the B1-horizon, but the B- and C-horizons are non-calcareous and the subsoil has moderate wetness.

The **Katspruit** (Ka) soil form has an orthic A- and G-horizon. It is usually categorised as Ka1 when it has a non-calcareous G-horizon and there is severe subsoil wetness. For example, the Katspruit soil form is characterised by water logging and anaerobic conditions. Its orthic topsoil is consequently grey or dark grey and weakly structured, and subject to wetness (Soil Classification Working Group, 1991).

The **Klapmuts** (Km) soil form has an orthic A-horizon and a pedocutanic B-horizon, which is a non-red horizon.

The **Mispah** (Ms) soil form has an orthic A-horizon and it is made up of hard rock. This soil form is referred to Ms1 when there is a bleached and a non-calcareous A-horizon and slight or no subsoil wetness.

The **Sepane** (Se) soil form has an orthic A-horizon, a pedocutanic B-horizon and contains unconsolidated material with signs of wetness. When the Sepane soil form is referred to as Se1, it means that it has a bleached A-horizon and medium-coarse to angular material in the B-horizon. It consists of non-calcareous B-and B-horizons, and displays severe subsoil wetness.

The **Sterkspruit** (Ss) soil form, which has an orthic A-horizon, also has a prismacutanic B-horizon. When the Sterkspruit form is allocated the symbol Ss1, it has a bleached A-horizon, a non-red B-horizon and moderate subsoil wetness.

The **Swartland** (Sw) soil form has an orthic A-horizon, a pedocutanic B-horizon and saprolite material. The Sw1 is the symbol used for the Swartland soil form subdivision when it has a bleached A-horizon and a non-red B-horizon. It consists of non-calcareous B- and C-horizons and has moderate subsoil wetness. The Sw2 symbol is given to the Swartland soil form when it consists of a bleached A-horizon and a non-red and fine-

structured B-horizon. It also has calcareous B- and C-horizons and moderate subsoil wetness. The Sw3 Swartland soil form has a bleached A-horizon, and a non-red coarse-structured B-horizon. It also has non-calcareous B- and C-horizons and a moderate subsoil wetness.

The Sw4 Swartland soil form designates a Swartland soil with a well-structured bleached A-horizon, a red or non-red B-horizon. It consists of non-calcareous B- and C-horizons, and it has moderate subsoil wetness.

The **Westleigh** (We) soil form consists of an orthic A-horizon and a soft, plinthic B-horizon. The We1 symbol refers to a luvic B-horizon combined with severe subsoil wetness (Soil Classification Working Group, 1991).

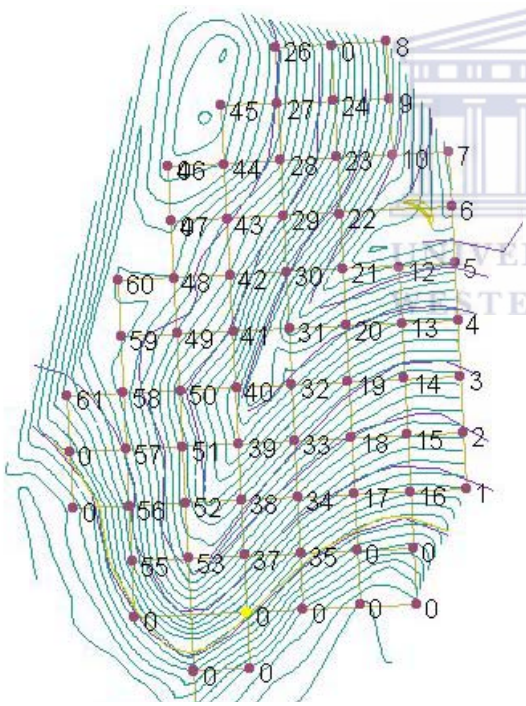

Figure 1.9 Contour map of the Goedertrou subcatchment indicating numbered soil pits (Source: de Clercq *et al.*, 2005)

All of these soil forms have, according to the Soil Classification Working Group's (1991) description, orthic topsoils (A-horizons) and occur over virtually the full range of soil-forming conditions encountered in South Africa. Orthic topsoils vary widely in organic carbon content, colour, texture, structure, base status and mineral composition, because of

the natural genetic relationship between topsoils and subsoils. However, in each case the nature of the topsoil can largely be deduced from the classification.

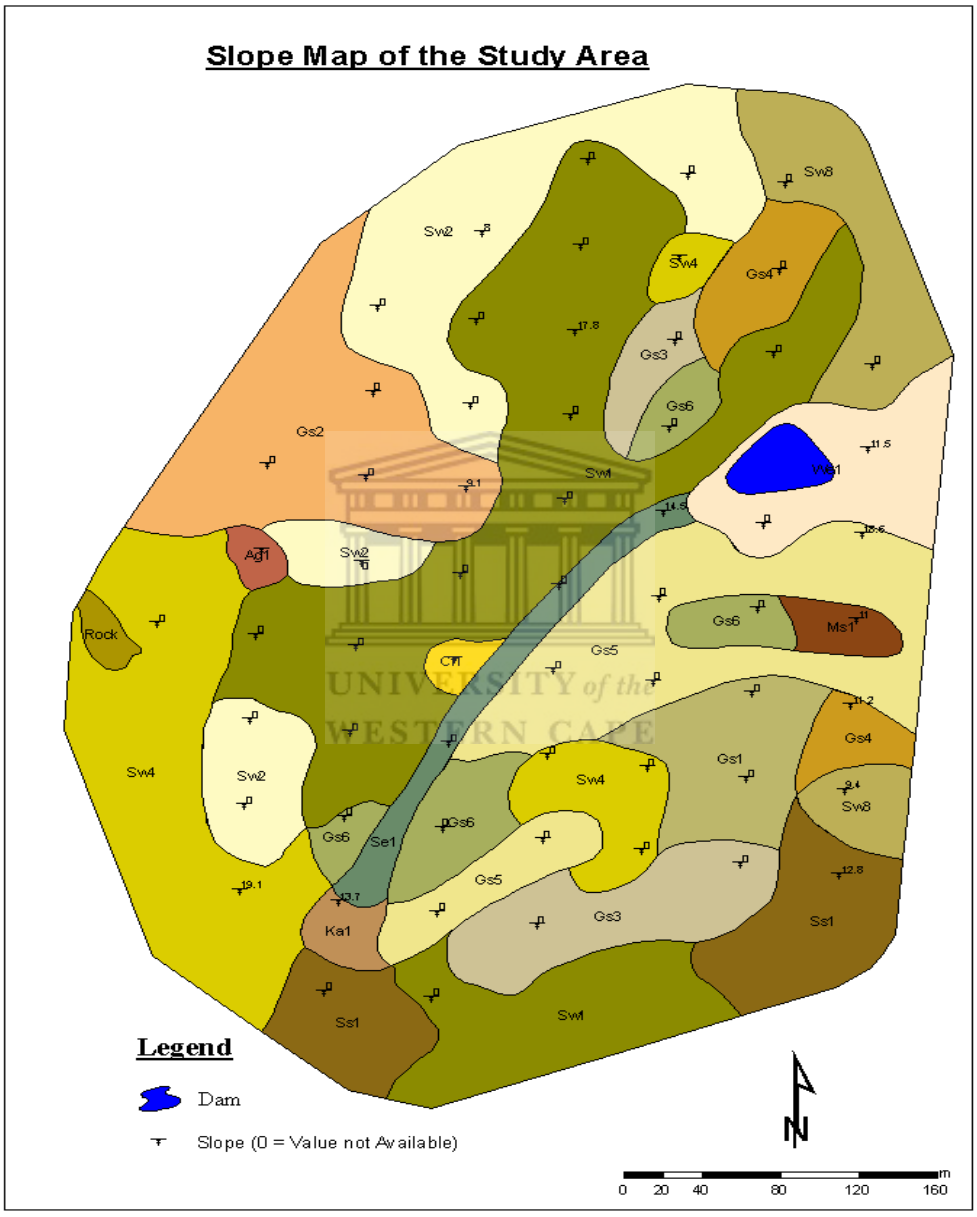

Figure 1.10 Distribution of soil forms and slope directions in the study area (source: de Clercq *et al.*, 2005)

The overall vegetation in the study area consisted of wheat planted in late autumn and covering more than 90% of the study area. Harvesting takes place in October, leaving a dry stubble land for most of the summer. The higher ground near the hill tops is mostly covered by vineyards irrigated in summer. Sheep and cattle use the stubble lands for grazing in summer. Some of the uncultivated areas carry an indigenous vegetation cover dominated by Renosterveld. Vegetation is the main factor for water loss through transpiration in the equation relating precipitation and run-off (FAO, 1992). However, the presence of a vegetation cover retards overland flow, giving the water more time to infiltrate the soil (De Clercq *et al.,* 2005).

Temperatures in summer average approximately 30 °C, with the maximum temperature in February (Figure 1.11) often increasing to 35 °C or higher. Winter temperatures fall to less than 10 °C in June, July and August. Rainfall averages approximately 53 mm per year, with the maximum rainfall in June, July and August (Figure 1.12).

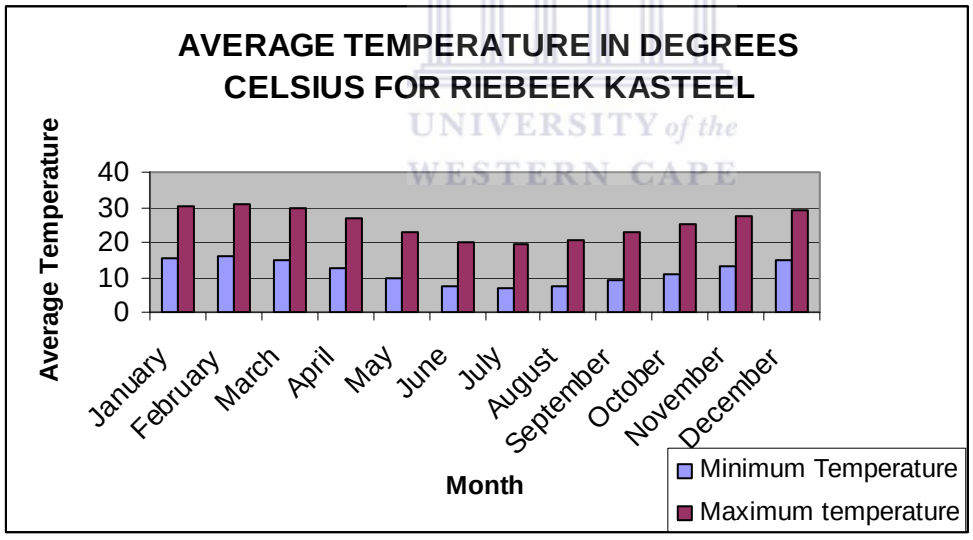

Figure 1.11 Average temperatures for Riebeek-Kasteel (source : www.capewestcoast.org)

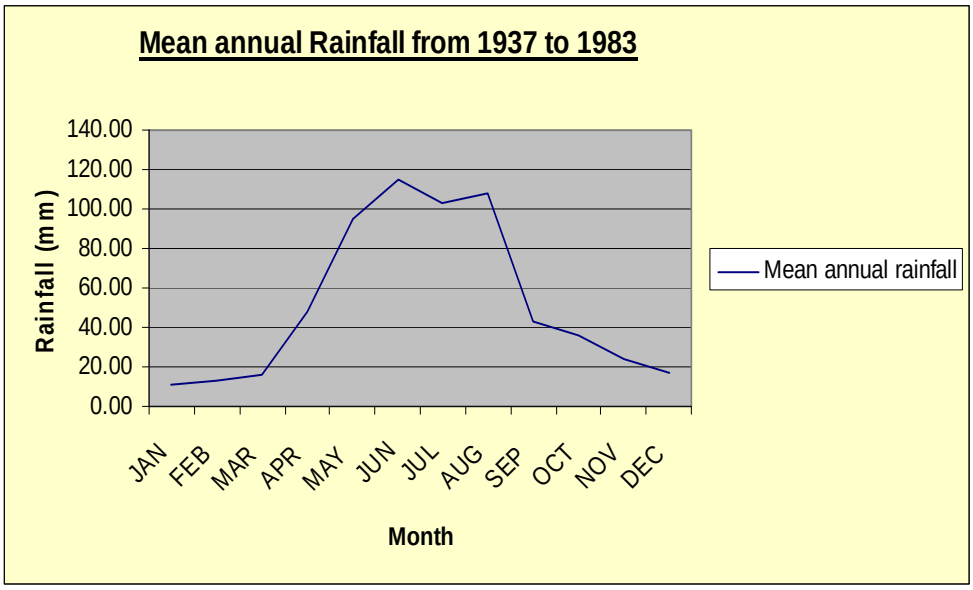

Figure 1.12 Mean monthly rainfall for Riebeek-Kasteel from 1937 to 1983 (Source: Water Research Commission, Volume IV, WRC Report No. 298/4.1/94)

The physical characteristics of the drainage basin, such as the terrain conditions affecting run-off, can be considered in two categories, namely conditions inherent in the natural landscape and conditions of land-use (De Clercq *et al.,* 2005). The main effects of temperature are related to elevation. At higher elevations, cooler temperatures result in less water loss through evapotranspiration processes (De Clercq *et al.,* 2005).

In a study done by the CSIR (2005), it was concluded that averaged total evaporation from a stand of Renosterveld vegetation exceeded the reference evapotranspiration by 60% on average for a period of 38 days. Strong relationships exist between the total evaporation measured at the site and the solar irradiance and reference evapotranspiration, indicating that the total evapotranspiration is strongly driven by solar irradiance.

The land-use in the study area, usually based on modern farming methods, is often responsible for the accelerated erosion and changes in natural drainage nets (De Clercq *et al.,* 2005).

Chapter 2

Evaluation of the infiltration

2.1 Introduction

Infiltration is a widely studied topic of importance to hydrologists, agronomists, soil erosion specialists, environmentalists and many more who are particularly concerned with water requirements and water quality. Erosion specialists, for example, are concerned with excess rainwater that accumulates on the soil surface, collects in depressions and concentrates as run-off in rills, gullies, streams and channels (Römkens *et al.,* 1995). However, before run-off happens, part of the rainfall will invariably infiltrate the soil. Infiltration is therefore the process by which precipitation moves downwards through the surface of the earth and replenishes soil moisture, aquifers and ultimately supports stream flow during dry periods (Viessman *et al.,* 1989; Viessman and Lewis, 2003).

A drop of water tends to spread out in a thin film over very small particles of soil, and capillary action is the tendency of a liquid to cling to the surface of solid material that can draw up the liquid against the pull of gravity. Similarly, water can run downward through holes made by worms or left by decayed roots (Leopold, 1974).

The volume of water that infiltrates into the subsurface soil depends on a number of factors Römkens *et al.,* 1995). Generally, the factors affecting infiltration are "precipitation, soil characteristics, soil saturation, land cover and land-use, slope of the land and evapotranspiration". The mineralogy of clay-sized particles and rainstorm characteristics are among the major factors that determine the nature of soil sealing (Mermut *et al.,* 1996). The development of surface seals during rainstorms is a known factor that reduces the infiltration rate and enhances surface run-off and erosion, with the

consequent loss of organic matter and nutrients (Mermut *et al.,* 1994). However, the study conducted by Poesen (1984) revealed that slope angle has a positive influence on infiltration rate for soils susceptible to surface sealing.

The greater infiltration rates near semi-arid vegetation have been attributed to soil properties, such as a lower bulk density under plants (Belsky *et al.,* 1993), a greater soil aggregate stability (Blackburn, 1975) and a greater density of macro pores (Dunne *et al.,*1991; Bergkamp *et al.,*1996). Nevertheless, the influences of plants on earth-surface processes involve in most environments weathering, erosion and deposition (Viles, 1990).

Previous studies have revealed that within semi-arid areas, light vegetation and related micro topography have an important effect on run-off at fine spatial scales (Yair and Lavee, 1976; Scoging, 1982; Wilcox *et al.,* 1988; Dunne *et al.,* 1991). The work done by Oostwoud and Poesen (1999), suggested that tillage action could expose the rock fragments on the surface. This is important, because of the ratio between the particle size of the largest and the smallest fraction that contribute to determine the percolation rates of the moisture (Middleton, 1970; Savage, 1987; Bridgwater, 1994). One of these effects is increased infiltration near vegetation, which reduces overland flow.

The most generally used methods for determining infiltration capacity are hydrograph analyses and infiltrometer studies (Viessman, 1989). Infiltrometers, however, do not provide absolute data and the results obtained from both flooding and sprinkling infiltrometers are of major value in comparative analysis (Gregory and Walling, 1973). Moisture contents are usually expressed as weight-percentage values, a percentage of the oven dry weight of soil (Gregory and Walling, 1973).

The purpose of this chapter is to examine infiltration in different soil types in the study area, as outlined earlier, and to investigate the factors that influence the downward movement of water in the vadoze zone.

To assess infiltration rates on different soil types in the study area, rainfall simulations were done, as mentioned earlier. Because the rainfall intensity generated by the simulator was known and could be adjusted as required, the infiltration capacity could be calculated by subtracting the run-off value from that of the rainfall intensity. Run-off values are usually measured as a volume, but in this case, they were converted to mm/h to make them comparable to the rainfall intensity. The following results were obtained.

2.2 Results and discussion

The main soil types in the study area are mentioned in section 1.4 of Chapter 1. Most of these contain various amounts of clay. Table 1 below summarises the clay content of surface material at the sites where rainfall simulations were done. Clay content varies from 25% at site 28 to low values of 10% at sites 1, 6, 53 and 59.

Table 2.1 The clay content for the various soil types on the simulation sites

Rainfall simulation site number	Soil type	Clay content (%)
1	Ss1	10.0
2	Sw3	13.5
3	Gs1	15.0
4	Ms1	12.5
5	Gs1	15.0
6	We	10.0
21	Km1	15.0
28	Sw1	25.0
40	Cf1	12.5
42	Gs2	15.0
45	Sw2	17.5
53	Ka1	10.0
55	Sw4	15.0
59	Ag1	10.0

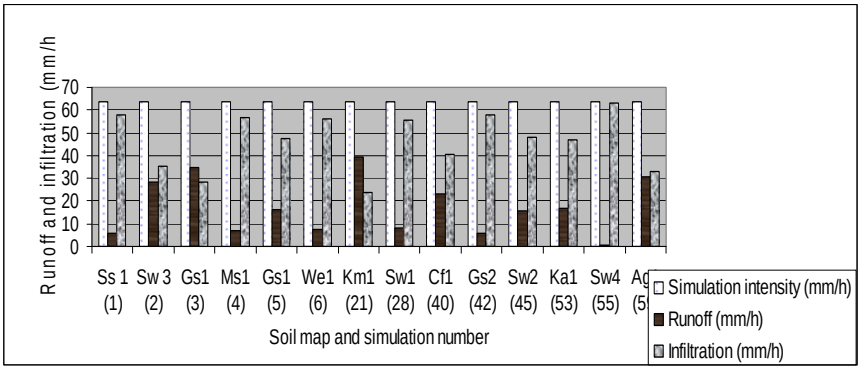

Figure 2.1 Indicates run-off and infiltration in mm/h generated through rainfall simulation at the various sites

Because the infiltration was calculated using the difference between the incoming simulated rainfall and the measured run-off as indicated above, there was an inverse relationship between run-off and infiltration. When run-off was low, the infiltration was high and vice versa.

Usually one would expect soils with high clay content to show low infiltration and high run-off rates, because of their low permeability. A comparison of the infiltration results displayed in Figure 2.1 with the clay content for each of the simulation sites in Table 2.1 clearly shows that this was not the case in the study area. The reason for this will be examined later in this chapter. In the following sections, the infiltration results for the different sites are discussed in detail.

Table 2.2 Summarises the infiltration results obtained with the simulations done on the various soil types under similar rainfall intensities

Simulation number and soil-map codes	Gradient of the soil surface (%)	Simulation period (min)	Infiltration rate (mm/h)		Moisture content (%) at different depths after simulation		
			At start	At end	Surface (10–20 mm)	100 mm	300 mm
1 (Ss1)	12.8	141	60	48	18	8	21
2 (Sw3)	9.4	87	55	22	20	12	4.5
3 (Gs 1)	11.2	88	46	18	21	13	6
4 (Ms1)	11	109	60	48	17	12	5
5 (Gs1)	18.5	72	58	30	15	10	6
6 (We1)	11.5	85	56	44	16	8	1.1
21 (Km1)	14.5	68	50	8	16	12	1

28 (Sw1)	17.8	108	61	42	14	14	8
40 (Cf1)	17.6	67	53	14	14	2	0.14
42 (Gs2)	9.1	141	62	41	20	18	13
45 (Sw2)	8.0	126	51	25	21	8	6
53 (Ka1)	13.7	69	50	11	14	4	3
55 (Sw4)	19.1	173	62	60	17	7	8
59 (Ag1)	10.5	80	50	15	17	9	5

The numbers in column 1 of Table 2.2 correspond to the grid number on the preliminary soil map of the Goedertrou area of June 2005, indicating where the particular simulation was done and the codes in brackets refer to the soil codes on the same map.

The gradient in column 2 is the slope gradient of the soil surface on which the simulation was done. The duration (in min) of the simulation is given in column 3. The infiltration rate in column 4 given in mm/h and this represents the difference between the simulated incoming rainfall and the measured run-off (converted to mm/h). These were calculated for the first sample taken after run-off was initiated, as well as for the last one of the simulation (given in column 5). Moisture content was determined for samples taken at various depths within the ring area after completion of the simulation and this is illustrated in column 5. Because all the simulations were done during summer, the initial moisture content of the soil for all the simulation sites was very low.

The results displayed in column 5, therefore, give some indication of the ease with which water infiltrated into the various soils towards the end of each simulation. Comparing these values with those from the other columns, as well as with the observed soil structure, could help to clarify the reasons for the variations in the infiltration rates for the various soils.

The section gives an overview of the infiltration results, focusing first on simulation sites showing relatively high infiltration rates (>40 mm/h), then looking at those with lower infiltration rates.

2.2.1 Simulation sites showing relatively high infiltration rates (more than 40 mm/h)

2.2.1.1 Simulation 55 (Sw4)

Simulation 55 had the longest "time to run-off" of all the simulations. The calculated infiltration curve for this simulation is illustrated in Figure 2.2.

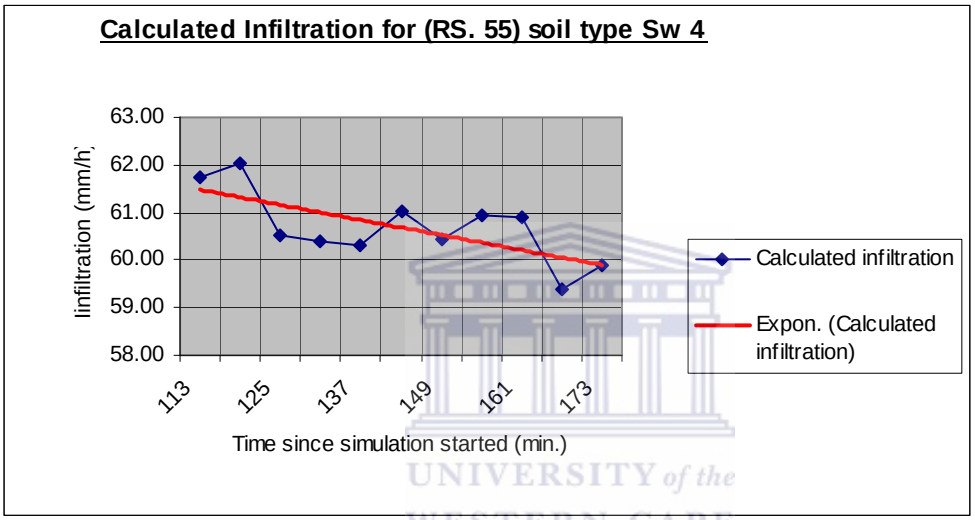

Figure 2.2 Indicates infiltration curve for simulation 55

Infiltration rates varied between 61.7 mm/h initially, when run-off started, and 59.9 mm/h towards the end of the simulation. The first run-off for this simulation happened only after 1 h and 53 min and the entire simulation process lasted for 2 h and 53 min.

This simulation was done on a south-facing slope of 19.1%. The soil type for this location was of the Swartland Form (Sw) and it had a clay content of 15%. The surface area within the ring where the simulation was done had a well-developed micro topography, with small depressions and slightly higher areas in between. A small tunnel of approximately 60 mm diameter created by a small rodent was also observed within the ring area. Such small tunnels were not the exception; they occurred frequently in the particular area.

During the simulation, water was concentrated in the depressions of the micro topography, which gradually filled up and when they eventually overflowed, the water was channelled downward by the animal conduit. The influence of animals and plants on earth-surface processes and landform development was termed "bio-geomorphology" by Viles (1988). In the past, this influence has often been neglected by scientists. It seems in this case to have played an important role in the observed high infiltration rates of site 55.

An analysis of the vertical distribution of moisture within the ring area directly under a wheat row revealed an interesting pattern. Because the ring enclosed a sloping surface and water dammed up slightly at the lower end of the slope, it was considered better to analyse the vertical moisture distribution at the upper end of the slope, from where the water would naturally drain away. The distribution is illustrated in Figure 2.3 below.

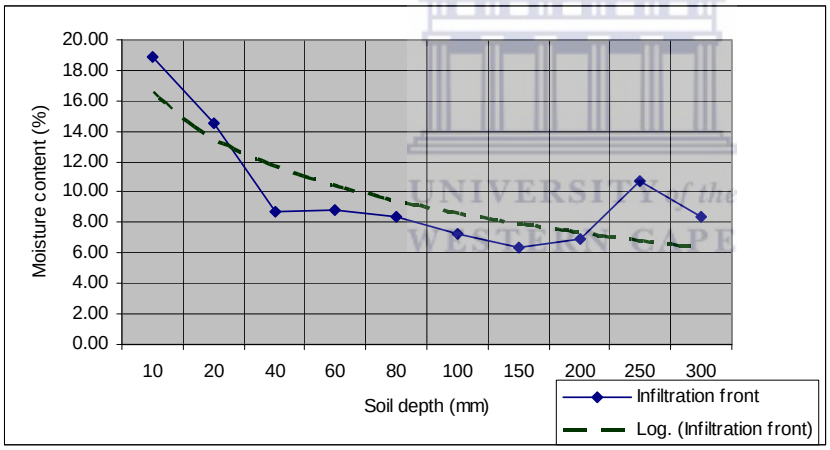

Figure 2.3 Indicates vertical distribution of moisture in the soil directly under a wheat row within the ring area of simulation 55

Figure 2.3 and Figure 2.4 indicate a general downward trend in the moisture content, decreasing from 19% at the surface to approximately 6% at 150 mm, then increasing again to approximately 8% at 300 mm depth.

The increase in moisture content at the depth from 200 to 300 mm is explained by the presence of the animal tunnel, which brought a large quantity of water to that depth. On

the other hand, close to the surface at about 10 mm of depth, more moisture was retained, because of a concentration of organic material.

Soil samples collected from between the wheat stem rows to investigate the absence or lower density of roots in the vadose zone on the moisture distribution, revealed a slightly different pattern. Figure 2.4 shows the moisture distribution for such an area. This diagram helps to evaluate the influence of roots. Here the topsoil held approximately 13.5% moisture, because no root systems were present, whereas the value at 300 mm barely reached 6%. Both values were slightly lower than those obtained in the previous case were.

It is thought, however, and confirmed by literature, especially from the work done by Leopold (1974), that rain falling on dry soil does not spread uniformly throughout that soil. It is partially controlled by the vegetation. It wets a certain depth of soil depending on the presence of vegetation, then, after the rain ends, the downward movement practically stops. The underlying soil then remains relatively dry until the rain continues again.

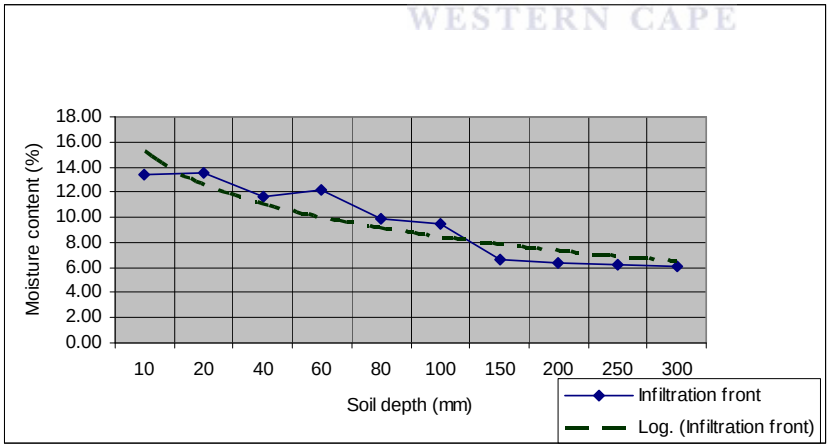

Figure 2.4 Indicates vertical distribution of moisture in the soil between wheat rows within the ring area of simulation 55

2.2.1.2 Simulation 42 (Gs2)

Simulation 42 is illustrated in Figure 2.5. Infiltration rates varied from an initial rate of 62.4 mm/h when run-off started, to 41.2 mm/h at the end of the simulation.
This simulation was done on a south-facing slope of approximately 9.1%, where the soil was of the Glenrosa Form (Gs) and had a clay content of 15%. The micro topography of the soil surface within the ring was similar to that of the previous simulation site, except that rodent tunnels were less noticeable, but other smaller cracks and ant tunnels were present.

The distribution of moisture in the soil within the ring area directly under a wheat row, after completion of the simulation, is illustrated in Figure 2.5. It indicates a general downward trend in the moisture content dropping from 24% at the surface to approximately 18% at 300 mm depth. This is slightly higher than at the previous site, probably because of different soil types.

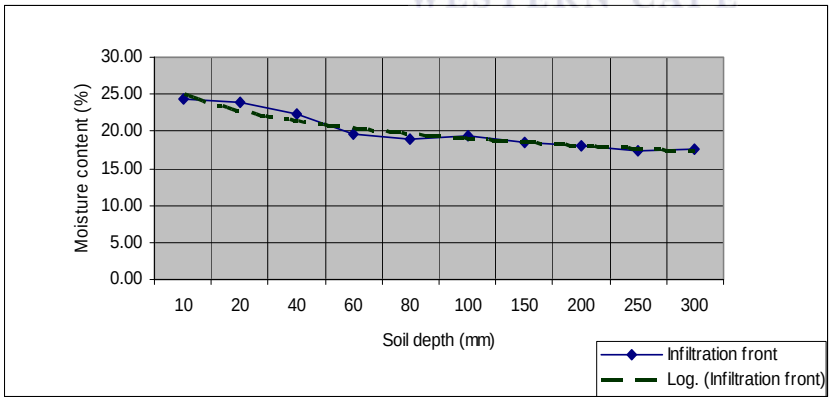

Figure 2.5 Indicates vertical distribution of moisture in the soil directly under a wheat row within the ring area of simulation 42

The "between-rows" distribution of soil moisture within the ring area is illustrated in Figure 2.6.

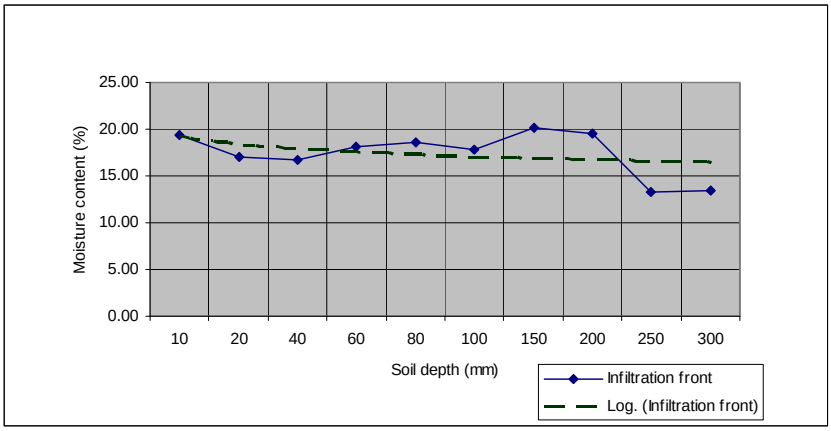

Figure 2.6 Indicates vertical distribution of moisture in the soil between wheat rows within the ring area of simulation 42

The general trend was a decrease in moisture ranging from 19.4% at the surface, to 13% at 300 mm depth. A slight increase in moisture occurred between 100 mm and 200 mm depth. This could have been because of the slightly flatter slope (9% against 19% in the previous case), which would not allow water to drain away as fast as in the previous case. This effect could have been enhanced by the shallow cracking pattern in the topsoil, as well as small termite-holes that were present.

2.2.1.3 Simulation 1 (Ss1)

Simulation 1 had a total duration of 2 h and 21 min and run-off started after 1 h and 14 min. The calculated infiltration curve for this simulation is illustrated in Figure 2.7.

The simulation was done on a north-facing slope with a gradient of 12.8%. The simulation site had soils belonging to the Sterkspruit Form, with a clay content of 10%. The surface simulation site was covered by dry wheat stems, where the root systems of the already harvested crops were slightly better developed. Some worm and termite channels, as well as cracks of different dimensions, were observed, especially in the areas close to the vegetated rows.

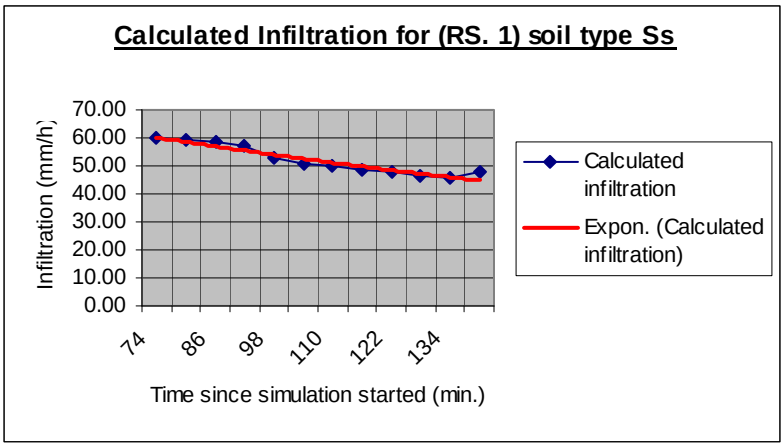

Figure 2.7 Indicates infiltration curve for simulation 1

At the beginning of run-off, the infiltration rate was 60 mm/h and at the end, it was 47.6 mm/h. The distribution of moisture after completion of the simulation in the soil within the ring area directly under a row is illustrated in Figure 2.8.

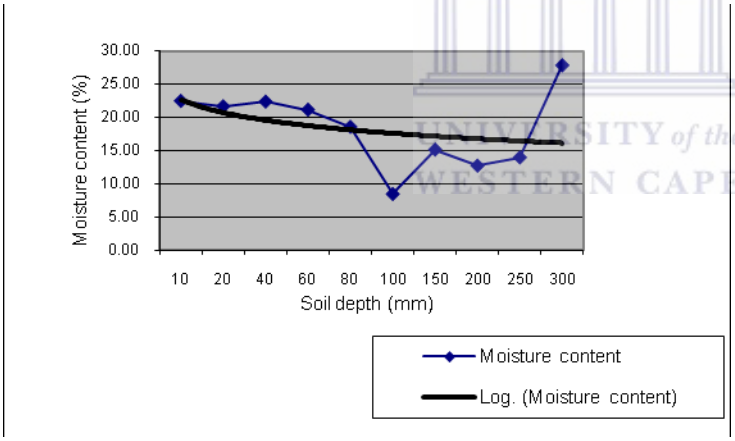

Figure 2.8 Indicates vertical distribution of moisture in the soil directly under a wheat row within the ring area of simulation 1

The moisture content decreased with depth from 22.4% at the surface, to a low value of 8.4% at a depth of 100 mm; then it increased to 12.7% at 200 mm and 27.8% at 300 mm depth.

This can be explained by the presence of a well-developed dry root system that left small tubes or tunnels in the ground, allowing the quick movement of water from the surface downwards to accumulate at a depth of 300 mm.

The distribution of moisture in the soil between the rows within the ring area is illustrated in Figure 2.9.

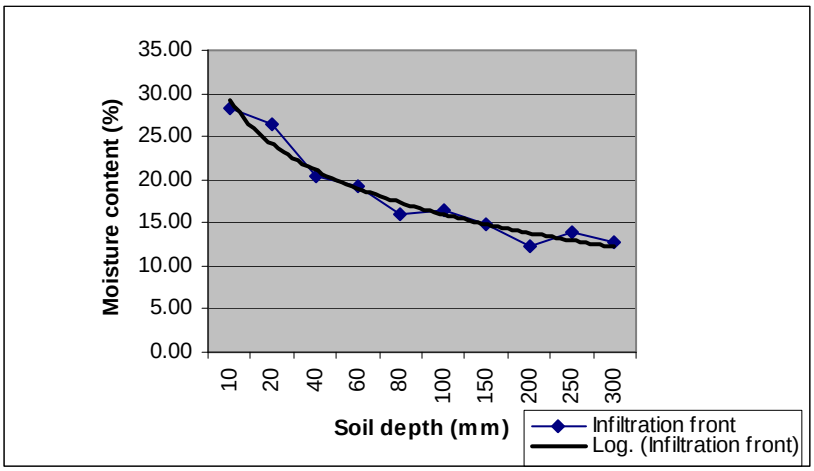

Figure 2.9 Indicates vertical distribution of moisture in the soil between wheat rows within the ring area of simulation 1

Figure 2.9 shows an evenly decreasing soil moisture content that varied from 28.3% at the surface to 12.8% at a depth of 300 mm. Because the slope was relatively flat, water did not flow away to the lower end of the ring area as quickly as on steeper slopes. This allowed the water more time to infiltrate at a particular position. Figure 2.9 shows a higher surface moisture content than Figure 2.8, probably because the water in the latter case infiltrated faster along the higher density of small tubes and cracks in the soil associated with the rows containing the dry roots of wheat. For the same reason, the water content at 300 mm depth was higher, as illustrated in Figure 2.8 and Figure 2.12 (at 250 mm).

The water accumulated at the lower end of the tubes and small cracks at 300 mm depth where roots occurred, whereas in the case of "in-between rows" this did not happen, resulting in slightly lower concentration of moisture.

2.2.1.4 Simulation 4 (Ms1)

Simulation 4 (Ms1) was done on a north-facing slope with a gradient of 11% and a surface covered by dry wheat stems, because it was after the harvesting season.

The soil for this particular site had a 12.5% clay content, and was of the Mispah Form. The first run-off happened after 43 min. The simulation process lasted for approximately 1 h and 49 min. The calculated infiltration curve for simulation 4 is illustrated in Figure 2.10 below.

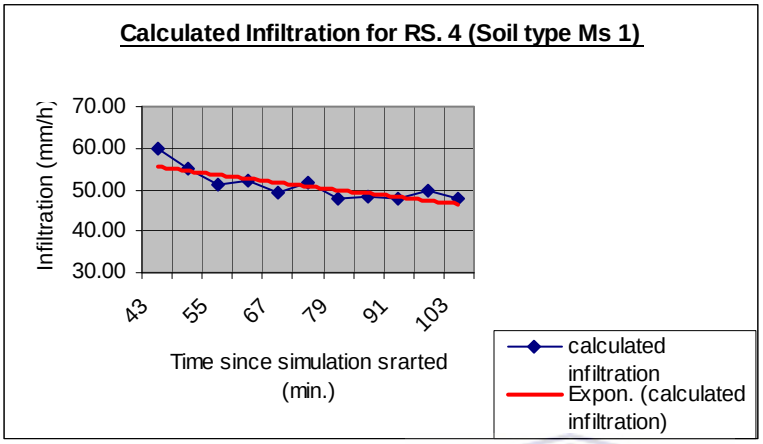

Figure 2.10 Indicates infiltration curve for simulation 4

The trend was a downward one as could have been expected, but it fluctuated slightly. The infiltration rate at the start of run-off was 59.8 mm/h and towards the end of the simulation, it was 47.6 mm/h.

The distribution of moisture in the soil beneath a wheat row in the ring area of simulation 4 is illustrated in Figure 2.11. The curve indicates a general decrease in moisture content, varying from 20.5% near the surface, to 13.9% at 80 mm depth. It then increased slightly to approximately 16.9% at 200 mm depth, before finally decreasing to 9.2% at a depth of 300 mm. The initial decrease of moisture between 60 mm and 100 mm depth could have been because of soil composition and soil material arrangement.

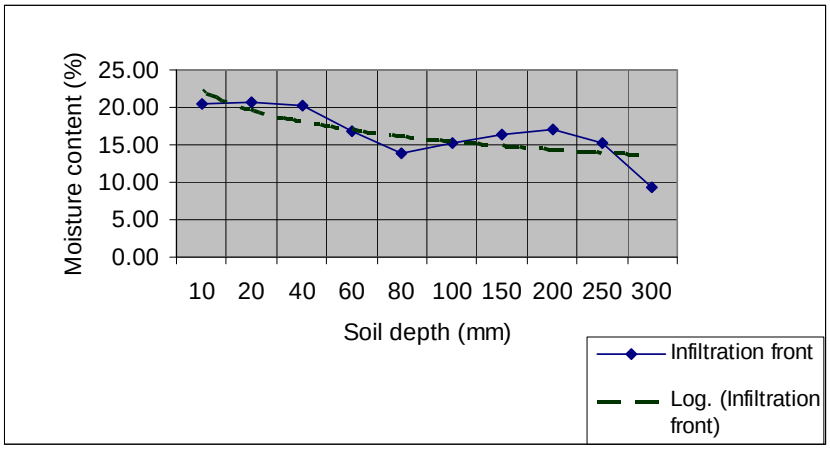

Figure 2.11 Indicates vertical distribution of moisture in the soil directly under a wheat row within the ring area of simulation 4

The increase in moisture content at about 200 mm depth could have been because of the presence of root systems, which had left open avenues as they decayed and dried off, allowing easy access of water to that particular depth. For the samples collected in-between rows, the results are shown in Figure 2.12.

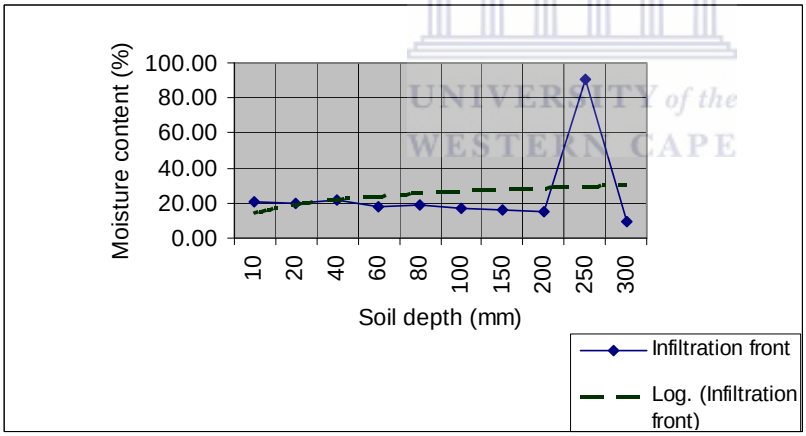

Figure 2.12 Indicates vertical distribution of moisture in the soil between wheat rows within the ring area of simulation 4

A very gentle decrease in the distribution of moisture with depth from 20.6% at the surface, to 15.2% at 200 mm depth is evident. A very high moisture content of 90.6% was found at 250 mm depth; it then decreased to 9.5% at 300 mm depth. This very high value was most likely the result of smaller channels/cracks that were feeding that point.

2.2.1.5 Simulation 6 (We1)

This simulation was done on a north-facing slope, where the gradient was approximately 11.5% and the surface had a 60% cover of dry wheat stems. The soil belongs to the Wesleigh Form (We1) and had a clay content of 10%. The calculated infiltration curve for simulation 6 is illustrated in Figure 2.13 below.

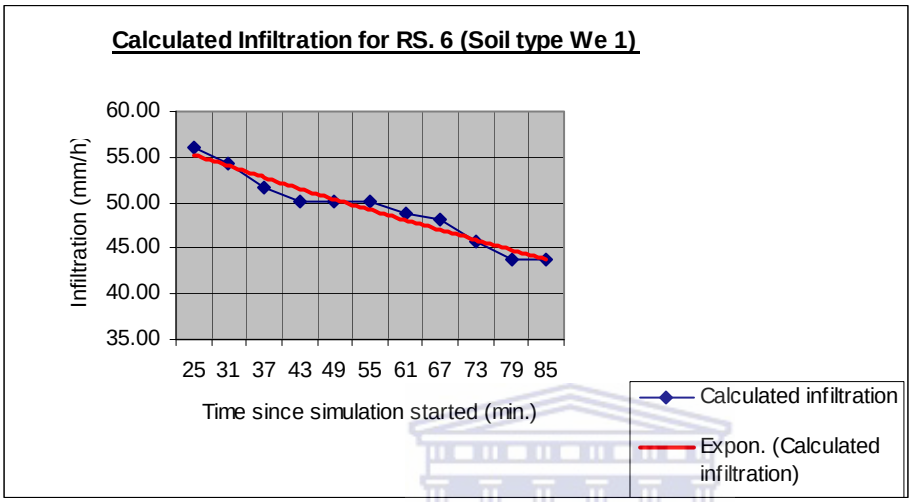

Figure 2.13 Indicates calculated infiltration curve for simulation 6

The infiltration rate at the start of run-off after 25 min of the simulation was 56 mm/h, dropping to 43.8 mm/h at the end of the simulation. The first run-off happened in the 25th min of simulation and the entire simulation took 1 h and 25 min.

The moisture content directly in the rows is illustrated in Figure 2.14. It varied between 20% at the surface and 2% at 300 mm depth. Interestingly, the rate of decrease in the profile was more or less constant, showing that the soil was relatively uniform in the top 300 mm beneath the rows.

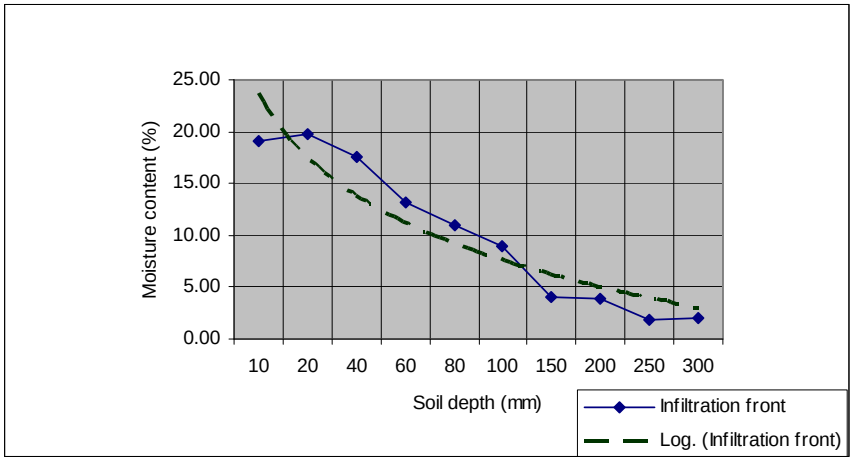

Figure 2.14 Indicates vertical distribution of moisture in the soil directly under a wheat row within the ring area of simulation 6

The distribution of moisture in the soil between the rows is illustrated in Figure 2.15. Here the moisture content reflects the presence of cracks and small animal-related tubes that supplied higher volumes of water to two main areas of the profile. The general trend was a decreasing moisture content, ranging from 17% at the surface to 2% at 300 mm depth, except at 20 mm depth, where the moisture content increased to 85% and at 150 mm depth, where it reached a value of 92%.

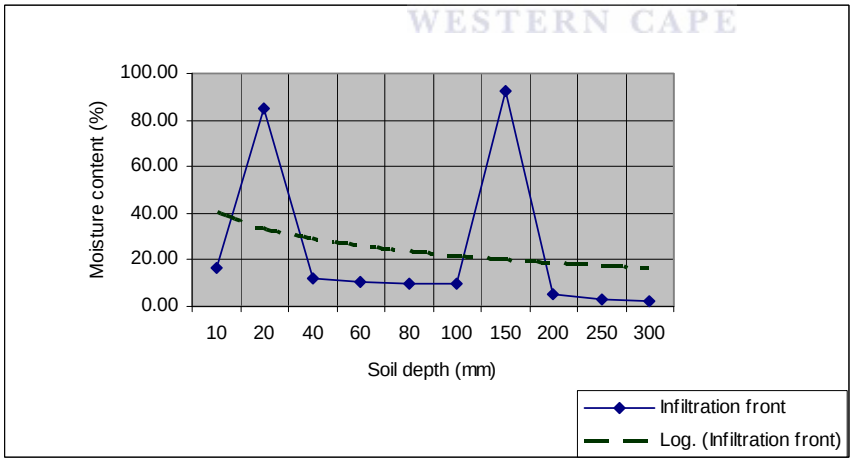

Figure 2.15 Indicates vertical distribution of moisture in the soil between wheat rows within the ring area of simulation 6

2.2.1.6 Simulation 28 (Sw1)

This simulation was the last one done in the category for sites with relatively high infiltration rates >40 mm/h. It was done on a south-facing slope with a gradient of 17.8% on soils of the Swartland Form (Sw). The clay content of 25% for this soil was the

highest of all the soils at the Goedertrou study site. The surface was covered by dry wheat stems (85% surface coverage), with well-developed root systems.

It has been widely reported in literature that roots can cause hydrological effects; when they increase surface roughness and soil permeability, they also increase the soil's infiltration capacity (Styczen and Morgan, 1995; Gray and Sotir, 1996). Cracks and the development of a visible micro topography were identified as the factors that allowed water to infiltrate into the soil with ease.

The calculated infiltration curve for simulation 28 is illustrated in Figure 2.16. It shows an infiltration rate of 61 mm/h at the start of run-off decreasing to 42.3 mm/h at the end of the simulation. Run-off started after 48 min of simulation and lasted for 1 h and 48 min.

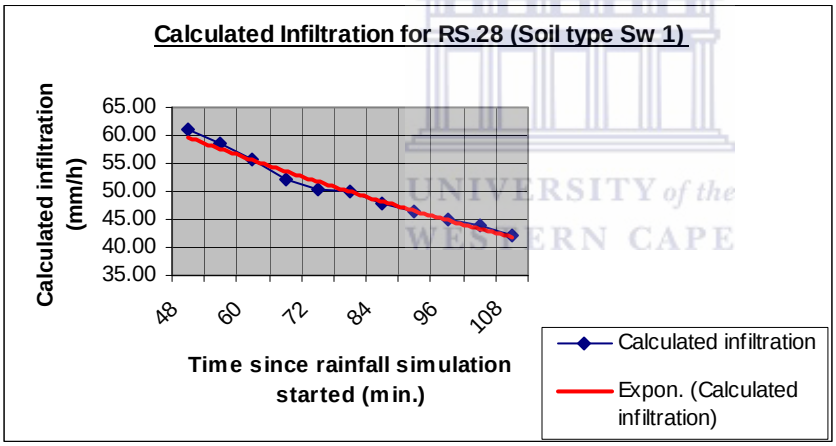

Figure 2.16 Indicates infiltration curve for simulation 28

The moisture content for the soils directly beneath a wheat row is shown in Figure 2.17. The moisture content ranged between approximately 17% at the surface and approximately 7% at 300 mm depth. In between the rows, the moisture content ranged between 17% at the surface and 11% at 300 mm depth. This is illustrated in Figure 2.17.

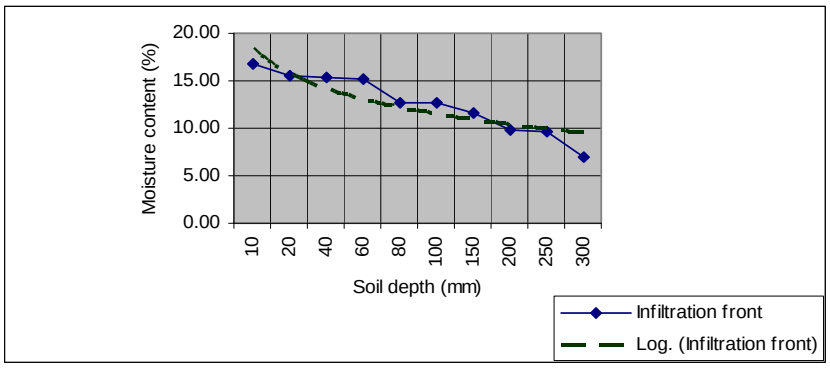

Figure 2.17 Indicates vertical distribution of moisture in the soil directly under a wheat row within the ring area of simulation 28

The moisture content for the soils directly beneath a wheat row is illustrated in Figure 2.18. It ranged between approximately 17% at the surface and approximately 11% at 300 m depth.

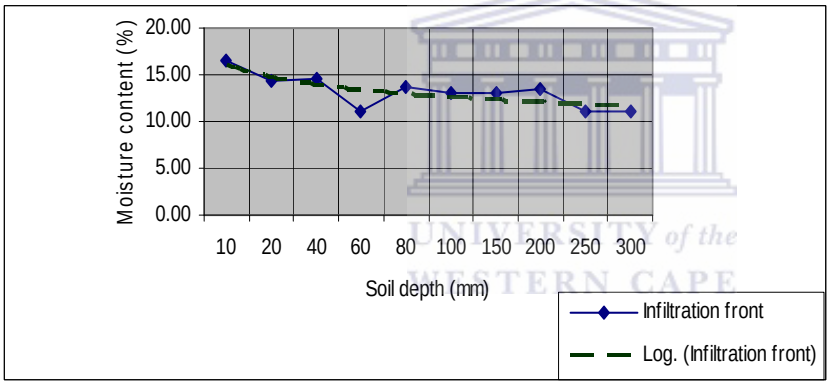

Figure 2.18 Indicates vertical distribution of moisture in the soil between wheat rows within the ring area of simulation 28

2.2.2 Simulation sites showing moderate infiltration rates (between 20 and 40 mm/h)

Simulation sites in this category were all on soils of the Swartland and Glenrosa Forms. "Time to run-off" during simulations varied between 12 min and 66 min and the infiltration rates at the end of simulations varied between 22 mm/h and 30 mm/h.

2.2.2.1 Simulation 5 (Gs1)

This simulation was done on an almost bare soil of Glenrosa Form (20% coverage with wheat stubbles), with a north-facing slope and a gradient of 18.5%. The clay content of the soil was 15%. The first run-off started in the 12th min of the simulation and the entire

process took approximately 1 h and 12 min. The calculated infiltration curve for the simulation is illustrated in Figure 2.19.

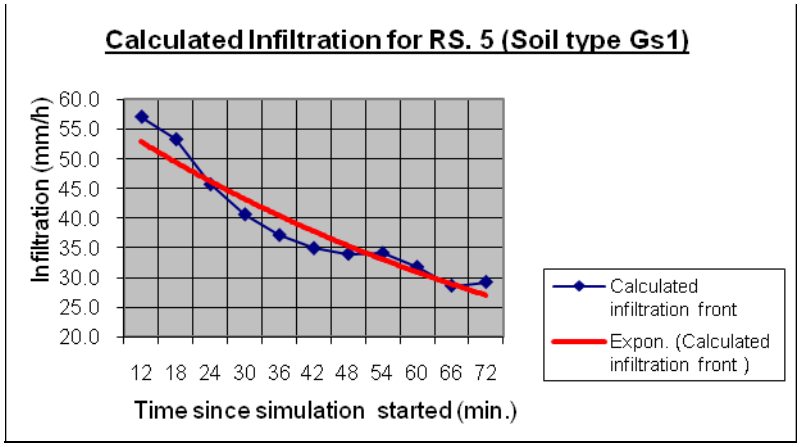

Figure 2.19 Indicates infiltration curve for simulation 5

The infiltration rate ranged between 57 mm/h at the start of run-off and 29 mm/h at the end of the simulation. The vertical distribution of moisture beneath the wheat rows in the ring area is illustrated in Figure 2.20. Here the moisture content decreased smoothly from 16.7% at the surface to 7.8% at a depth of 300 mm, except at a depth of 40 mm, where the value increased to 88.9%. It seems that, because of the steeper slope (18.5%) and the low vegetation density, water drained away quite quickly, allowing little time to infiltrate to greater depths. This could have been the reason for the higher concentration at a shallow depth of 40 mm.

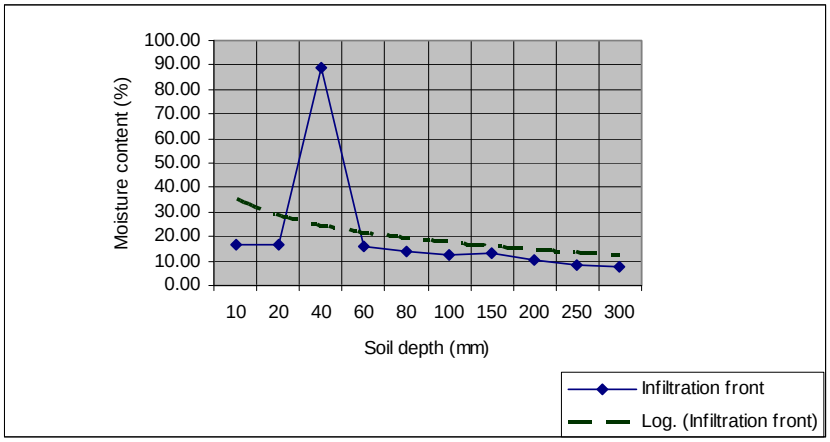

Figure 2.20 Indicates vertical distribution of moisture in the soil directly under a wheat row within the ring area of simulation 5

The vertical moisture distribution for the "in-between rows" situation is illustrated in Figure 2.21. Here the moisture decreased from 19.5% at the surface to 8.4% at 150 mm depth, then it increased to 92% at 200 mm and 84% at 300 mm depth.

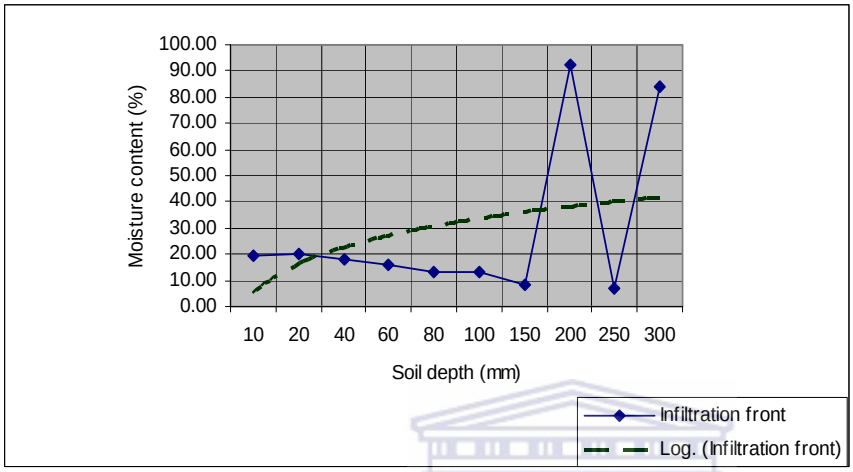

Figure 2.21 Indicates vertical distribution of moisture in the soil between wheat rows within the ring area of simulation 5

The two peaks of high concentration were probably related to soil cracks present in the relatively bare soil surface between the rows, allowing a deeper infiltration of water in these areas.

2.2.2.2 Simulation 45 (Sw2)

This simulation was done on a south-facing slope with a gradient of 8%. The soil for this site had a clay content of approximately 17.5% and was of the Swartland Form (Sw). The surface had a 15% wheat stubble cover with well-developed root systems and many visible cracks. The first run-off happened in the 66th min of the simulation, which lasted for 2 h and 6 min. The calculated infiltration curve for simulation 45 is illustrated in Figure 2.22.

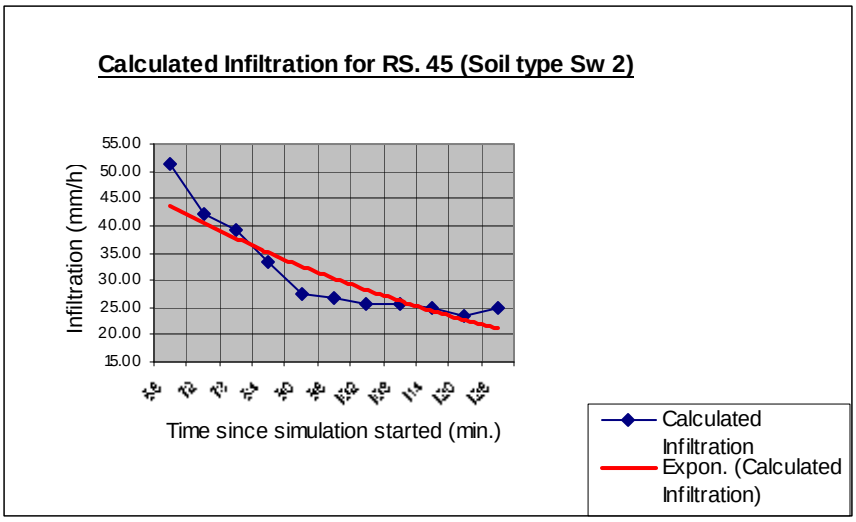

Figure 2.22 Indicates infiltration curve for simulation 45

The infiltration rate at the start of the run-off was 51.4 mm/h, decreasing sharply to 27.6 mm/h around 90 min of simulation, and then levelling at a moderate 24.7 mm/h towards the end of the simulation.

The vertical distribution of moisture beneath wheat rows is illustrated in Figure 2.23. The moisture content decreased smoothly from 24% at the surface to 5.5% at 250 mm depth, then it increased slightly again to 10% at 300 mm depth.

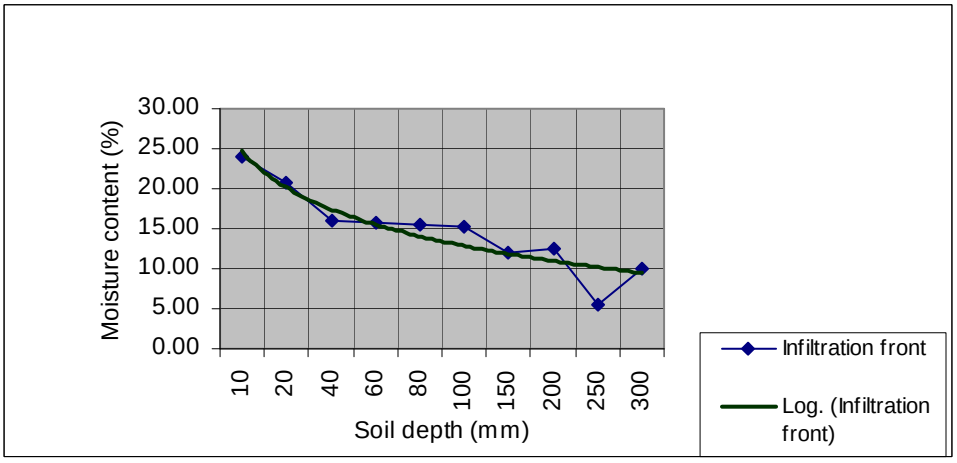

Figure 2.23 Indicates vertical distribution of moisture in the soil directly under a wheat row within the ring area of simulation 45

The numerous cracks and the dry root system of the wheat probably influenced the downward movement of water, resulting in the slight increase in moisture content at 300 mm depth.

The vertical moisture distribution for the area between rows at simulation site 45 is illustrated in Figure 2.24.

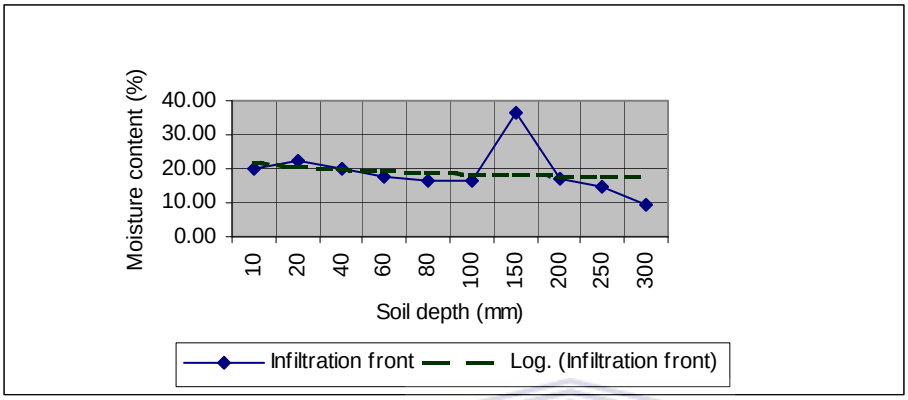

Figure 2.24 Indicates vertical distribution of moisture in the soil between wheat rows within the ring area of simulation 45

The general trend in moisture content was a decreasing one, with moisture content at the surface of about 19.8%, then decreasing to 9.4% at 300 mm depth. The exception was at 150 mm depth, where the moisture content increased to 36.4%. Here again, as in so many of the other cases, openings created by cracking and other biological activity, could have piped the water to that depth, thus causing the higher concentration.

2.2.2.3 Simulation 2 (Sw3)

Simulation 2 was done on a north-facing slope with a gradient of 9.4% in a Swartland Soil (Sw) with a clay content of 13.5%. The soil had a dense (75%) wheat stubble coverage with well-developed root systems.

The first run-off happened 27 min after rainfall simulation started and the entire simulation process lasted approximately 87 min. The calculated infiltration curve for this simulation is illustrated in Figure 2.25.

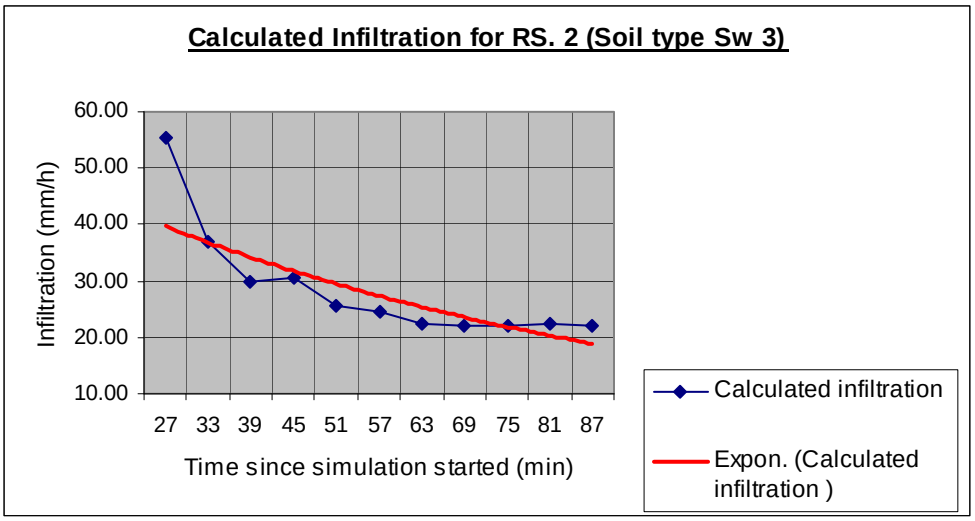

Figure 2.25 Indicates infiltration curve for simulation 2

At the start, the infiltration rate was high, at approximately 55 mm/h, then decreasing to a moderate 22 mm/h at the end of the simulation, after approximately 87 min. The distribution of moisture in the soil beneath the wheat row within the ring area is illustrated in Figure 2.26.

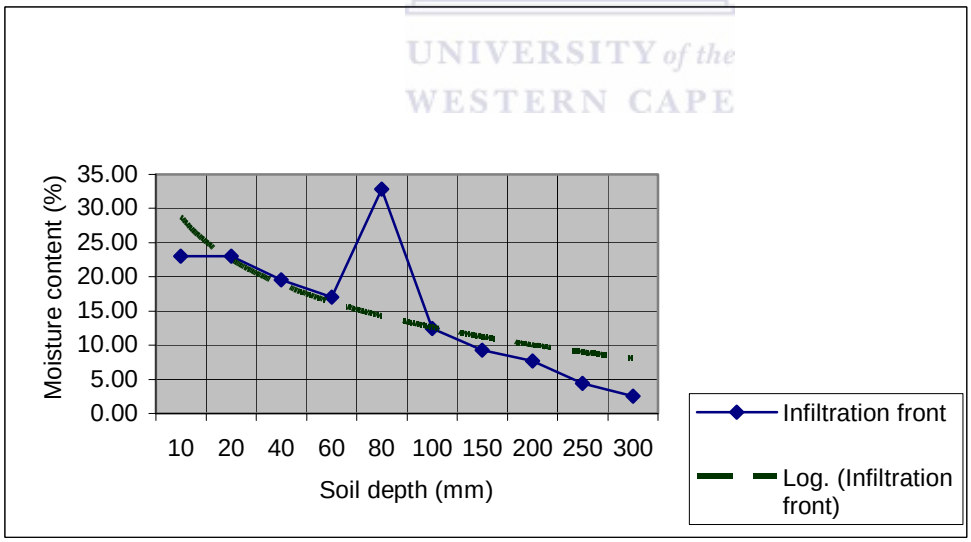

Figure 2.26 Indicates vertical distribution of moisture in the soil directly under a wheat row within the ring area of simulation 2

The moisture content generally decreased from approximately 23% at the surface to approximately 3% at 300 mm depth, with an exception at 80 mm depth where the moisture content increased to almost 33%. This could have been because of a channel

observed in the ring area, as well as minor cracks near the surface. It seems, therefore, that the root system and the physical structure of the soil surface influenced the infiltration of this particular simulation. This is supported by the study of Mermut *et al.* (1996). The vertical moisture distribution for the area between rows at simulation site 2 is illustrated in Figure 2.27.

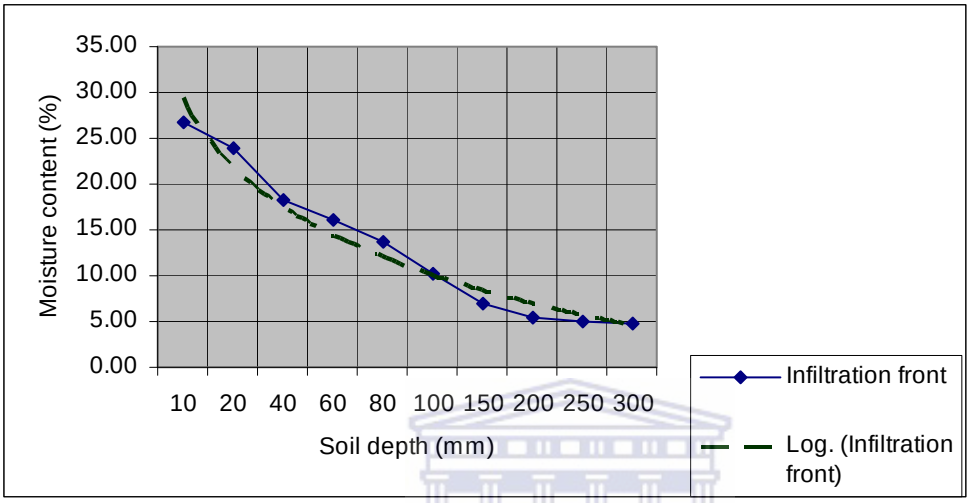

Figure 2.27 Indicates vertical distribution of moisture in the soil between wheat rows within the ring area of simulation 2

Figure 2.27 indicates an evenly decreasing distribution of the moisture content during the simulation. It is clear that a large percentage of the moisture was concentrated at the surface, where material such as clay was present. At the surface, the moisture content was approximately 27%, decreasing to approximately 5% at a depth of 300 mm. There was a little bit of moisture input between 40 mm and 100 mm (the values were slightly higher than expected).

This small variation could have been caused by either the presence of nearby roots or a few small cracks that supplied avenues for water movement in the topsoil. The figure also indicates that from approximately 200 mm upwards, the infiltration was stable. A possible explanation is that the water flowed downward through the network of avenues, but encountered frictional resistance that increased with an increase of the depth of the network. Such an increase in friction with depth of wetting slows the rate of downward

movement and it consequently impedes the rate of entrance of "new" water from the surface (Leopold, 1974).

2.2.3 Simulation sites showing low infiltration rates (less than 20 mm/h)

Simulations on sites in this category were done on a variety of soils, including the Glenrosa Augrabies, Cartref, Katspruit and Klapmuts Forms. "Time to run-off" during the simulations varied between 7 and 28 min, and the infiltration rates at the end of simulations ranged between 8 mm/h and 18 mm/h.

2.2.3.1 Simulation 3 (Gs1)

The first simulation in this group with low infiltration rates was simulation 3, with an infiltration rate at the end of the simulation of only 18 mm/h. This simulation was done on a north-facing slope with a gradient of 11.2%, where the soil was of the Glenrosa Form (Gs) and had a clay content of 15%.

The surface was covered by wheat stems (85%) that remained after wheat harvesting. The first run-off happened in the 28th min of simulation and the entire simulation took 88 min. The infiltration rate was 46 mm/h at the start of the simulation and it is illustrated in Figure 2.28.

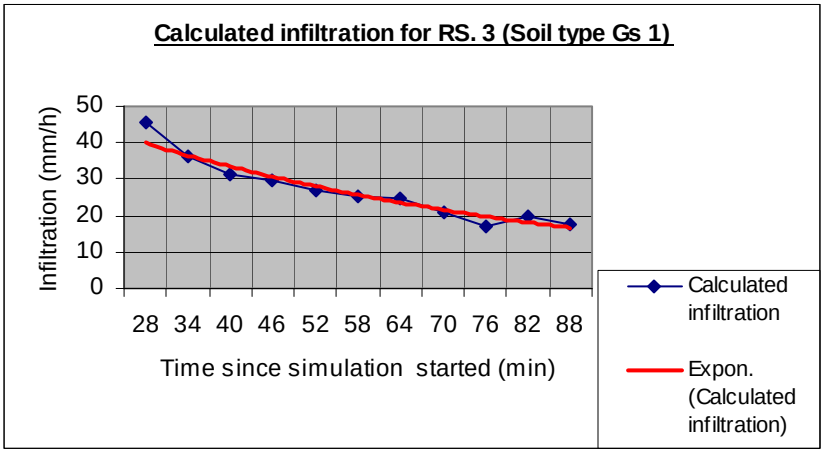

Figure 2.28 Indicates infiltration curve for simulation 3

The vertical distribution of moisture within the ring area directly below a wheat row is illustrated in Figure 2.29.

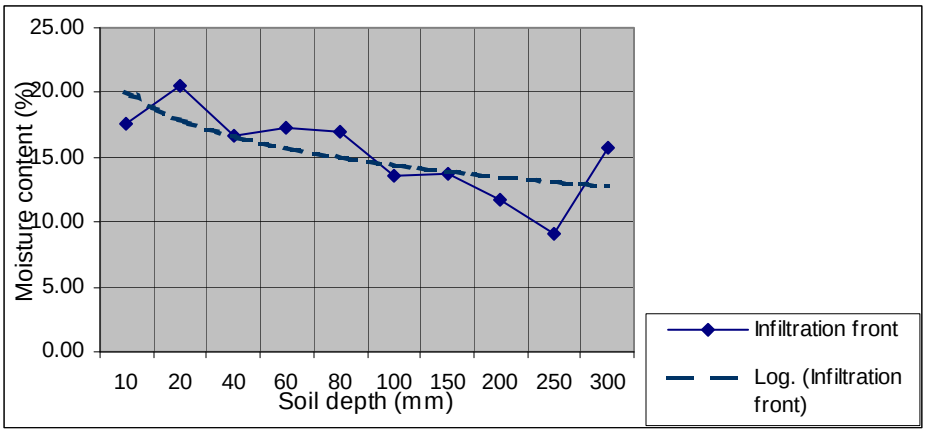

Figure 2.29 Indicates vertical distribution of moisture in the soil directly under a wheat row within the ring area of simulation 3

The curve shows a fluctuating, but slowly decreasing moisture content ranging between approximately 20% near the surface and approximately 9% at a depth of 250 mm, then increasing again to close on 16% at 300 mm depth. The higher value at 300 mm depth could have been related to the high coverage (85%) of dry wheat stubbles where the dry root systems supplied avenues along which water could infiltrate. It could also have been that the soil horizons at this depth became more difficult to infiltrate and that the water, therefore, accumulated here without infiltrating farther down. The vertical distribution of moisture in the area between rows is illustrated in Figure 2.30.

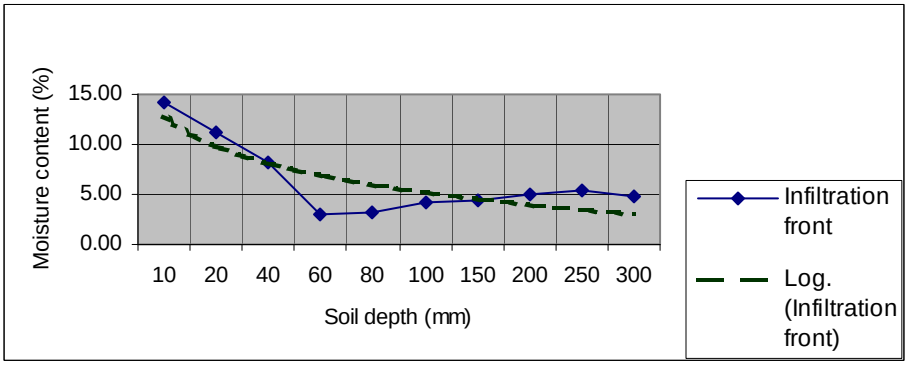

Figure 2.30 Indicates vertical distribution of moisture in the soil between wheat rows within the ring area of simulation 3

The moisture content decreased sharply from 14% at the surface to approximately 3% at a depth of 60 mm. It then increased gradually to approximately 4.8% at a depth of 300 mm. From the curve, it is clear that water only really infiltrated the upper soil horizon,

resulting in the relative short "time to run-off" of approximately 28 min. The clear influence of the wheat roots, allowing water to infiltrate (whereas the opposite applies where roots are absent), was well illustrated in this simulation.

2.2.3.2 Simulation 59 (Ag1)

Simulation 59 was the second of the group of low infiltration soils with infiltration rates of less than 20 mm/h. The simulation was done on a south-facing slope with a gradient of approximately 10.5% on soils of Augrabies Form (Ag1) with a clay content of 10%.

The surface was covered with wheat stems (45%) that remained from the previous harvesting, and by well-developed cracks and small ant tunnels. Run-off happened 20 min after the start of the simulation and the entire simulation lasted for 80 min. The calculated infiltration curve for simulation 59 is illustrated in Figure 2.31.

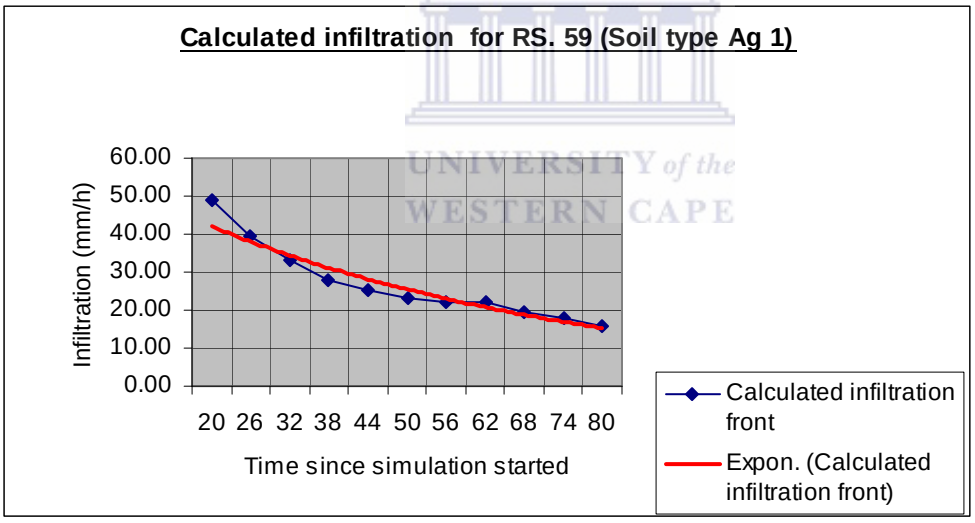

Figure 2.31 Indicates infiltration curve for simulation 59

The curve reveals an evenly decreasing infiltration rate, ranging from 49 mm/h when run-off started to approximately 15.8 mm/h at the end of the simulation. The vertical distribution of moisture in the ring area directly beneath a wheat row is illustrated in Figure 2.32.

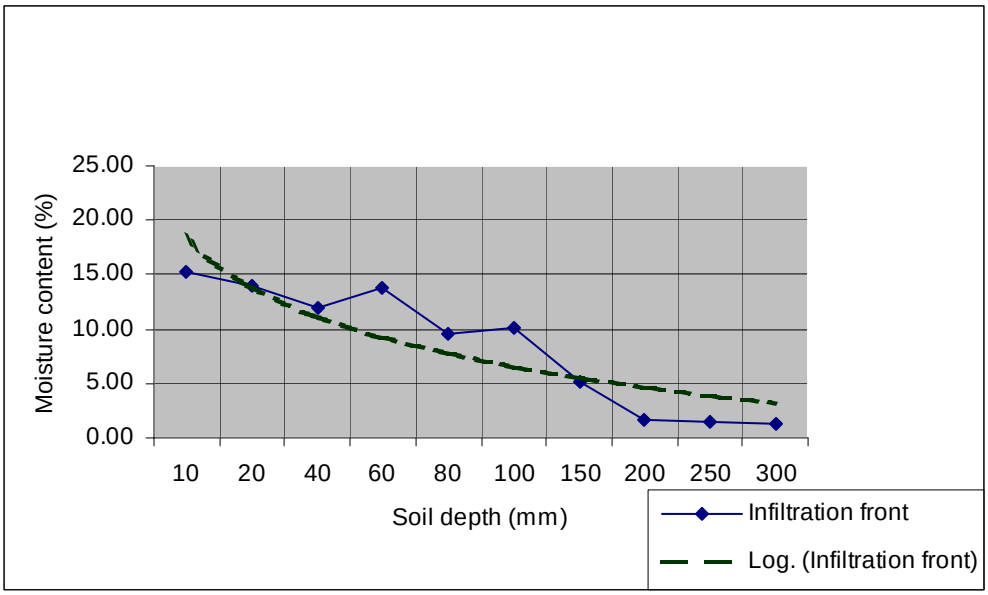

Figure 2.32 Indicates vertical distribution of moisture in the soil directly under a wheat row within the ring area of simulation 59

Moisture content decreased from 15% at the surface to less than 2% at a depth of 300 mm. It is clear that the low infiltration rate of less than 20 mm/h does not allow water to infiltrate deep into the soil. Although the observed small cracks and ant tunnels might have played a role, they appeared to be rather shallow, only allowing water to soak into the upper 100 mm of soil, as can be seen from the slightly higher moisture content at 60 mm and 100 mm depth in Figure 2.32.

The distribution of moisture in the ring area between the rows is illustrated in Figure 2.33.

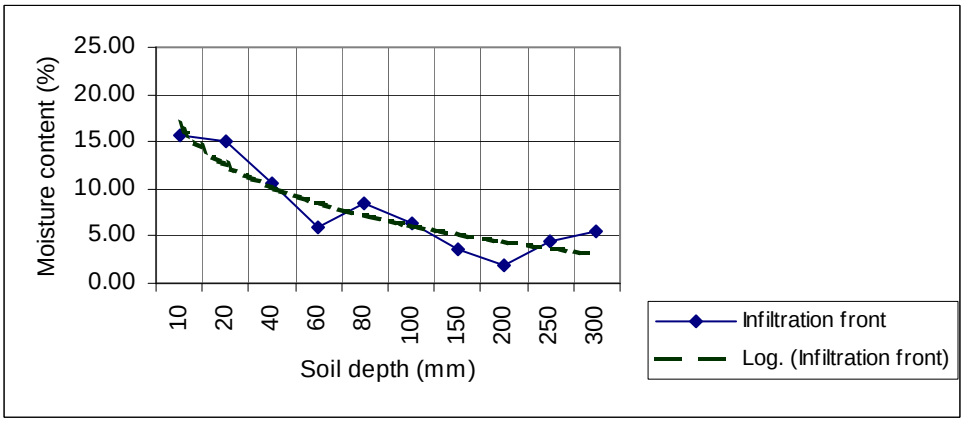

Figure 2.33 Indicates vertical distribution of moisture in the soil between wheat rows within the ring area of simulation 59

The curve shows decreasing moisture content, ranging from 15.7% at the surface to approximately 5% at 300 mm depth. A slight increase in the moisture content was evident at 80 mm depth, indicating the influence of the observed small cracks and ant tunnels.

2.2.3.3 Simulation 40 (Cf1)

This simulation was done on a south-facing slope with a gradient of 17.6% on a soil of Cartref Form. The soil had a clay content of 12.5% and coverage of wheat stems of approximately 70%. The first run-off happened 7 min after the simulation started and the entire simulation took approximately 1 h and 7 min. The infiltration rate when the first run-off happened was 53 mm/h and at the end of the simulation was 14 mm/h. The calculated infiltration rate for simulation 40 is illustrated in Figure 2.34.

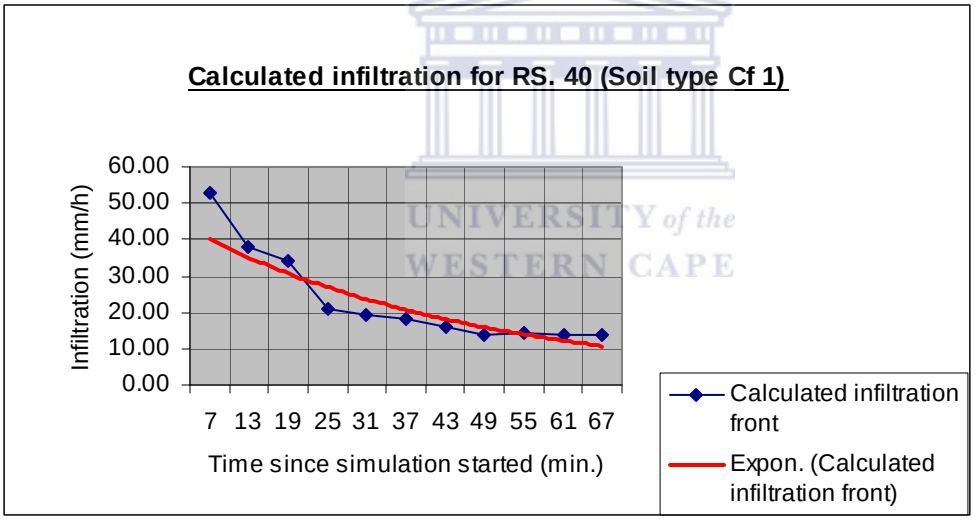

Figure 2.34 Indicates infiltration curve for simulation 40

As can be seen from the curve, the infiltration rate decreased sharply to approximately 20 mm/h in the first 25 min; it then evened out at approximately 14 mm/h. The vertical distribution of moisture in the soil beneath a wheat row within the ring area is illustrated in Figure 2.35.

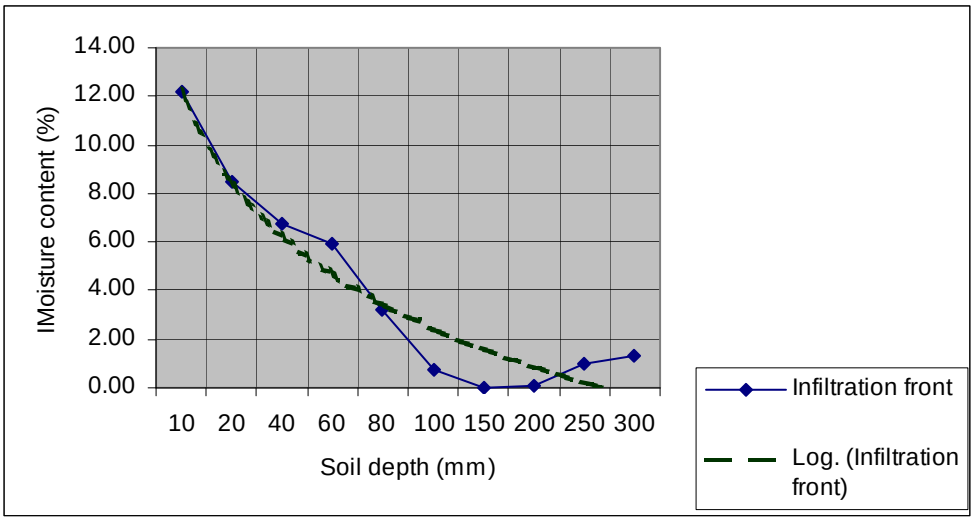

Figure 2.35 Indicates vertical distribution of moisture in the soil directly under a wheat row within the ring area of simulation 40

The moisture content, as revealed by the Figure 2.35, varied between 12% at the surface and less than 2% at 300 mm depth, with a lowest moisture content of 0.1% at a depth of 150 mm. The distribution of moisture in the soil between rows within the ring area is illustrated in Figure 2.36.

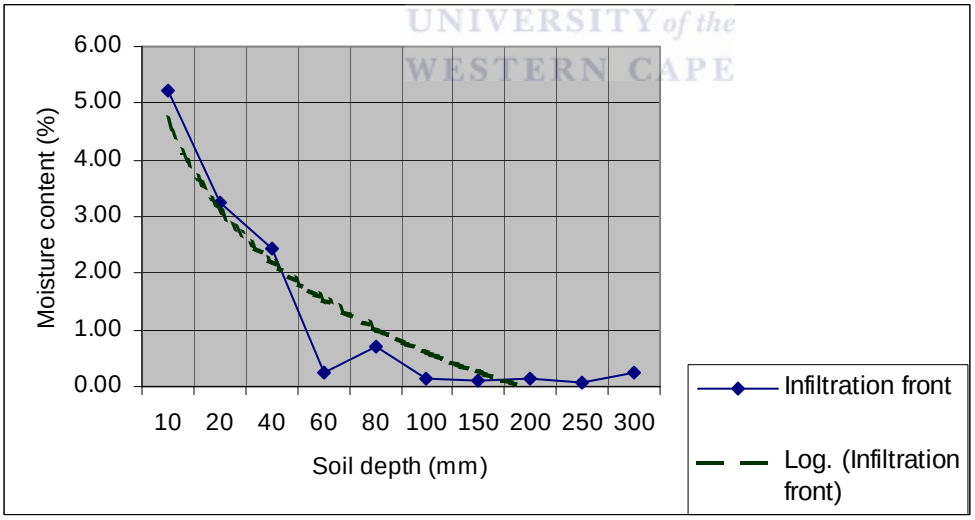

Figure 2.36 Indicates vertical distribution of moisture in the soil between wheat rows within the ring area of simulation 40

As in the previous case, the moisture content of the soil was very low, ranging from approximately 5% at the surface to approximately 0.2% at 300 mm depth. This is

understandable, considering the low infiltration rate of 14 mm/h. The latter also explains the short delay before run-off happened (only 7 min before run-off started).

2.2.3.4 Simulation 53 (Ka1)

Simulation 53, which displayed the second lowest infiltration rate, was done on a south-facing slope, with a gradient of 13.7%. The soil was of the Katspruit Form and had a 10% clay content.

The first run-off happened in the 9th min of simulation and the entire simulation lasted for 1 h 9 min. Besides the dry wheat stems that covered 65% of the surface, termite activity was also observed.

The calculated infiltration curve for simulation 53 is illustrated in Figure 2.37.

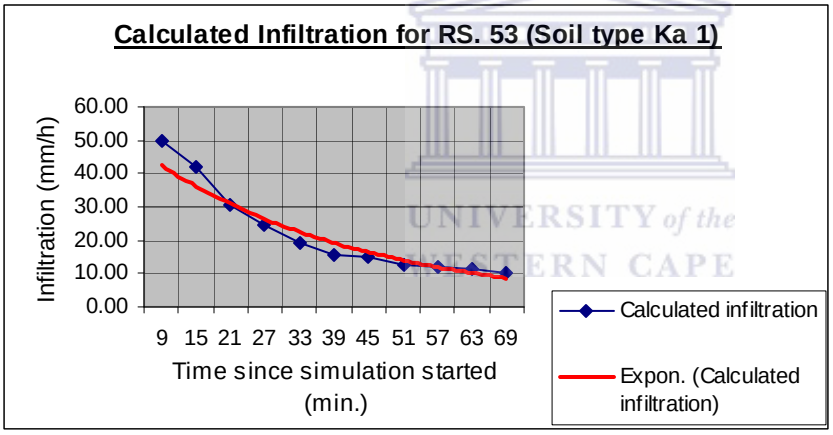

Figure 2.37 Indicates infiltration curve for simulation 53

Infiltration for simulation 53 varied from 49.6 mm/h at the start of run-off to approximately 10.5 mm/h at the end of the simulation. The vertical moisture distribution in the soil beneath the wheat rows in the ring area is illustrated in Figure 2.38.

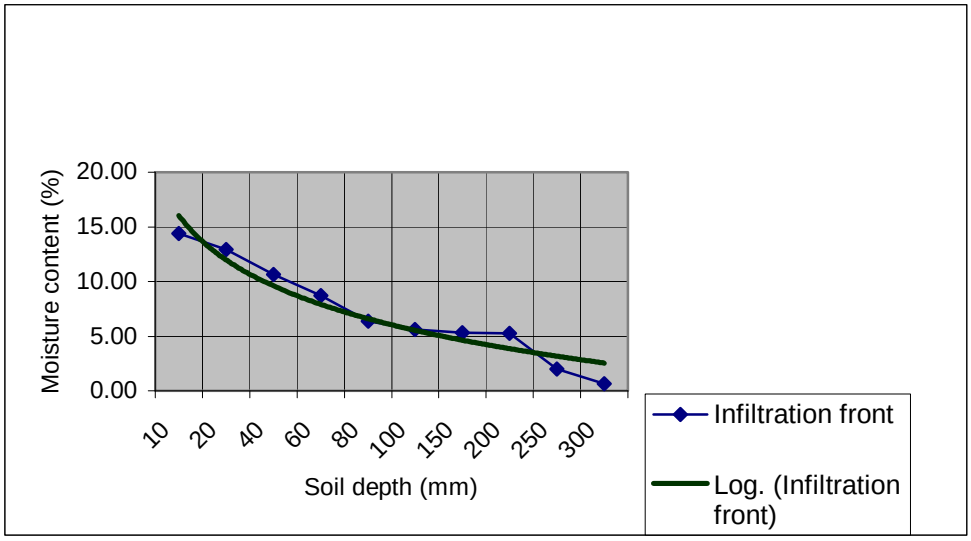

Figure 2.38 Indicates vertical distribution of moisture in the soil directly under a wheat row within the ring area of simulation 53.

Moisture content decreased from 14.4% at the surface to less than 1% (0.7%) at a depth of 300 mm. The situation for the area between rows was slightly different. Moisture content varied from 17% at the surface to less than 1% at 200 mm depth; it then increased again to approximately 6% at 300 mm depth. This is illustrated in Figure 2.39.

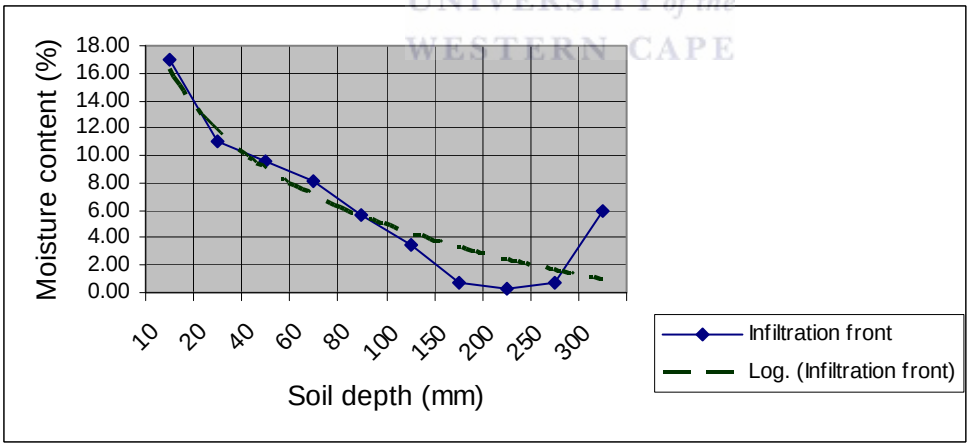

Figure 2.39 Indicates vertical distribution of moisture in the soil between wheat rows within the ring area of simulation 53

The increasing values at 300 mm depth might have be related to the presence of termite activity in the soil, which allowed water to infiltrate along these small tunnels to depths of 300 mm.

2.2.3.5 Simulation 21 (Km1)

Simulation 21 had the lowest infiltration rate of all the simulations. It was done on a south-facing slope of approximately 14.5%, with a wheat stem coverage of approximately 70%. Soils were of the Klapmuts Form and had a clay content of 15%. The first run-off happened in the 8th min of the simulation and the entire simulation took 68 min. The infiltration rates were 50 mm/h at the beginning when run-off started and 8 mm/h at the end of the simulation. This is illustrated in Figure 2.40.

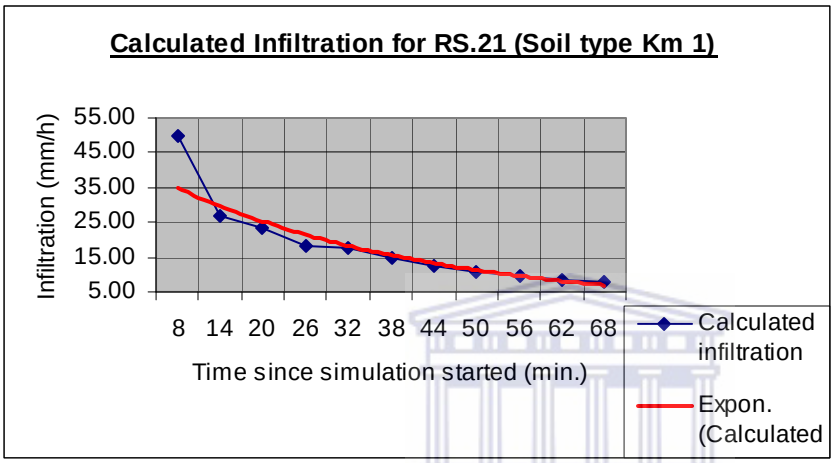

Figure 2.40 Indicates infiltration curve for simulation 21

As can be seen from the curve, the infiltration rate decreased rapidly from the initial value of 50 mm/h, to approximately 26 mm/h after only 14 min; it then decreased at a lower rate down to the end value of 8 mm/h. The vertical moisture distribution for the area beneath a wheat row in the ring area of simulation 21 is illustrated in Figure 2.41.

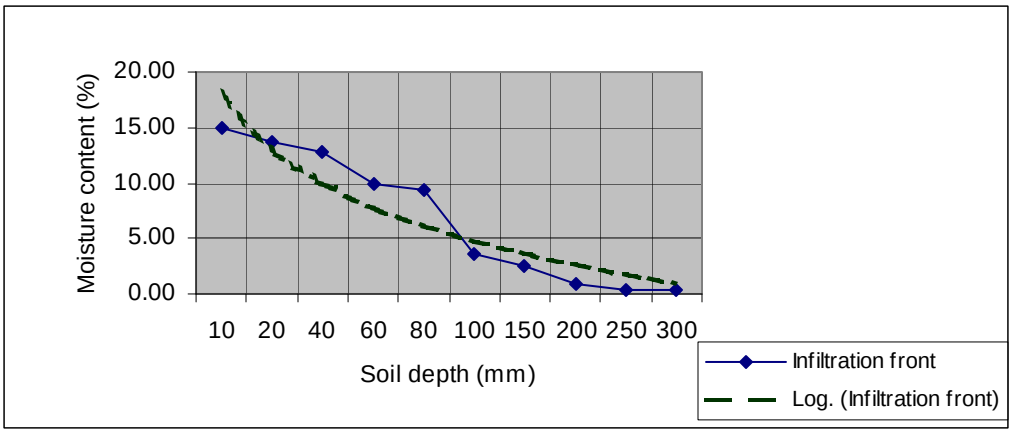

Figure 2.41 Indicates vertical distribution of moisture in the soil directly under a wheat row within the ring area of simulation 21

Moisture content decreased from 15% at the surface, to approximately 0.4% at 300 mm depth, although the moisture content at a depth of 40 mm to 80 mm seems to be slightly higher than expected. Again, it is clear that the low infiltration rate of 8 mm/h towards the end of the simulation did not allow water to penetrate much deeper than approximately 100 mm depth. The vertical moisture distribution for the area between rows is illustrated in Figure 2.42.

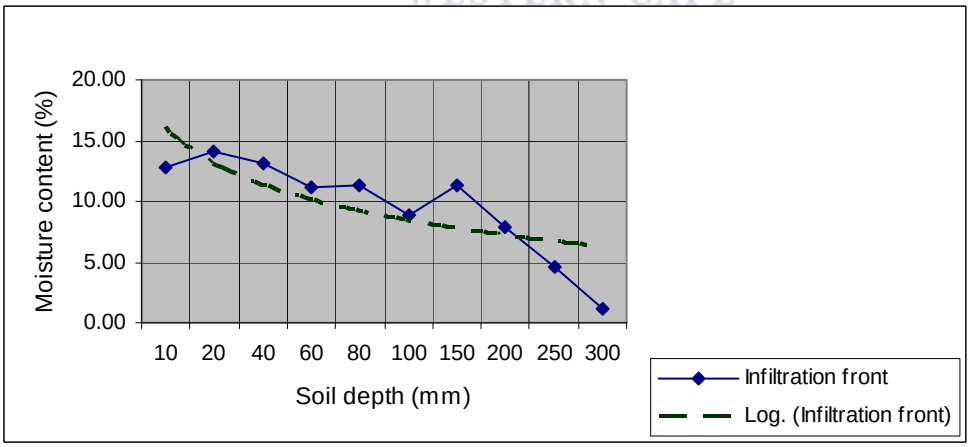

Figure 2.42 Indicates vertical distribution of moisture in the soil between wheat rows within the ring area of simulation 21

Moisture varied from approximately 14% in the upper 20 mm, to 11% at 150 mm depth, then it decreased sharply to 1% at 300 mm depth. The infiltration characteristics in Figure 2.42 depict clearly the influence of the soil properties during the simulation process. The

clay content was relatively high and without a well-developed crack pattern, nor any biological activity in this particular soil, therefore water could not infiltrate to greater depths.

2.3 Conclusions

The project conducted on a small-scale catchment at Goedertrou was done to gain a better understanding of the hydrological processes in the soil mantle and vadose zone. An evaluation of infiltration using rainfall simulation was therefore done. The analysis to determine the moisture content was done using the basic gravimetric method.

From the infiltration curves and moisture distribution curves shown earlier, it is clear that the vertical movement of water through the topsoil was largely governed by a well-developed soil structure. This was further enhanced by the presence of mainly dry root systems of wheat that formed small tubes along which water could infiltrate. The tunnelling activities of termites and other small animals additionally produced larger tunnels, which that often resulted in abnormally high infiltration rates. It seems that the water was usually concentrated in the depressions of the micro topography, before being channelled downward by the above-mentioned factors.

Considering the results, one might conclude that decayed root systems from the rows of plants, soil cracks, small channels and openings created by small animals, as well as slope orientation and, therefore, soil composition, all played a major role in influencing the ability of the soil to absorb the simulated rainfall.

More detailed information on the hydrological influence of cracks of different dimensions on the infiltration rates of soils at the beginning of the winter season, before surface sealing occurs, is needed. It would be interesting to establish whether disturbing the soil structure by tilling the soil could result in deeper or better infiltration.

In the next chapter, the focus changes to an overview of the run-off characteristics generated by rainfall simulation on the various soils.

Chapter 3

Evaluation of run-off

3.1 Introduction

The term run-off has been described as water moving over the earth surface because of precipitation and snowmelt (Warren *et al.,* 1995). It is the part left over after infiltration has taken away as much as the porosity and permeability of the ground will allow (Leopold, 1974).

The initial loss, also known as initial abstraction, results from many factors, such as crack filling, micro topography and vegetation cover (Gribbin, 2002; Poesen, 1987). Previous studies have revealed that within semi-arid areas, light vegetation and related micro topography have an important effect on run-off at fine spatial scales (Yair and Lavee, 1976; Scoging, 1982; Wilcox *et al.,* 1988; Dunne *et al.,* 1991). One of these effects is the increased infiltration near vegetation, which reduces overland flow.

Another effect is the direct influence of micro topography on concentrating or diverging run-off, which was an important field observation in this study as well. It is clear that for run-off generation, the approach has always been to examine the larger scale, whereas the effect of micro topography has so far only received slight attention (Bergkamp, 1998).

Another effect that might also play an important role is the slope of the surface on which run-off is generated. Slope is negatively related to Hortonian run-off volume on soils prone to surface sealing (Poesen, 1984).

To understand the effect of individual vegetation patches and surface micro topography on run-off at the slope scale, new properties, patterns and processes that are observed at the broader scale have to be taken into consideration. For example, the presence of

interrows, and the concentration of flow in these, significantly affects the measurement of run-off at the slope scale (Roels, 1984).

Therefore, run-off characteristics cannot be assessed with ease from measurements at the individual vegetation patch scale alone (Bergkamp, 1998). For this reason, to scale up run-off production within semi-arid regions, one must understand the discontinuity in run-off related to the short duration and small size of storms, as well as the heterogeneity in surface properties (Wolman and Gerson, 1978; Yair and Lavee, 1985; Wood *et al.*, 1986; de Boer and Campbell, 1989; Malcolm, 1996).

On a seasonal scale, it might be difficult to evaluate the different processes related to micro topography, because rainfall could be variable. To overcome these problems, and to work effectively, rainfall simulation offers an acceptable alternative, as mentioned earlier.

The principal environmental issues associated with run-off are the impacts to surface water, groundwater and soil through transport of water pollutants. Ultimately, these consequences result in human health risks, ecosystem disturbances.

For this study, however, the main focus was to address some of the hydrological processes active on different soil types in the research catchment as discussed earlier in sections 1.2 and 1.3 of Chapter 1. One of the processes mentioned, was run-off generation.

Therefore, the aim of studying the run-off was answering the question of how the different soil types and infiltration rates could influence run-off. This chapter gives an overview of run-off characteristics in the Goedertrou catchment. The methodology used, was discussed in detail earlier in section 1.3 of Chapter 1, and will not be repeated here. Figures 3.1 and 3.2 shows the simulation setting and Table 3.1 a summary of the simulation results obtained.

Figure 3.1 Indicates simulation setting avoiding wind interference.

Figure 3.2 Indicates simulation ring over stubble land

Table 3.1 Indicating simulation summary.

Soil map symbol and grid number	Gradient of simulation area (%)	Time to run-off (min)	Simulation period (min)	Run-off (mm/h)
Ss1 (1) #	12.8	74	141 VLG	15.9 L
Sw3 (2) #	9.4	27	87 LG	41.4 M
Gs1 (3) #	11.2	28	88 LG	45.7 H
Ms1 (4) #	11	43	109 VLG	6.80 L
Gs 1 (5) #	18.5	12	72 MT	34.3 M
We1 (6) #	11.5	25	85 LG	19.7 L
Km1 (21) #	14.5	8	68 MT	55.5 H
Sw1 (28) $	17.8	48	108 VL	21.2 L
Cf1 (40) $	17.6	7	67 MT	49.8 H
Gs2 (42) $	9.1	81	141 VL	22.7 L
Sw2 (45) $	8.0	66	126 VL	38.7 M
Ka1 (53) $	13.7	9	69 MT	53.0 H
Sw4 (55)$	19.1	113	173 VL	3.6 L
Ag1 (59)$	10.5	20	80 LG	47.6 H

= North-facing simulation area (slope), $ = South-facing simulation area.

H (high run-off) = >45 mm/h

M (Moderate run-off) = 22 to 44 mm/h

L (Low run-off) = <22 mm/h

VL: Very Long simulation period (>100 min)

LG: Long simulation period (≥80 min)

MT: Medium simulation period (<80 min)

Considering the run-off data of the above table, one could divide it into three categories: the high run-off category (H), moderate run-off category (M) and the low run-off category.

The high run-off category included five simulations: simulation 21 (Km1), 53 (Ka1) and 3 (Gs1), which were done on moderate north-facing slopes (10–15%): simulation 40

(Cf1) done on a steeper south-facing slope (>15%), and simulation 59 (Ag1) done on a moderate south-facing simulation area The moderate run-off category conversely consisted of the following four simulations: simulation 2 (Sw3) that was done on a low-gradient (<10%), north-facing simulation area with vegetation; simulation 45 (Sw2) that was done on a low south-facing simulation area; simulation 5 (Gs1), which was completed on a steep north-facing simulation area with vegetation; and simulation 42 (Gs2), which was done on a low south-facing simulation area with vegetation, cracks and animal-related openings.

The low run-off category comprised five simulations: simulation 28 (Sw1) that was done on a steep, south-facing simulation area where vegetation was noticed and cracks were present; simulation 6 (We1), which was done on a moderate north-facing simulation area with the presence of vegetation; simulation 1 (Ss1), which was done on a moderate north-facing simulation area with vegetation; simulation 4 (Ms1), which was completed on a moderate north-facing simulation area with vegetation; and simulation 55 (Sw4), which was done on a steep south-facing simulation area with presence of cracks and animal openings.

It is clear that simulations 55 (Sw4), 28 (Sw1), 5 (Gs1) and 40 (Cf1) had been expected to have high run-off because of their relatively steep gradients >15%. However, only simulation 40 (Cf1) had the expected high run-off. Simulations 28 (Sw1) and 55 (Sw4) had the lowest run-off, although they had been expected to have high run-off, because of their higher gradients. Similarly, simulations 2 (Sw3), 45 (Sw2) and simulation 42 (Gs2) had moderate run-off, although they had been expected to have low run-off, because of their low gradients.

A number of factors could be expected to play a major role in influencing the run-off. Soil type is one of these and this aspect was very important in this study, because it gave the structural pattern where the cracks that play a major role, develop. The soil type with or without a clay content influences the vegetation growth and the development of the

root system, and the vegetation roots conversely influence infiltration and, therefore, also run-off.

The other factor is the micro topography, which influences run-off in the way that water collects in depressions created by the microtopography over a period until it overcomes the height of the micro topography and eventually starts the motion of run-off.

3.2 Discussion

In general, simulations lasted longer or shorter in time and, therefore, resulted in higher or lower run-off, because of the observed factors mentioned before: vegetation root systems in the vadose zone, animal (worms) and termite channels, soil cracks of different dimensions and geometry, micro topography or surface roughness, which influence the initial losses and probably the soil moisture deficit (Gregory and Walling, 1973).
Simulation (55) Sw4 had the smallest run-off of all simulations evaluated at 0.46 mm/h and it lasted longer (173 min) than the other simulations.

The first run-off only happened in the 113th min, which was the longest period before run-off took place for all of the simulations. However, these variations could be related to factors that have been observed and that were specific to this simulation. For simulation (55) Sw4, the observed factors were: the micro topography, the developed root system and the animal channel of 60 mm diameter in the soil profile. Therefore, more water was infiltrating through these different channel systems, resulting in less run-off.

The other simulation that had a low run-off quantity was 42 (Gs2). The simulation process took 141 min and the first run-off happened in the 81st min. The reason for the low run-off similar to that of simulation 55 (Sw4) might be linked to the fact that the soil cracks of different orientations allowed water to seep downward in the soil and the developed dry root system in the soil profile facilitated infiltration of the water. However, the same factors also affected simulations 28 (Sw1) 6 (We1) 4 (Ms1) and 1 (Ss1), which had the additional factor of termite channels.

In other cases, the degree of run-off might have been influenced simply by aspect, making certain areas facing the sun harder, and in that way facilitating run-off formation.
Conversely, simulations 21 (Km1) 3 (Gs1) and 59 (Ag1) had relatively high run-off of greater than 40 mm/h, but their simulation time varied between 60 and 90 min.
The reason for this could be linked to the local soil properties, such as soil hydraulic conductivity and soil moisture content, as suggested by Gaillard *et al.* (1995), Taha *et al.* (1997) and Latron and Gallart (2006).

The north-facing simulations (seven simulations in total) all lasted longer than 1 h. One simulation, Ss1 (1), lasted for 2 h 20 min. The slope gradient in most cases varied between 10 and 15%. Only two cases showed a gradient of less than 10%.

Unlike the north-facing simulations, three out of seven simulations on the south-facing slopes had durations exceeding 2 h, with one simulation lasting for almost 3 h. Only one simulation lasted for approximately 1 h 40 min. Three simulations lasted for a time varying between 1 and 1.5 h. The gradient of three simulation areas varied between 17 and 19%. Two simulation areas had gradients varying between 10 and 14% and the two remaining ones had a gradient of less than 10%. This implies that gradient did not influence the generation of run-off largely, but that there were openings in the soil profile, allowing water to infiltrate and, therefore, taking more time for run-off generation.

3.3 Conclusions

Gradient did not influence the generation of run-off significantly, because of openings in the soil profile, which allowed water to infiltrate and, therefore, to take longer for run-off production.

The reason for high run-off production could be linked to the local soil properties, such as soil clay content, which influenced soil cracks and soil moisture content. In this study, the factors that influenced run-off were found to be micro topography, soil moisture, root systems, animal activity in the soil profile, soil crack dimensions and hydraulic conductivity.

Chapter 4

Evaluation of sediment mobilisation

4.1 Introduction

Particles smaller than 65 μm in size are subject to mobilisation, if storm rainfall occurs (Poesen, 1981). Fine particles, when washed away as a result of a rainfall event, can pollute a river, especially one in a Mediterranean-type environment, such as the Berg River.

Land degradation is one of the major environmental concerns in the Mediterranean-type regions of the world (Imeson, 1993; Oldeman and van Lyden, 1998; Ruysschaert *et al.*, 2004). According to Govers *et al.* (1990), concentrated flow erosion is defined as the detachment and displacement of soil particles by concentrated water flow, resulting in the development of rills and gullies. Studies done in the past indicate that gully erosion represents an important sediment source in many environments (Poesen *et al.,* 2003). This causes serious problems for large areas, such as Europe, particularly the hilly regions of Belgium (Gyssels and Poesen, 2003).

Prosser *et al.* (1995) showed that the critical-flow shear stress decreased by clipping off the above ground vegetation. In their study, the dense root network prevented the surface from significant smoothness and sediment transport.

Although they did not measure the effect, their observations indicate the importance of roots in protecting soil against erosion. Plant roots have a mechanical effect on soil strength. By penetrating the soil mass, roots reinforce the soil and increase the soil shear strength (Styczen and Morgan, 1995).

Given that roots bind soil particles at the soil surface and increase surface roughness, they decrease the susceptibility of the soil to rill and gully erosion. Roots also have hydrological effects. By increasing surface roughness and soil permeability, roots enhance soil infiltration capacity. Dealing with sediment mobilisation is to deal indirectly with sediment detachability. Erodibility as an erosion factor, is usually considered as static and rather used as an erodibility index by Bryan (1968), Yamamoto and Anderson (1973), Erodibility was used as a constant value in erosion models by Meyer and Wischmeier (1969), David and Beer (1975), Foster and Meyer (1975) and Moeyersons and De Ploey (1976).

Although not much information is available on the dynamic properties of the sediments used in erosion processes, Poesen (1981) concluded that particle detachability is linked to grain size and could be less with finer particles.

To answer research question 3 mentioned in Chapter 1, this study looked at the grain size of the particles that are vulnerable to mobilisation during intense rainfall events.

Particle-size classification is important for the investigation of depositional environments. The transport of sediment by overland flow involves two steps: the first is erosion and entrainment of sediment from the bed and the second is subsequent, sustained down current movement of sediment along the bed (Boggs, 1995). However, more energy is usually required to initiate particle movement than to keep particles in motion after entrainment (Boggs, 1995). As the velocity and shear stress of a fluid moving over a sediment bed increase, a critical point is reached, where grains begin to move downward. Usually, the smallest move first. As shear stress increases, larger particles are dragged into motion and grain motion is common everywhere on the bed (Boggs, 1995; McLaren, 1981). This critical threshold, however, for grain movement is a direct function of multiple variables, including the boundary shear stress and fluid viscosity (Boggs, 1995).

The fine and clay-sized particles resist movement, because of cohesiveness that arises from electrochemical bonds between these small grains (Boggs, 1995; Curtis, 1977; Gieskes, 2007).

The motive forces that fluid flow must generate to overcome the resistance to movement imposed by these retarding factors include a "drag force" that acts parallel with the bed. That force is related to the boundary shear stress, and a "lift force" because of the Bernoulli effect of fluid flow over projecting grains (Boggs, 1995). This is why the influence of slope is recognised in this study. Generally, particle size and quantity is positively correlated with slope.

According to the Encyclopaedia Britannica (2007), grain-size scale is a division of a continuous range of particle sizes into a series of discrete groups. However, several scales have been devised for standardizing terms and providing a basis for statistical analysis. On most scales, therefore, the finest particles are designated clay and silt, whereas sand, granules, gravel, pebbles and boulders constitute the coarser fraction.

The scale was devised by the American sedimentary petrologist Udden (1898) and was adapted by Wentworth (1922), who expanded the definitions of various grades to conform to actual usage by researchers. Consequently, most scientists have adopted the Udden scale with Wentworth's modifications (Boggs, 1995).

The φ scale, which is used by sedimentologists, is often meaningless to engineers and biologists that report grain size as measured in metric units (Pierce and Graus, 1981). However, the Udden–Wentworth scale easily adapts to the phi-logarithmic transformation (Leeder, 1982).

In the process of particle-size analysis of this study, the Udden–Wentworth scale provided sieve ranges that varied from the lowest to the highest aperture of 3.9, 31, 63, 125, 250 and 500 μm.

4.2 Material and methods

Material and methods used for the simulation process that produced the results reported in the results section, as well as the figures, were discussed in Chapter 1.

Sediment mobilisation produced during rainfall simulations over wheat stubble lands was done in a small-scale catchment at Goedertrou Farm in the Riebeek-Wes District. During the study, attention was given specifically to sediment yield brought by overland flow. A site description was given earlier in section 1.5 of Chapter 1. Ten soil samples were collected from each simulation of the A-horizon. The depths where these samples were collected from were referred to in section 1.3 of Chapter 1. Samples were always collected from wheat rows and from between the wheat rows, so that the influence of the root system could be evaluated.

The simulation site gradient was measured to evaluate its influence in sediment movement during rainfall simulation. The rainfall simulator that was used to generate artificial rainfall was discussed in section 1.3 of Chapter 1. Each simulation was done on a different soil type to evaluate the wetting front after rainfall simulation.

Run-off, time to run-off, soil type, gradient, depth of wetting, rate of infiltration and sediment yield were the variables used for this study. Analyses of the particle size were somewhat problematic initially, because the mobilised particles mostly came from the fine fraction (smaller than 65 μm).

In the process of analysing the size of the yielded sediments, the samples were mixed with separation fluid to de-agglomerate the particles. A low-power stereomicroscope was used as an aid in sample preparation.

After the microscopic process, and photographing the particles, “Image J” software processing was used to analyse particles using options such as Image-Adjust-Contrast-Apply, Process-Binary-Threshold (specifying the direction, such as Northing) and Process-Analyse-Particles.

Rhodes (1998) found that no single physical dimension sufficiently described the size of irregularly shaped particles, just as a single dimension cannot portray the shape of a cylinder.

Figure 4.1 provides an example of the sediment distribution within a sediment sample. This method had the capacity to indicate agglomeration of particles and from this picture, it is clear that agglomeration occurred mainly with smaller particles. This result had enormous bearing on the specific particle-size analytical method used and the sample preparation methods used. Methods that cause a dispersion of the particles would show a wrong particle-size distribution if one has to analyse the suspension load. For this reason, the decision was made to analyse the suspension load without adding a spreading agent. Figure 4.1 and Figure 4.2 show a typical suspension load distribution.

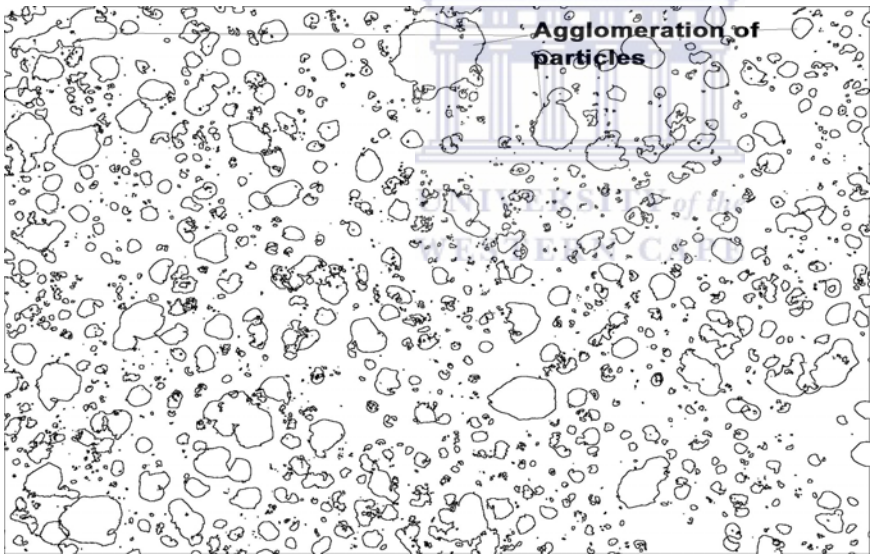

Figure 4.1 Indicates the agglomeration of smaller particles from simulation Ag1 (59) using the microscopic photograph (× 50 magnification)

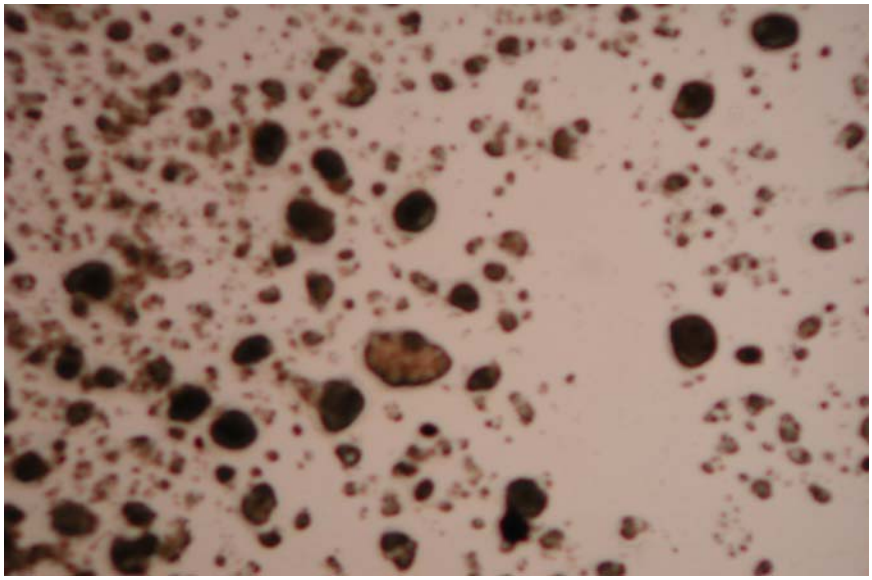

Figure 4.2 Indicates sediment properties of simulation Gs1 (5) after microscopic photography with × 50 magnification using "Image J" software processing.

Because of the high clustering level of the particles and not being able to assess the classes and other properties of the grains in a proper way, it was decided to focus on another method of particle-size analysis, namely the use of the Laser method for sediment analysis. Here a Micromeritics instrument was used in a specialised laboratory and with DemoDigisizer software to convert the measured distribution into more practical classes (Rhodes, 1998).

However, a population of particles described by a particle-size distribution could also be expressed as frequency-distribution curves or as cumulative curves. Conversely, the two curves are mathematically related such that the cumulative distribution is the integral of the frequency distribution (Rhodes, 1998).

The Oxford English Dictionary (2007) defines cumulative as designating a probability distribution that is the integral up to a particular value of a probability density function, and therefore represents the probability that this value is not exceeded by a random variable with this distribution. For this reason, frequency-distribution curves and cumulative curves were used.

In the following comparison between A-horizon samples and the rainfall-simulation overland-flow samples, it is important to note that the rainfall simulation was done on a 1 m^2 soil surface and the volume of the A-horizon material was 0.2 m^3. The soil sample from this area had a volume of 1 l and the sediment sample taken from this was 50 g. The overland-flow sample had a sediment load of approximately 15 g. This 15 g has to be compared with the reserve of 0.2 m^3 in the field.

4.3 Results and Discussion

4.3.1 Mobilised Sediments

Run-off generated by the simulator described in Chapter 1 was sampled on a 5-min interval for the analysis of its suspended load. Throughout the experiments, mobilised sediments were greater in the first sample than in the last sample. For example, simulation 1 (Ss1) exhibited initially high sediment yield, and decreasing for the last sample. Table 4.1 lists the different parameters that played major roles in the mobilisation of sediments.

Table 4.1 Indicates sediments mobilisation parameters.

Simulations	Ss1 (1)	Gs2 (42)	Sw4 (55)	Ms1 (4)	Gs1 (5)	Sw1 (28)	Cf1 (40)	Km1 (21)	Ka1 (53)	We1 (6)	Gs1 (3)	Ag1 (59)	Sw2 (45)	Sw3 (2)
Gradient %	12.8	9.1	19.1	11	18.5	17.8	17.6	14.5	13.7	11.5	11.2	10.5	8	9.4
Slope facing	N	S	S	N	N	S	S	N	S	N	N	S	S	N
Vegetation Cover (%)	25	55	45	35	5	70	55	55	60	45	70	30	15	60
Clay Content (%)	10	15	15	12.5	15	25	12.5	15	13.7	10	15	10	17.5	13.5
Infiltration Start (mm/h)	60	62	51	60	58	60	53	50	50	56	46	50	51	55
End (mm/h)	48	41	25	48	30	42	14	8	11	44	18	15	25	22
Total runoff (L)	12.9	12.4	12	11.7	18.3	13.4	24.5	42.4	18.3	10.1	48.4	38.3	30.6	38.9
Mobilized sediments (g/L)	9.06	4.24	3.39	2.22	1.52	1.25	1.01	0.84	0.81	0.61	0.51	0.44	0.32	0.32
Time to firstrunoff (min.)	74	81	113	43	12	48	7	8	9	25	28	20	66	27
Simulation length (min.)	141	141	173	109	72	108	67	68	69	85	88	80	126	87

N = North

S = South

Comparing the values of mobilised sediments for all simulations, one might suggest that in many of the simulations the sediment yield might have been influenced by soil type (soil chemistry, soil structure).

Table 4.1 shows that the mobilised sediments generally decreased from the first to the last sample in each simulation, whereas vegetation cover fluctuated. Total run-off varied between 10.1 l and 48.4 l, but did not seem to correlate with the total time of the simulations. Although not very prominent, it seems that in general a higher amount of sediment had been generated on the steeper slopes and lower amounts on the flatter ones.

The above observation of higher amounts of mobilised sediments at the beginning of a rainfall event seems to +correlate with the seasonal pattern of sediment transport from a river catchment. As soon as the rain starts, the river turns muddy because of sediment load, and when rain continues over time, the river becomes clearer again. These results agree with those of Steegen, *et al.* (2001), who investigated sediment transport by water from an agricultural catchment in the Loam Belt of Central Belgium.

4.3.2 Particle-size analysis

The methodology for analysing the particle-size distribution was outlined in the previous paragraph. This section deals mainly with the obtained results for simulations on the various soil types.

Sediment particles in the A-horizon ranged in size from clay particles to large boulders, as had been indicated earlier. One should also note that grain size is usually expressed as a linear dimension (Leeder, 1982). The grain size of clastic sediment is a measure of the energy of the depositing medium and the energy of the basin of deposition (Reineck and Singh, 1980.)

4.4 Rainfall simulation Sw4 (55)

The Swartland soil form (Sw) was described and discussed in Chapter 1, in the description of the study area .

4.4.1 Frequency distribution

The method of frequency distribution entails plotting the particle volume frequency on the *y*-axis against the particle size on the *x*-axis. Figure 4.3 presents a sediment analysis of the A-horizon of the soil where the rainfall simulation was run. It also presents the analysis of the sediments mobilised during the rainfall simulation. It is important to note that both are expressed in terms of a volume frequency percentage and that the total area below each line should be the same.

The A-horizon result depicts the distribution of the available sediment. It is therefore clear from the similar shapes of the two curves that sediment sizes <20 µm can in total be mobilised and that sediment fractions coarser than 20 µm are more resistant to mobilisation. Hence, this result shows the specific sediment size that is prone to mobilisation during a rainfall event with similar impact to that of the rainfall simulator.

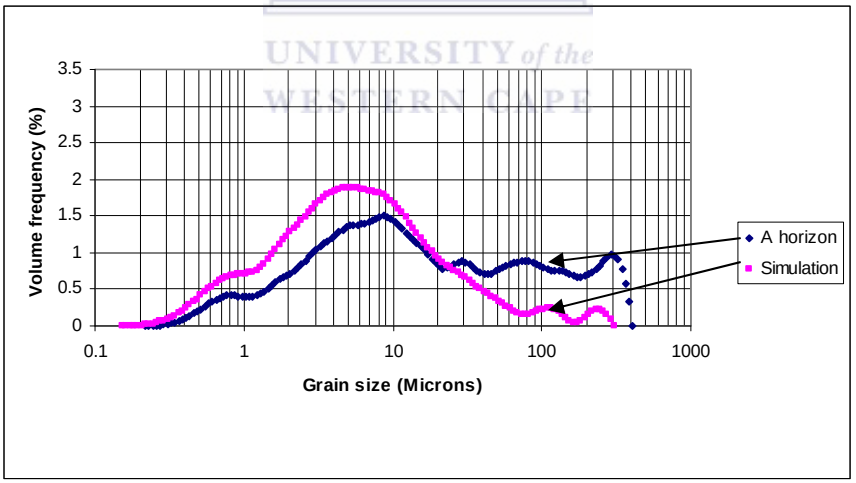

Figure 4.3 Indicates frequency distribution of particles of the A-horizon (pit 55) and sediment mobilised by the simulation at site 55 (Sw4).

A visual examination of the grain size distribution of the mobilised sediments revealed important variations within one single rainfall event. Figure 4.3 depicts the results of small particles ranging from 0.16 to 60 µm. Particles bigger than 100 µm could have been the aggregated particles. The grain-size class ranging from 0.4 to 0.7 µm had almost equal values, where A-horizon results represent 9.09% and simulation 9.02%. The other

class ranged from 0.8 to 1.5 µm where the A-horizon is represented the same way as the previous range of 9.09%, whereas simulation event has mobilized 9.02%. For the class ranging from 1.6 to 10 µm for this particular comparison, the results were almost equal, because the A-horizon had 25.76%, whereas simulation represented approximately 25.56%. However, the figure 4.3 above indicates that sediments smaller than 20.1 µm had been washed away by the rainfall-simulation event.

In Figure 4.4, the particle distribution for both the A-horizon sample and the overland-flow sample is illustrated in terms of the Wentworth sieve classes. This presentation indicates in a better way the total amount of sediment available in each class than the amount mobilised in each class.

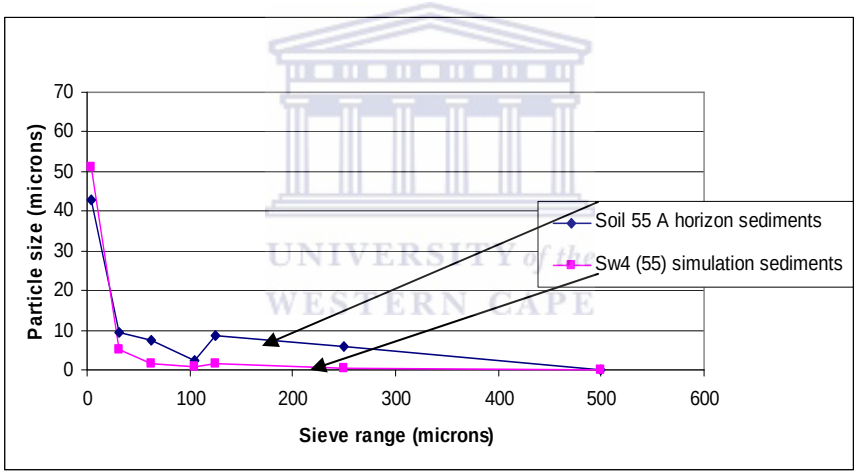

Figure 4.4 Indicates particle-size distribution of the A-horizon sediment and the particles mobilised by rainfall-simulation at site 55 (Sw4).

The graph (Figure 4.4) demonstrates clearly that the sediments available in the A-horizon, were large in diameter, up to 43 µm. The rainfall-simulation event washed away all particles smaller than or equal to 51 µm. This means that the particles ranged from clay particles to coarse silt (Allaby, 1999). However, the reason why even the large particles were mobilised is that factors such as the rainfall-simulation intensities and the slope gradient played a major role.

4.4.2 Cumulative particle size

Figure 63 shows that 10% of the particles were approximately 0.82 µm in size, and the A-horizon had a grain size of approximately 1.60 µm. Approximately 50% of the simulation particles had a size of 5.6 µm, whereas the A-horizon sediments were approximately 12.96 µm. Almost 100% of the simulation particles were up to 300 µm, whereas the A-horizon particles ranged up to 400 µm.

Figure 4.5 also shows the available sediment of the A-horizon in this soil, as well as the mobilised fraction of the rainfall-simulated material. What is of interest here is the nick point in Figure 4.6 in the A-horizon sample at approximately 20 µm. This nick point is an indication of the weathering process and indicates a larger amount of coarser particles present above this point. Particles above this point showed resistance to movement and this was possibly related to the slope gradient and natural rainfall impact on this site.

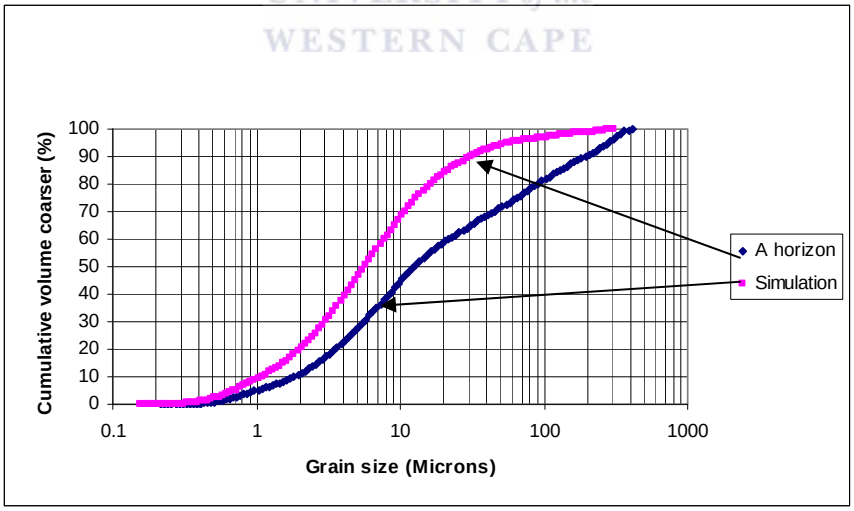

Figure 4.5 Indicates particle-size cumulative frequency distribution of A-horizon sediment (pit 55) and sediment mobilized by simulation at site 55 (Sw4).

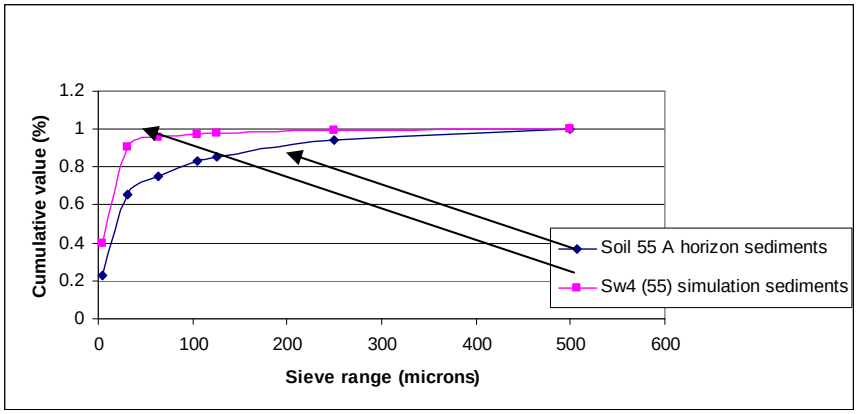

Figure 4.6 Indicates particle-size cumulative frequency distribution of A-horizon sediment and particles mobilised by rainfall-simulation at site 55 (Sw4).

The graph (Figure 4.6) shows that mobilised sediment in the A-horizon had particles less than 35 µm in size, because of decreased run-off and only particles of that range were vulnerable to be washed away.

4.5 Rainfall simulation Gs2 (42)

Soil form Gs2 was described and discussed in Chapter 1, in the description of the study area .

4.5.1 Frequency distribution

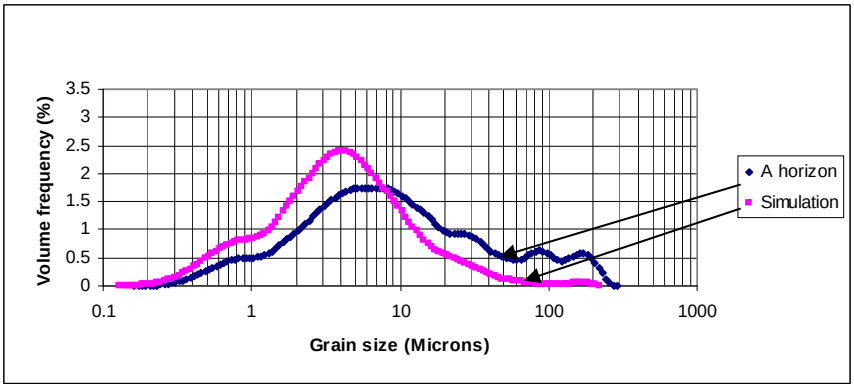

Figure 4.7 Indicates frequency distribution of particles of the A-horizon (pit 42) and sediment mobilised by rainfall-simulation at site 42 (Gs2).

In this single rainfall-simulation event, there were variations in sediment supply where four classes could be identified. The first class ranged between 0.1 and 0.3 µm, where the A-horizon represented 12.21% and the material generated by the simulation, 15.38%. The

second size class ranged from 0.4 to 0.7 µm, with the A-horizon having 9.16% and the material from the simulation, 9.23%. The third class ranged from 0.8 to 1.5 µm, where the A-horizon had 9.16% and the simulation had 9.23%. The fourth class ranged from 1.6 to 10 µm, available sediments in the A-horizon formed 25.95% and those from the simulation, 26.15%. Although a wide range of grain sizes was transported, the predominant finer material <7.5 µm were mobilised. Nevertheless, Figure 4.7 shows the prevailing sizes that ranged from 0 to 70 µm. Grains larger than this could have been mobilised because of the clustering of particles.

To compare the grain size of particles mobilised by the rainfall simulation with the grain sizes available in the A-horizon, one can plot the particle size on the *y*-axis and the sieve range on the *x*-axis. This is illustrated in Figure 4.8.

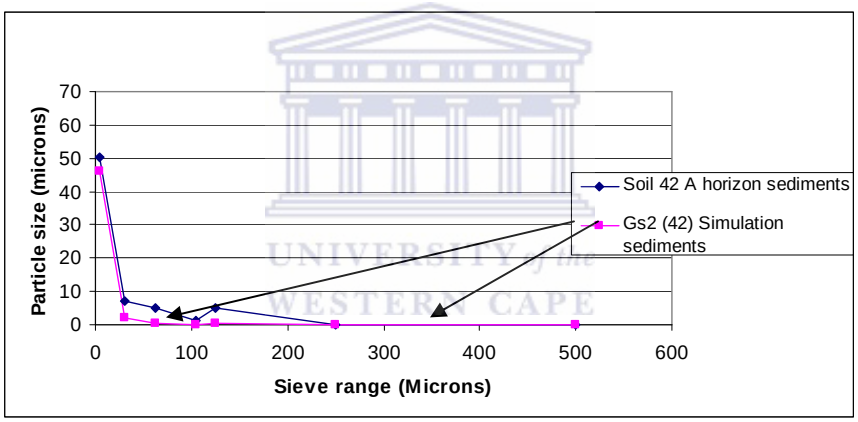

Figure 4.8 Indicates particle-size distribution of the A-horizon sediment and the particles mobilised by rainfall-simulation at site 42 (Gs2) (42).

This graph (Figure 4.8) shows that in the A-horizon the available particles ranged from very fine clay particles to coarse silt of 51 µm. The mobilised sediments were more or less of the same size, ranging from fine clay to coarse silt of 46 µm size (Wentworth, 1922).

4.5.2 Cumulative grain size

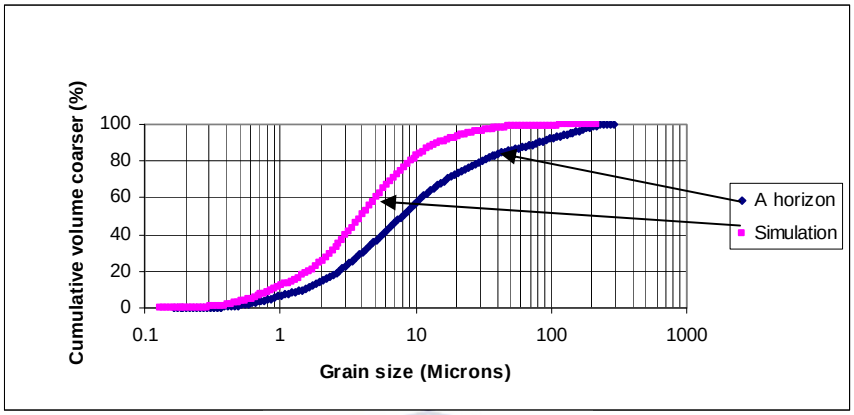

Figure 4.9 Indicates grain size cumulative distribution of the A-horizon sediment (pit 42) and sediment mobilised by rainfall-simulation at site 42 (Gs2).

Figure 4.9 demonstrates that at 10%, the simulation had mobilised sediments of 1.50 µm in size, and the A-horizon had particles of 1.50 µm available. At 20%, the simulation mobilised particles of 1.6 µm, whereas the A-horizon had particles of up to 2.7 µm available. At 50%, the A-horizon had sediments of 7.71 µm in size available, whereas the simulation mobilised 4.09 µm size material. At 100%, both the A-horizon and the material mobilised by the simulation showed coarse sediments of a similar size of approximately 193.86 µm.

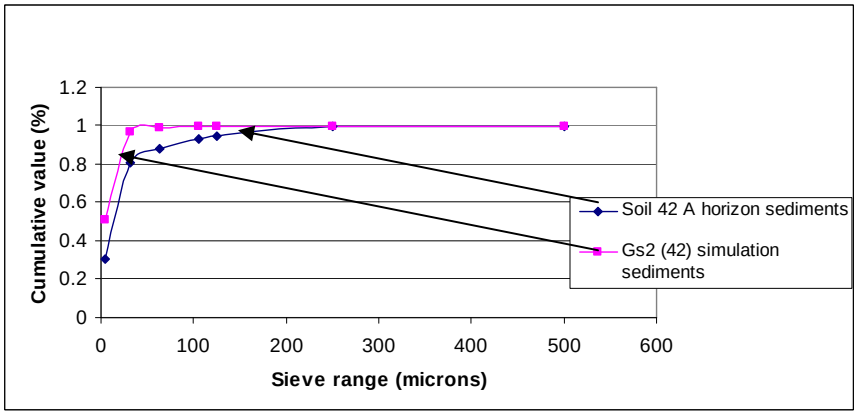

Figure 4.10 Indicates particle-size cumulative frequency distribution of A-horizon sediment and particles mobilised by rainfall- simulation at site 42 (Gs2).

This graph in Figure 4.10 shows a pattern of similarity of the A-horizon particles and the sediments washed away by the rainfall-simulation event.

4.6 Rainfall simulation Ms1 (4)

The Ms1 soil form was discussed in the first chapter, in the description of the study area.

4.6.1 Frequency distribution

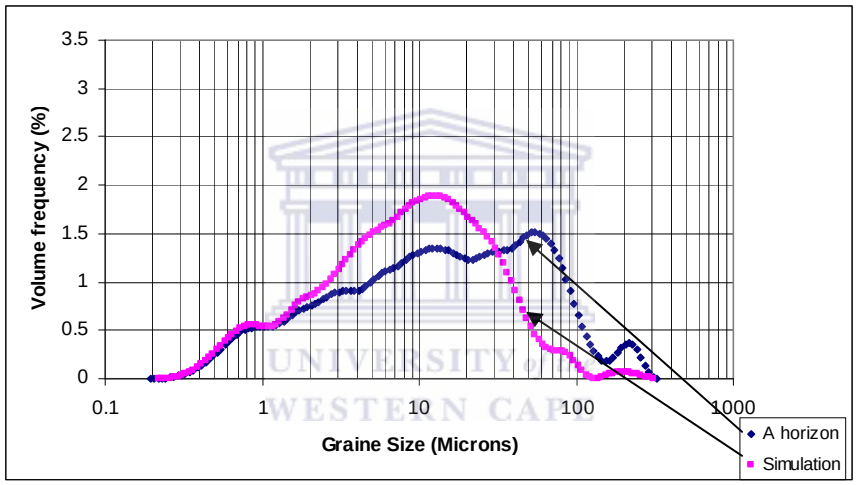

Figure 4.11 Indicates frequency distribution of particles of the A-horizon sediment (pit 4) and sediment mobilised by rainfall- simulation at site 4 (Ms1).

Four classes were recognised for this distribution frequency (Figure 4.11), where the first one ranged from particles with size of 0.1 to 0.3 µm. The simulation mobilised 8% of the material range. The second class encompassed sizes varying from 0.4 to 0.7 µm, where the A-horizon ha 9.23% and simulation mobilised only 9.45% of that range. The third class ranged from 0.8 to 1.5 µm. The A-horizon had 9.23% of that material and the simulation mobilised 9.45% of that same size. The fourth class ranged in size from 1.6 to 10 µm, where the A-horizon had 26.15% and simulation mobilised 26.77%.

It is obvious that in all classes both A-horizon material and simulation sediments had very similar values. However, the finer material smaller than 30 µm in size had been

predominantly washed away. Figure 4.11 shows that the bigger sizes mobilised by rainfall simulation were ≤ 70 µm.

As before, one can also represent the particle distribution graphically, by plotting the particle size on the *y*-axis and the sieve range on the *x*-axis (Figure 4.12). This shows in a better way the total amount of sediment available in each class than the amount mobilised in each class.

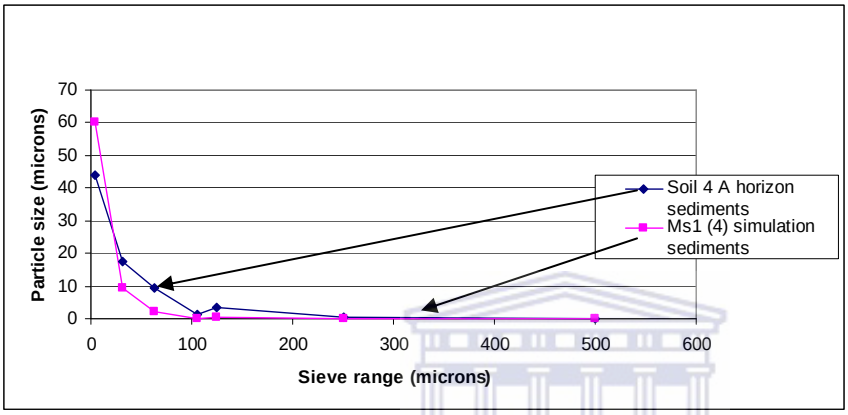

Figure 4.12 Indicates particle-size distribution of the A-horizon sediment (pit 4) and the particles mobilised by rainfall-simulation at site 4 (Ms1).

The particles available in the A-horizon varied in size from clay to coarse silt up to 44 µm. The rainfall event washed away all particles ≤61 µm. The reason for this was probably high run-off, as demonstrated earlier in the chapter dealing with run-off.

4.6.2 Cumulative grain size

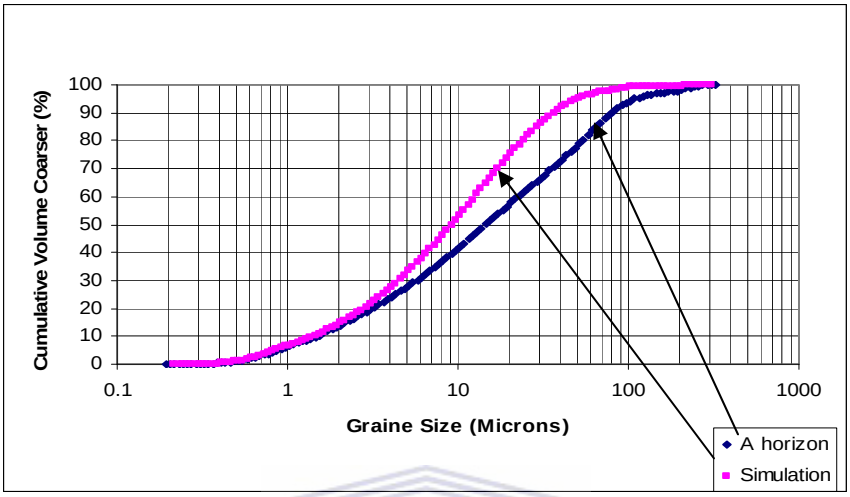

Figure 4.13 Indicates particle-size cumulative frequency distribution of the A-horizon sediment (pit 4) and sediment mobilised by rainfall-simulation at site 4 (Ms1).

Figure 4.13 illustrates that at a cumulative value of 10%, both the A-horizon and the material mobilised by the simulation had the same particle size of 1.45 µm. The same applied at 20%, where both the A-horizon and sediment mobilised by simulation had sizes of 2.90 µm. It also applied at 100%, where both had particles of 307.26 µm in size.

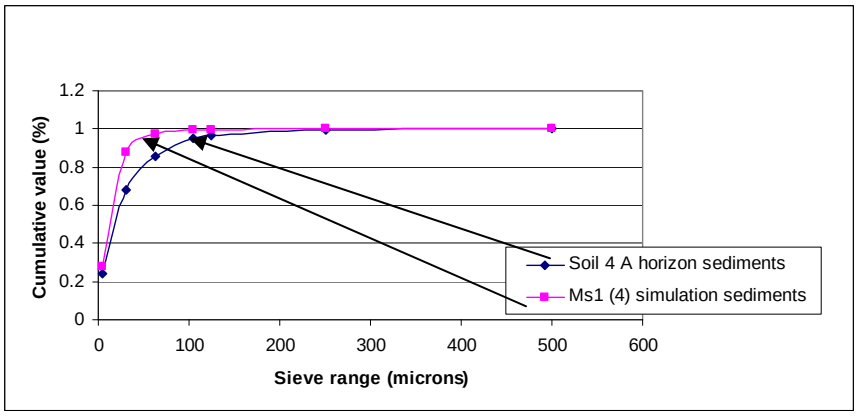

Figure 4.14 Indicates particle-size cumulative frequency distribution of the A-horizon sediment and particles mobilised by rainfall- simulation at site 4 (Ms1)

4.7 Conclusions

Sediment mobilisation using rainfall simulation on a stubble land was evaluated on a small-scale catchment in the Riebeek-Kasteel district. Factors that played a major role in influencing sediment mobilisation within the rain-simulated area appeared to be the micro topography within the ring, the slope gradient and length, the vegetation cover and the simulated rainfall intensity.

From the above analyses, it seems that with storm rainfall, particles up to 65 μm are subject to mobilisation. These are fine particles, and when mobilised, can pollute the surface water. Therefore, adequate methods and practices for tillage as mitigation measures should be applied, such as planting mixed-crops, strip-cropping and maintaining the existing contours for trapping the sediments that are being washed away. Care must be taken to maintain a vegetation cover, and not to expose the land surface in bare form for too long. To attain the latter, farmers must leave a crop residue cover behind after the annual harvest.

Chapter 5

Summary, conclusions and recommendations

The study was conducted on the Goedertrou Farm in the Riebeek-Kasteel district. The area drains towards the Berg River, which is situated in a Mediterranean-type climatic environment of the Western Cape.

The focus of this study was to address some of the hydrological processes active in the research catchment, namely infiltration, run-off and sediment mobilisation on different soil types. It was done as part of a bigger investigation on the origin of Berg River pollutants.

The study reports the results of a field evaluation of infiltration, run-off and sediment mobilisation from different soil forms and families from field experiments and laboratory measurements. An evaluation of infiltration using rainfall simulations was done in conjunction with an evaluation of run-off and sediment mobilisation.

The first research objective was to evaluate the vertical and horizontal distribution of moisture in the A-horizon by analysing the infiltration and run-off characteristics of different soils in the research catchment and to determine the factors that played a major role in this. This was described in Chapters 2 and 3 dealing with infiltration and run-off.

The discussion in Chapter 2 demonstrated that infiltration in the study area was dominated by a number of factors. Among these, soil structure, accompanied by secondarily created small-scale tunnelling (mainly by termites, but also by larger animals, such as rodents), as well as openings created by decaying root systems, contributed to increase the infiltration rates. Another notable factor was the micro topography, where the water was concentrated in the small depressions, then channelled downward by the different factors referred to above. Considering the results, one could conclude that

decayed root systems from the rows of plants, soil cracks, small channels and openings created by small animals, as well as slope orientation and, therefore soil, composition, all played a major role in influencing the ability of the soil to absorb the simulated rainfall. A study to gather information that is more detailed on the hydrological influence of soil cracks of different dimensions on the various soils in the study area at the beginning of winter, before surface sealing happens, could be a future avenue for research.

Run-off was discussed in detail in Chapter 3. It was demonstrated that high run-off production was linked to the local soil properties, such as soil hydraulic conductivity and soil moisture content. The same factors that influenced infiltration also played a major role in determining run-off, namely micro topography, root systems, animal activities in the soil profile, soil crack dimensions and hydraulic conductivity.

The second research question referred to in Chapter 1 dealt with the material most vulnerable to mobilisation during rainfall events. This aspect was addressed in Chapter 4, where a detailed analysis was done of the particle size of solids present in run-off water generated by the various simulations.

The major factors that influenced sediment mobilisation are firmly believed to be the micro topography within the ring area of the simulation, slope gradient and length, vegetation cover and rainfall-simulation intensity.

Particle-size analyses were done using the Laser method for sediment analysis. A Micromeritics instrument was used in a specialised laboratory at the Engineering Faculty of the University of Stellenbosch. DemoDigisizer 5200 V1.09 software was used to convert the measured distribution into more practical distributions. In this process, the Udden–Wentworth scale provided sieve ranges.

The study revealed that fine particles, ranging from clay to coarse silt, are subject to mobilisation by storm rainfall. The Goedertrou small catchment therefore contributes to sedimentation of fine particles in the Berg River. This is probably true for most of the

small catchments in the Berg River drainage area. Farmers in this area should therefore be aware that with storm rainfall, fine particles <65 µm are subject to mobilisation. Well-planned and appropriate land-use types are therefore crucial, for the contribution of solids to the Berg River catchment to be controlled effectively in future.

References

Allaby, A. & Allaby, M., 1999. Udden-Wentworth Scale: a dictionary of Earth Sciences. Encyclopedia. [on line] available at http://www.encyclopedia.com.

Belsky, A. J., Mwonga, S. M., Amondson, R. G., Duxbury, J. M., and Ali, A. R. 1993. Comparative effects of isolated trees on their under canopy environments in high and low rainfall savannas. Journal of Applied Ecology, 30: 143–155.

Bergkamp, G., Cammerat, L. H., and Martinez-Fernandez, J. 1996. Water movement and vegetation patterns on scrublands and an abandoned field in two desertification threatened areas in Spain. Earth Surface Process and Landforms, 21: 1073–1090.

Bergkamp, G., 1998. A hierarchical view of the interactions of runoff and infiltration with vegetation and microtopography in semi arid shrublands. Catena 33201-220.

Blackburn, W. H. 1975. Factors influencing infiltration and sediment production of semiarid rangelands in Nevada. Water Resource, 11 (6): 929–937.

Boggs, S. 1995. Principles of Sedimentology and Stratigraphy. Prentice-Hall, Inc. 2nd edn.: 79–107.

Bridgwater, J. 1994. Mixing and segregation mechanisms in particle flow. *In* Mehta, A., Granular Matter: An Interdisciplinary Approach. , Springer: 161–193.

Bryan, R. B. 1968. The development, use and efficiency of indices of soil erodibility. Geoderma 2: 5–26. *In* Poesen, J., 1981. Rain-wash experiments on the erodibility of loose sediments. Earth surface processes and landforms 6: 285–307.

Climate [On line] available at http://www.Capewestcoast.org/RegionalInfo/RegionalInfoIndex.htm

Crosby, C. T., McPhee, P. J., and Smithen, A. A. 1983. Introduction of the Universal Soil Loss Equation in the Republic of South Africa. Unpublished paper No. 83–2072, presented at the 1983 summer meeting of ASAE, Bozeman, Montana, June.

CSIR. 2005. Geohydrology and meteorology. *In* Water Research Commission Project No. K5/1503. Land use impacts on salinity in Western Cape Waters Progress Report, November 2005.

Curtis, C. D. 1977. Sedimentary geochemistry: environments and processes dominated by involvement of an aqueous phase. Journal of Mathematics and Physical Sciences, 286: 353–372. *In* Poizot, E., Mear, Y., Biscara, L., 2007. Sediment trend analysis through the variation of granulometric parameters: A review of theories and applications. Earth-Science Review.

David, W. P., and Beer, C. E. 1975. Simulation of soil erosion. I. Development of a mathematical erosion model. Transactions of the ASAE, 18, 126–129, 133. *In*
Morgan, R. M., and Bull, P. A., 2007. The use of grain size distribution analysis of sediments and soils in forensic enquiry. Journal of Science and Justice.

De Boer, D. H., and Campbell, I. A. 1989. Spatial scale dependence of sediment dynamics in a semi-arid badland drainage basin. Catena, 16: 277–290.

De Clercq, W. P., Fey, M. V.; Ellis, F., Rozanov, A., Folefoc, D., and Schloms, H. 2005. Land use impacts on salinity in Western Cape waters. Water Research Commission Project No. K5/1503, Progress Report, P. 1–14. (Unpublished)

De Graaff, J., 1992. Social and economic aspects of soil and water conservation: Part I. Wageningen Agricultural University. Department of Irrigation and Soil and Water Conservation.200–509.

Dunne, T., Zhang, W., and Aubury, B. F. 1991. Effects of rainfall, vegetation and micro topography on infiltration and runoff. Water Resource, 27: 2271–2285.

FAO, 1988. State of Food and Agriculture. Food and Agricultural Organization, Rome.

FAO/UNEP, 1983. Guidelines for the control of soil degradation. Food and Agricultural Organization, Rome.

FAO, 1992. Risk analysis in dryland farming systems, by Anderson J. and Dillon J.: Farm Systems Management Series No 2. Rome.

Foster, G. R., and Meyer, L. D. 1975. Mathematical simulation of upland erosion by fundamental erosion mechanics: Present and Prospective technology for predicting sediment Yields and sources. Proceedings of the sediment yield workshop, Oxford, Mississippi, USDA-ARS, 40, 190–207. *In* Poesen, J. 1981. Rain wash experiments on the erodibility of loose sediments. Journal of Earth Surface Processes and Landforms, 6: 285–307.

Gaillard, E., Lavabre, J., Isbérie, C., and Normand, W. 1995. Etat hydrique d'une parcelle et écoulement dans un petit basin versant du massif cristallin des Maures. Le Journal de l'Hydrogéologie, 4: 41–48.

Gieskes, J. M. 2007. Deep-sea drilling interstitial water study: implicationhs for chemical alteration of the oceanic crust, Layers I and II. *In* Poizot, E., Mear, Y., Biscara, L. , 2007. Sediment trend analysis through the variation of granulometric parameters: A review of theories and applications. Earth-Sciences Review.

Gray, D. H., and Sotir, R. B. 1996. Biotechnical and soil bioengineering slope stabilization: A practical Guide for erosion control. John Wiley and Sons, Toronto.

Gregory, K. J., and Walling, D. E. 1973. Drainage Basin Form and Processes: A geomorphological approach. Edward Arnold, London.

Gribbin, J. E. 2002. Introduction to hydraulics and hydrology with applications for storm water management. Delmar, Thomson Learning, Albany, NY.

Gyssels, G., and Poessen, J. 2003. The importance of plant root characteristics in controlling concentrated flow erosion rates. Journal of Earth Surface Processes and Landforms, 28: 371–384.

Hoffman T., and Ashwell A. 2001. Nature divided: Land degradation in South Africa. University of Cape Town Press, Lansdowne, pp. 3–9.

Imeson AC. 1993. The physical, chemical and biological degradation of the soil. *In* Fantechi R., Peter, D., Balabanis, P., and Rubio, J. L., 2002. Desertification in a European context. Bruxelles: European Commission, 153–168, Ed. *In* Pardini, G., Gispert, M., Dunjóo, G. Runoff erosion and nutrient depletion in five Mediterranean soils on NE Spain under different land use. The science of the Total Environment, 309: 213–224.

Latron, J., and Gallart, F. 2006. Seasonal dynamics of runoff-contributing areas in a small Mediterranean research catchment (Vallcebre, Eastern Pyrennees). Journal of Hydrology, doi: 10.1016/j.jhydrol.2006.11.012.

Lavee, H., Poesen, J., and Yair, A. 1997. Evidence of high efficiency water-harvesting by ancient farmers in the Negev desert, Israel. Journal of Arid Environments, 35: 341–348.

Leeder, M. R. 1982. Sedimentology: Process and Product. Allen and Unwin, London, 35–43.

Leopold, L. B. 1974. Water: a primer. Freeman, San Francisco, California, pp. 9–115.

Lindholm, R. C. 1987. A practical approach to Sedimentology. Allen and Unwin, London.

Loch, R. J. 2000. Using rainfall simulation to guide planning and management of rehabilitated areas: 1. Experimental methods and results from a study at the North Parkes mine. Journal of Land Degradation and Development, 11: 221–240.

Loch, R. J., Robotham, B. G., Zeller, L., Masterman, N., Orange, D. N., Bridge, B. J., Sheridan, G., and Bourke, J. J. 2001. A multi-purpose rainfall simulator for field infiltration and erosion studies. Australian Journal of Soil Research, 39: 599–610.

Malcolm, N. 1996. Hydrology and the river environment. Clarendon Press, Oxford.

McLaren, P. 1981. An interpretation of trends in grain size measures. J. Sediment. Journal of Petrol, 51 (2): 611–624. *In* Poizot, E., Mear, Y., and Biscara, L. 2007. Sediment trend analysis through the variation of granulometric parameters: A review of theories and applications. Journal of Earth-Sciences Review, doi: 10.1016/jearscirev.2007.07.004

Meyer, L. D., and Wischmeier, W. H. 1969. Mathematical simulation of the process of the process of soil erosion by water. Transactions of the ASAE, 12, 754–758, 762. *In* Poesen, J. 1981. Rainwash experiments on the erodibility of loose sediments. Journal of Earth Surface Processes and Landforms, 6: 285–307.

Mermut, A. R., Luk, S. H., Römkens, M. J. M., and Poesen, J. W. A. 1994. Micromorphological and mineralogical components of surface sealing in loess soils from different geographic regions. Geoderma, 66: 71–84.

Mermut, A. R., Luk, S. H., Römkens, M. J. M., and Poesen, J. W. A. 1996. Soil loss by splash and wash during rainfall from two loess soils. Geoderma, 75: 203–214.

Middleton, G. V. 1970. Experimental studies related to problems of flysch sedimentation. Geological Association of Canada Special Paper, 7: 253–272.

Moeyersons, J., and De Ploey, J. 1976. Quantitative data on splash erosion, simulated on unvegetated slopes. Zeitschrift für Geomorphologie, Supplement band, 25, 120–131. *In* Poesen, J. 1981. Rainwash experiments on the erodibility of loose sediments. Journal of Earth Surface Processes and Landforms, 6: 285–307.

Morini, J., and Benyamini, Y. 1977. Rainfall infiltration into bare soils. Water Resources Research, 13: 813–817.

Oldeman, L. R., and van Lynden, G. W. I. 1998. Revisiting the GLASOD methodology. *In* Methods for assessment of Soil Sciences, Ed. by Lal, R., Blum, W. R., Valentin, C., and Stewart, B. A., CRC Press, Boca Raton, FL.

Oostwoud, W., D., and Poesen, J. 1999. The effect of soil moisture on the vertical movement of rock fragments by tillage. Journal of Soil and Tillage Research, 49: 301–312.

Oxford English Dictionary, 2007. Oxford University Press. Online [available] at www.oed.com/

Partridge, T. C., and Maud, R. R. 1987. Geomorphic evolution of southern Africa since the Mesozoic. South African Journal of Geology, 90: 179–208.

Pierce, J. W., and Graus, R. R. 1981. Use and misuses of phi-scale: discussion. Journal of Sedimentology and Petrology, 51: 1348–1350.

Poesen, J. 1981. Rainwash experiments on the erodibility of loose sediments. Journal of Earth surface processes and landforms, 6: 285–307.

Poesen, J. 1984. The influence of slope angle on infiltration rate and Hortonian overland flow volume. Journal of Geomorphology, 49: 117–131.

Poesen, J. 1987. The role of slope angle in surface seal formation. International Geomorphology; Part II. John Wiley and Sons Ltd, Belgium.

Poesen, J., Nachtergaele, J., Verstraeten, G., and Valantin, C. 2003. Gully erosion and environmental change: importance and research needs. Catena, 50: 91–133. *In* De Baets, S., Poesen, J., Gyssels, G., and Knapen, A. Effects of grass roots on the erodibility of topsoil during concentrated flow. Journal of Geomorphology, 76: 54–67.

Prosser, I. P., Dietrich, W. E., and Stevenson, J. 1995. Flow resistance and sediment transport by concentrated overland flow in grassland valley. Geomorphology 13, 71–86. *In* De Baets, S., Poesen, J., Gyssels, G., and Knapen, A. 2005. Effects of grass roots on the erodibility of topsoil during concentrated flow. Journal of Geomorphology, 76: 54–67.

Riebeek-Kasteel & Riebeek-Wes [On line] available at http://www.CapeWestCoast.org/Towns/town.php?town=Riebeek

Reineck, H. E., and Singh, I. B. 1980. Depositional Sedimentary Environments, with Reference to Terrigenous Clastics. 2nd edn., Springer Verlag, New York.

Reynolds, S. G. 1970. The gravimetric method of soil moisture determination. Pts. 1, 2 and 3. Journal of Hydrology II: 258–300.

Roels, J. M. 1984. Surface runoff and sediment yield in the Ardeche rangelands. Journal of Earth Surface Processes and Landforms, 9: 371–381.

Rhodes, M. J. 1998. Introduction to particle technology. John Wiley, New York.

Römkens, M. J. M., Luk, S. H., Poesen, J. W. A, and Mermut, A. R. 1995. Rainfall infiltration into loess soils from different geographic regions. Catena, 25: 23–32.

Ruysschaert, G., Poesen, J., Verstraeten, G., and Govers, G. 2004. Soil loss to crop harvesting: significance and determining factors. Journal of Progress in Physical Geography, 28(4): 467–501.

Savage, S. B. 1987. Interparticle percolation in granular materials: A review. *In* Developments in Engineering Mechanics, Ed. by Selvadurai, A. P. S. Elsevier, Amsterdam.

Scoging, H. M.. 1982. Spatial variations in infiltration, runoff and erosion on hill slopes in semiarid Spain. *In* Badlands Geomorphology and Piping, Ed. by Bryan, R., and Yair, A., Geo Books, Norwich.

Sfeir – Younis, A., 1985. Soil conservation in developing countries: a background report (unpublished draft). Washington D.C.

Soil Classification Working Group, 1991. Soil Classification: A Taxonomic System for South Africa. Memoirs on agriculture in Southern Africa, No. 15. Department of Agricultural Development, Pretoria.

Steegen, A**.,** Govers, G., Takken, I., Nachtergaele, J., Poesen, J., and Merckx, R. 2001. Factors controlling sediment and phosphorus export from two Belgian agricultural catchments. Journal of Environmental Quality, 30: 1249-1258.

Styczen, M. E., and Morgan, R. P. C. 1995. Engineering properties of vegetation. *In* Morgan, R. P. C., and Rickson, R. J.(eds) Slope Stabilization and Erosion Control: A Bioengineering Approach. E and F. N. Spon. London, pp. 5–58. *In* De Baets, S., Poesen, J., Gyssels, G., and Knapen, A. 2005. Effects of grass roots on the erodibility of topsoil during concentrated flow. Journal of Geomorphology, 76: 54–67.

Taha, A., Grésillon, J. M., and Clothier, B. E. 1997. Modelling the link between hill slope water movement and stream flow: application to a small Mediterranean forest watershed. Journal of Hydrology, 203: 11–20.

Viessman, W., Lewis, G. L., and Knapp J. W. 1989. Introduction to hydrology. 3rd edn., Harper and Row, New York.

Viessman, W., and Lewis, G. L. 2003. Introduction to hydrology. 5th edn., Prentice Hall.

Viles, H. A. 1988. Biogeomorphology. Basic Blackwell, Oxford.

Viles, H. A. 1990. The agency of organic beings: a selective review of recent work in biogeomorphology. *In* Thornes J.B., Vegetation and Erosion: Processes and Environments. Chichester: John Wiley and Sons: 5–24.

Warren Viessman, Jr. & Gary Lewis, L., 1995. Introduction to Hydrology. University of Florida. Addison Wesley Longman. 4th Ed.

West Coast Tourism Organization. (2000). Climate. [Online]. Available http://www.capewestcoast.org/RegionalInfo-Index.htm

Wilcox, B. P., Wood, M. K., and Tromple, J. M.. 1988. Factors influencing infiltrability of semiarid mountain slopes. Journal of Range Management, 41: 197–206.

Wolman, M. G., and Gerson, R. 1978. Relative scale of time and effectiveness of climate and watershed geomorphology. Journal of Earth Surface and Landforms, 3: 189–208.

Wood, E. F., Sivapalan, M., and Beven, K. 1986. Scale effects in infiltration and runoff production. IAHS Publication, 156: 375–387.

Yair, A., and Lavee, H. 1976. Runoff generative process and runoff yield from arid talus mantled slopes. Earth Surface and Processes Landforms, 1: 235–247.

Yair, A., and Lavee, H. 1985. Runoff generation in arid and semi-arid zones. *In* Ed. by Anderson, M. G., Burt, T. P. Hydrological Forecasting. Wiley, Chichester.

Yamamoto, T., and Anderson, H. W. 1973. Splash erosion related to soil erodibility indexes and other forest soil properties in Hawaii. Water Resources Research, 9: 336–345. *In* Poesen, J. 1981. Rainwash experiments on the erodibility of loose sediments. Journal of Earth Surface Processes and Landforms, 6: 285–307.

Appendix 1

Graphs indicating measured distribution of particles using Micromeritics equipment

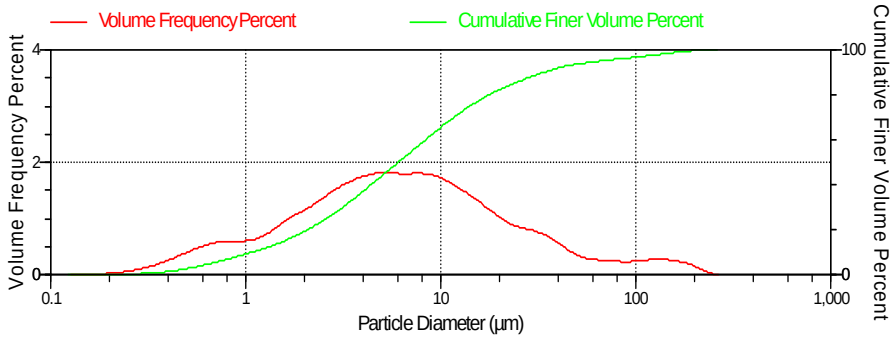

Figure 1.1 Volume frequency vs. diameter for sediment from Sw3 (2)

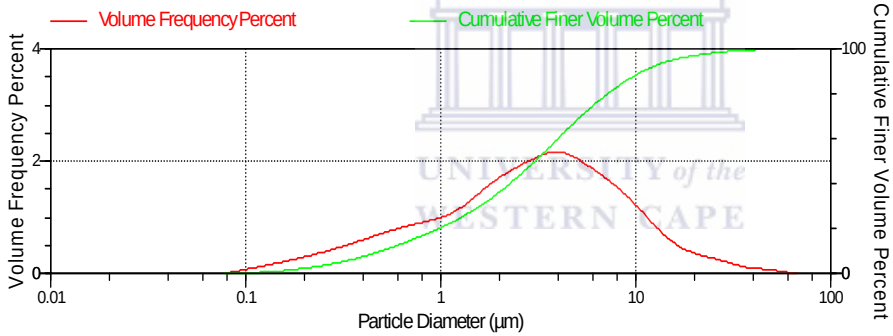

Figure 1.2 Volume frequency vs. diameter for sediment from Gs1 (3)

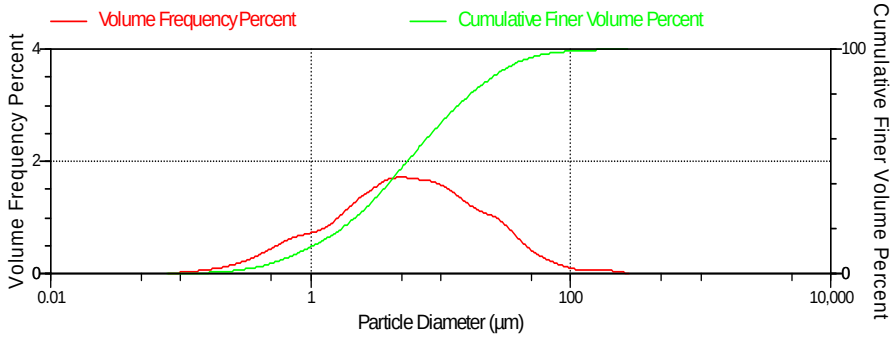

Figure 1.3 Volume frequency vs. diameter for sediment from Gs (5)

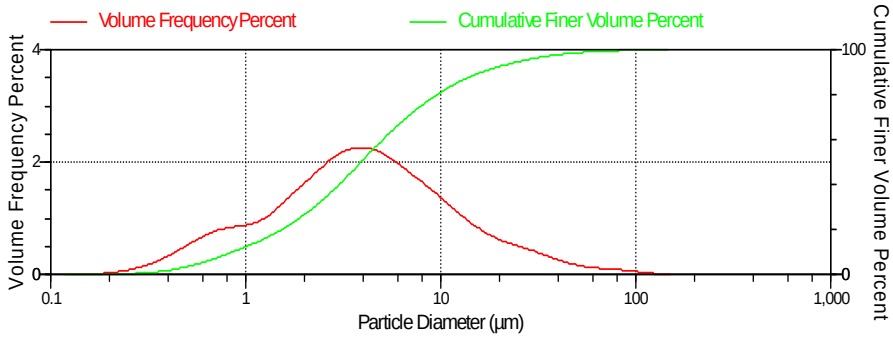

Figure 1.4 Volume frequency vs. diameter for sediment from Sw2 (45)

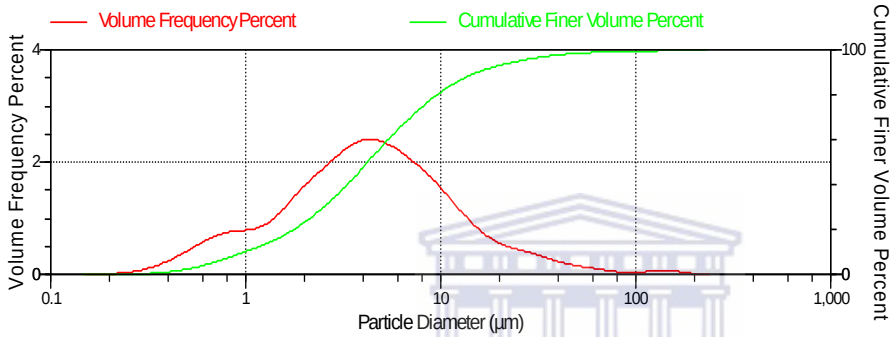

Figure 1.5 Volume frequency vs. diameter for sediment from Ag1 (59)

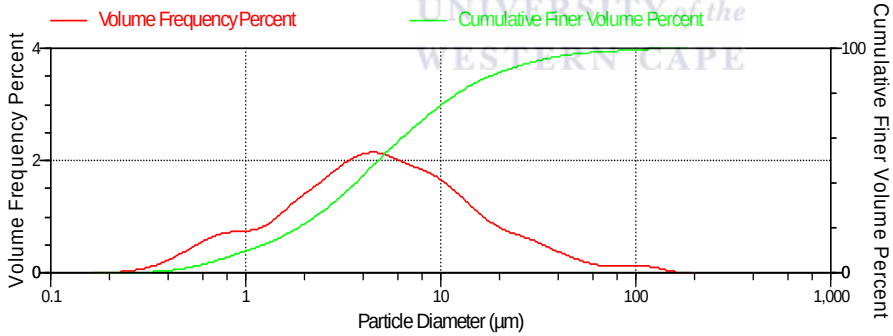

Figure 1.6 Volume frequency vs. diameter for sediment from Sw1 (28)

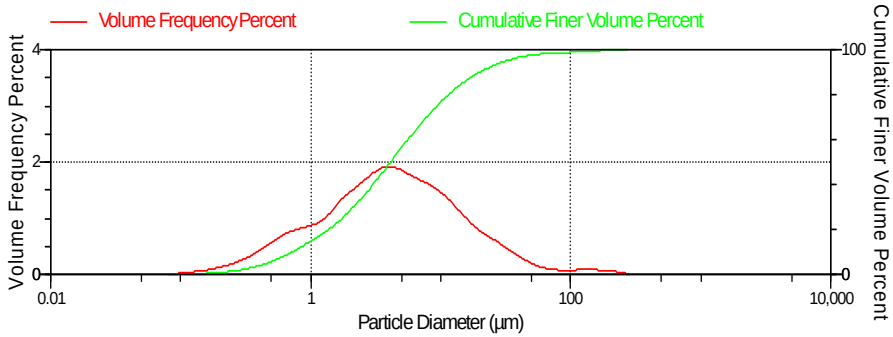

Figure 1.7 Volume frequency vs. diameter for sediment from Ss1 (1)

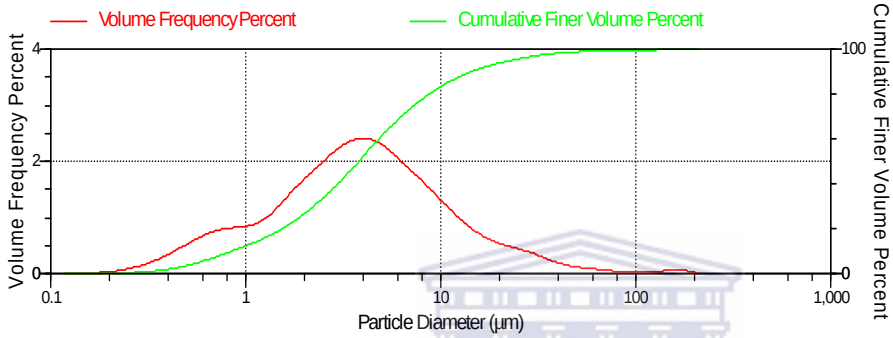

Figure 1.8 Volume frequency vs. diameter for sediment from Gs2 (42)

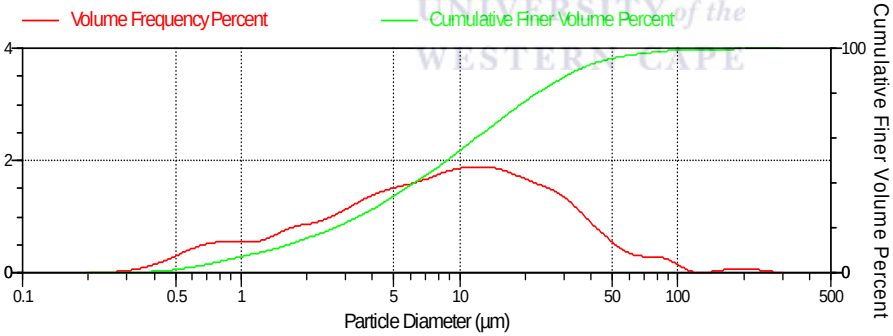

Figure 1.9 Volume frequency vs. diameter for sediment from Ms1 (4)

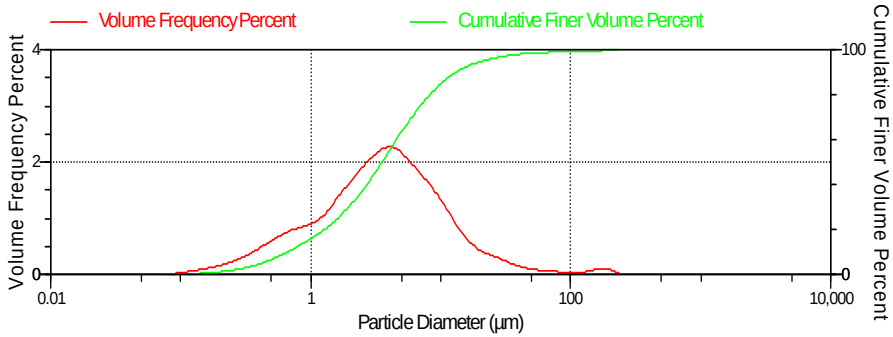

Figure 1.10 Volume frequency vs. diameter for sediment from Km1 (21)

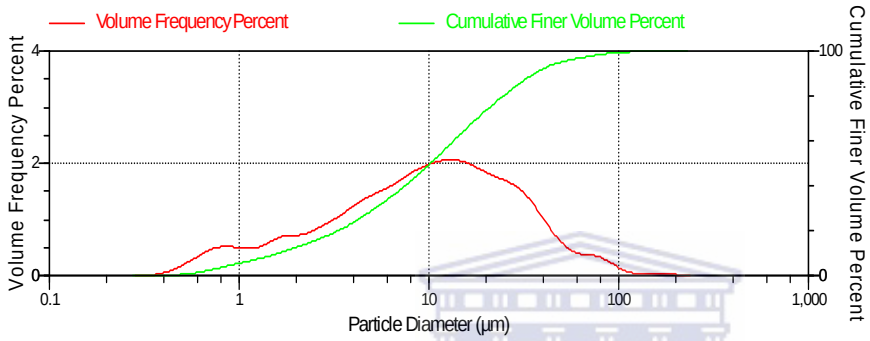

Figure 1.11 Volume frequency vs. diameter for sediment from We1 (6)

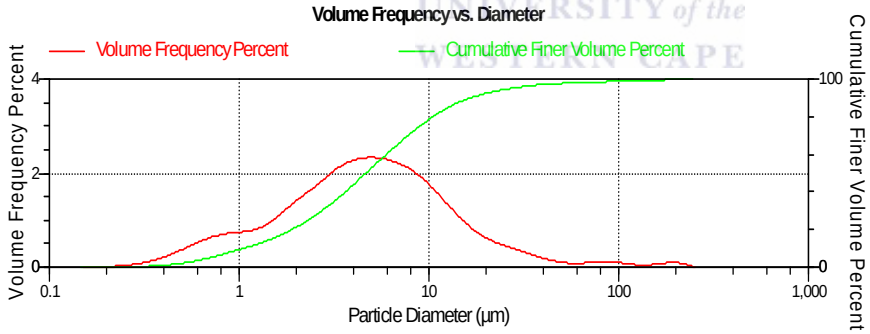

Figure 1.12 Volume frequency vs. diameter for sediment from Cf1 (40)

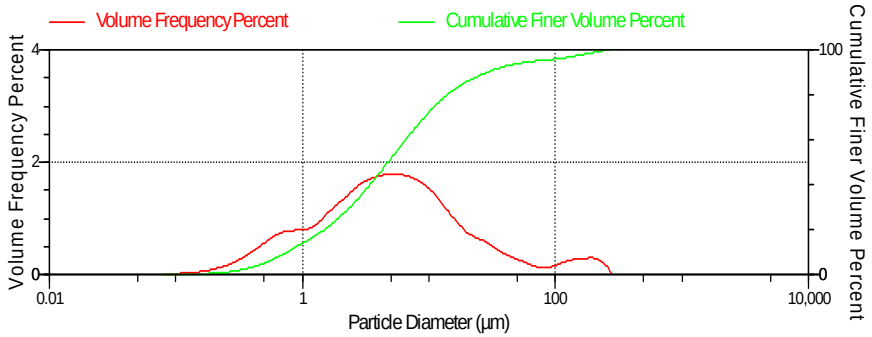

Figure 1.13 Volume frequency vs. diameter for sediment from Ka1 (53)

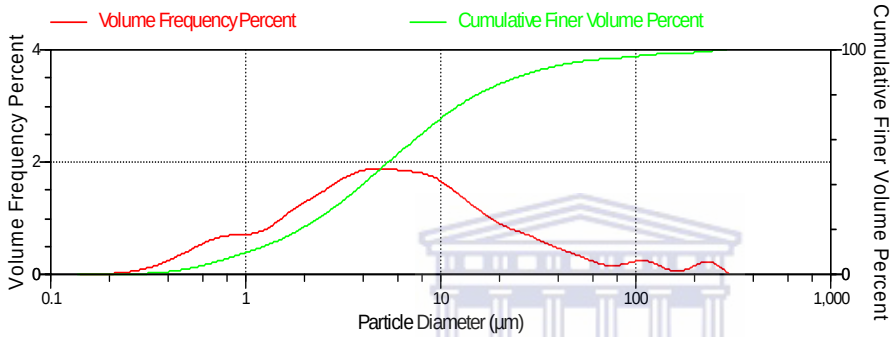

Figure 1.14 Volume frequency vs. diameter for sediment from Sw4 (55)

Appendix 2

Combination of A-horizon, Wischmeier plot and simulation Cf1 (40) sediments

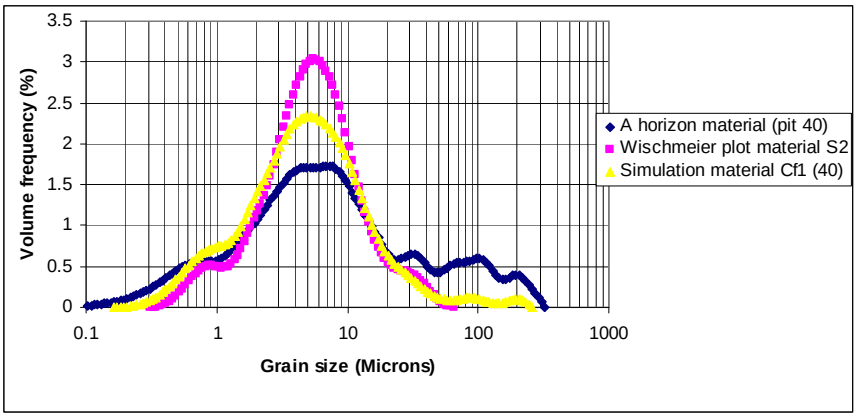

Figure 2.1 Showing distribution frequency between A-horizon (pit 40), Wischmeir plot S2 and simulation Cf1 (40)

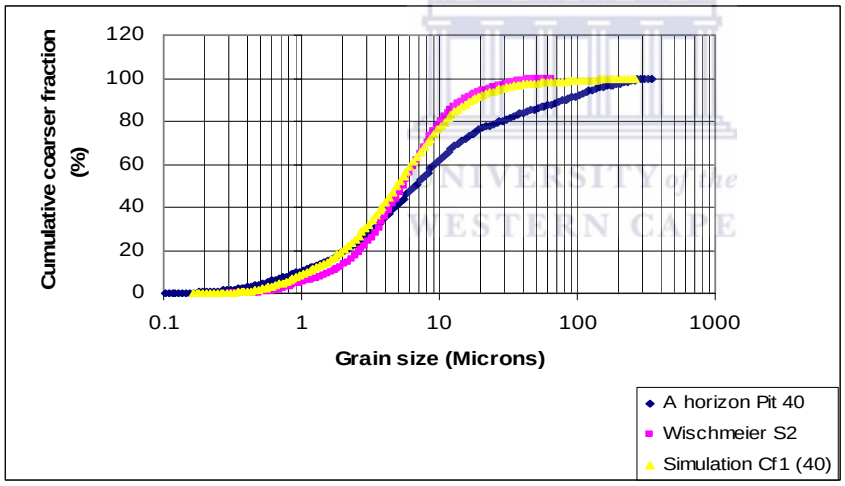

Figure 2.2 Showing cumulative frequency distribution between A-horizon (pit 40), Wischmeir plot S2 and simulation Cf1 (40)

Combination of A-horizon, Wischmeier plot and simulation Gs1 (3) sediments

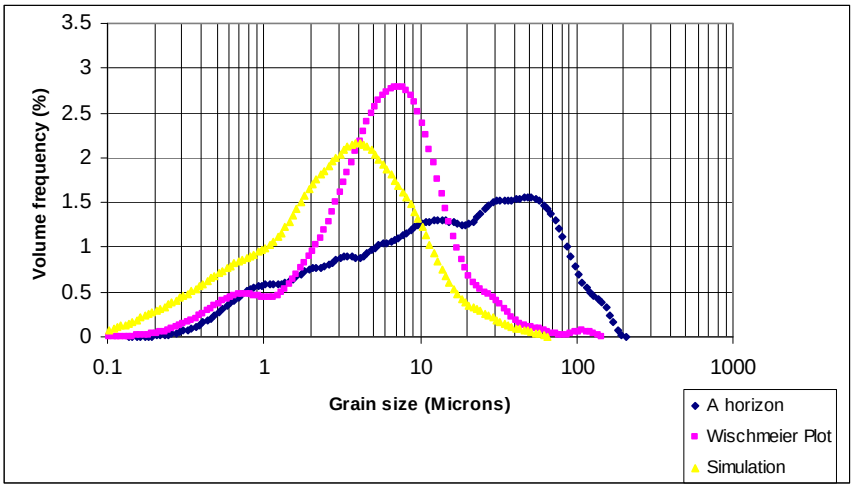

Figure 2.3 Showing distribution frequency between A-horizon (pit 3), Wischmeir plot S1P1T1 and simulation Gs1 (3)

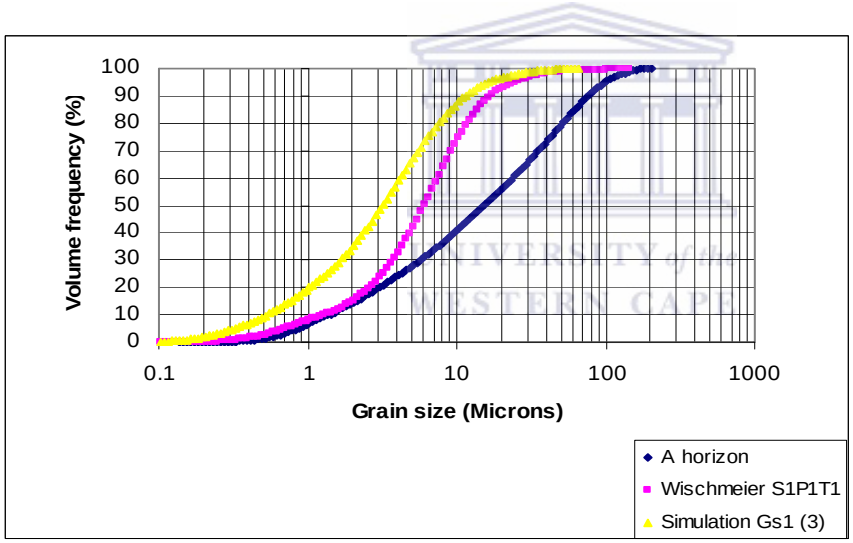

Figure 2.4 Showing cumulative frequency distribution between A-horizon (pit 3), Wischmeir plot S1P1T1 and simulation under Glenrosa soil (Gs1–3)

Appendix 3

Allaby (1999)

Millimeters	µm	Phi (ϕ)	Wentworth size class	
		-20		
4096		-12	Boulder (-8 to -12ϕ)	
1024		-10		
256		-8	Pebble (-6 to -8ϕ)	
64		-6		
16		-4	Pebble (-2 to -6ϕ)	Gravel
4		-2		
3.36		-1.75		
2.83		-1.50	Gravel	
2.38		-1.25		
2.00		-1.00		
1.68		-0.75		
1.41		-0.50	Very coarse sand	
1.19		-0.25		
1.00		-0.00		
0.84		0.25		
0.71		0.50	Coarse sand	
0.59		0.75		
1/2 0.50	500	1.00		
0.42	420	1.25		
0.35	350	1.50	Medium sand	
0.30	300	1.75		Sand
1/4 0.25	250	2.00		
0.210	210	2.25		
0.177	177	2.50	Fine sand	
0.149	149	2.75		
1/8 0.125	125	3.00		
0.105	105	3.25		
0.088	88	3.50	Very fine sand	
0.074	74	3.75		
1/16 0.0625	63	4.00		
0.0530	53	4.25		
0.0440	44	4.50	Coarse silt	
0.0370	37	4.75		
1/32 0.0310	31	5		
1/64 0.0156	15.6	6	Medium silt Fine silt	
1/128 0.0078	7.8	7	Very fine silt	
1/256 0.0039	3.9	8		Mud
0.0020	2.0	9		
0.00098	0.98	10		
0.00049	0.49	11	Clay	
0.00024	0.24	12		
0.00012	0.12	13		
0.00006	0.06	14		

Appendix 4

Figure 4.1 Showing a Satellite image of the study area (Europa Technologies, 2006)

Appendix 5.

Particle-size distribution

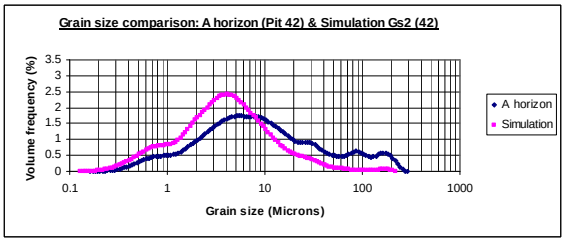

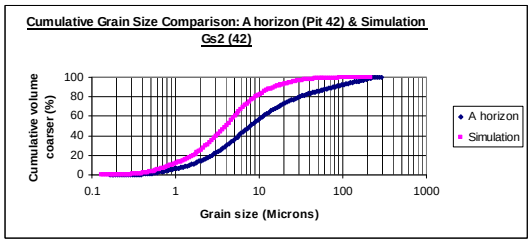

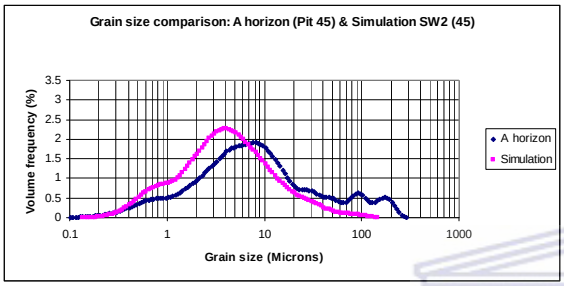

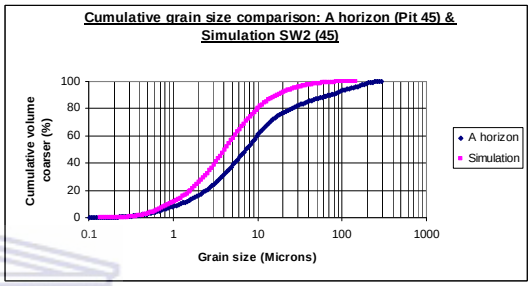

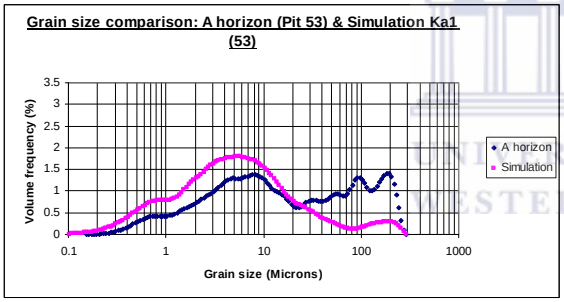

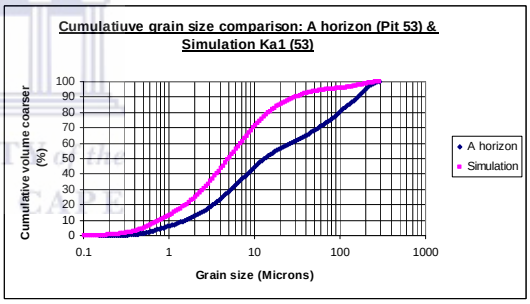

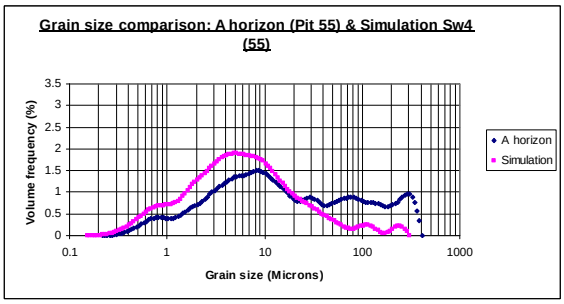

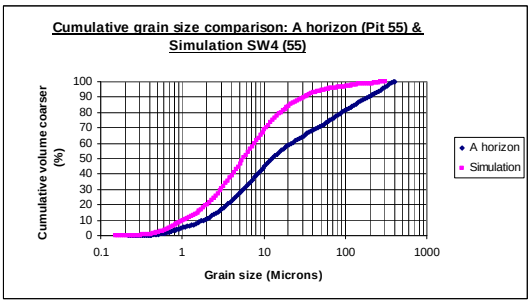

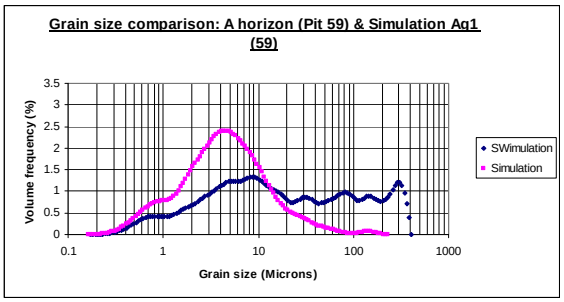

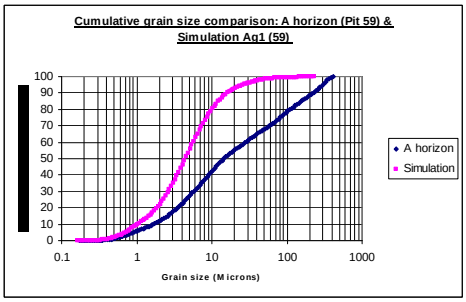

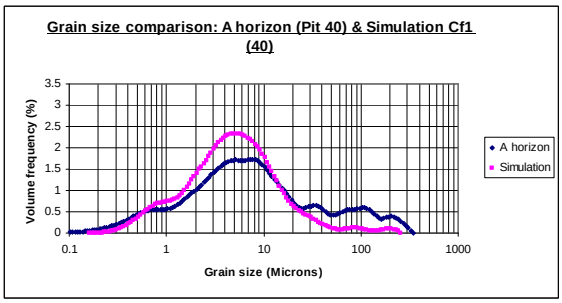

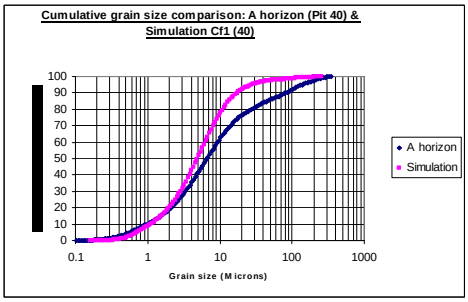

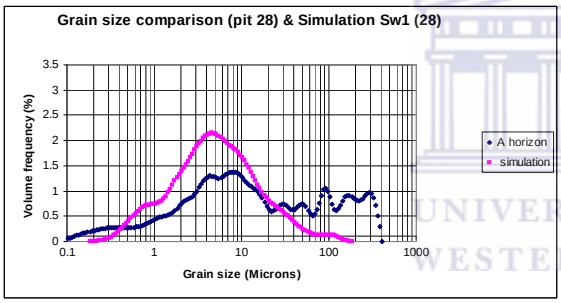

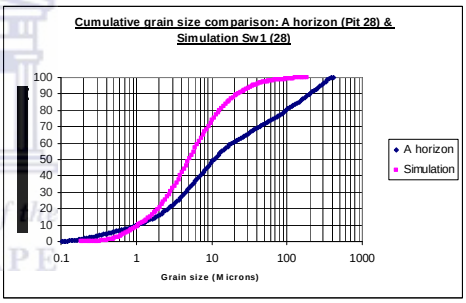

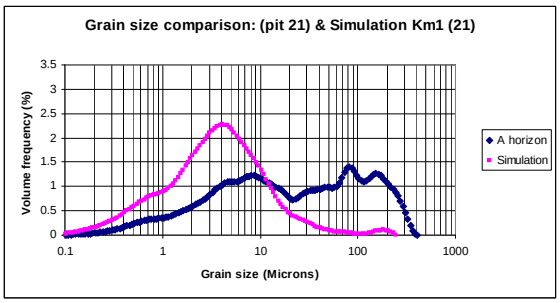

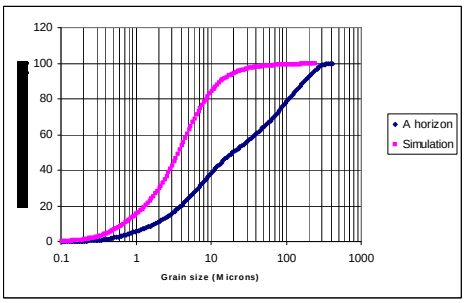

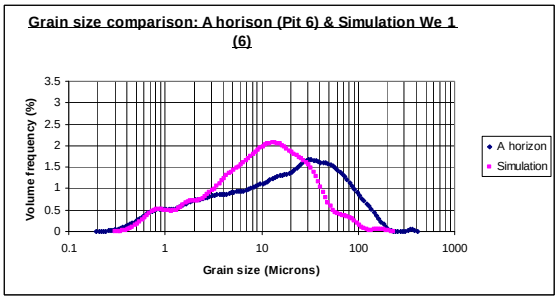

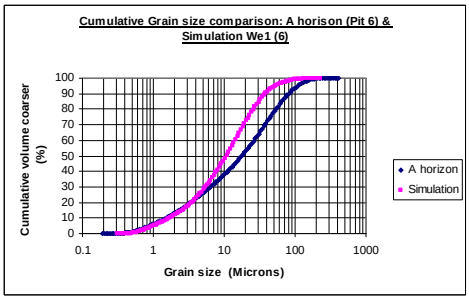

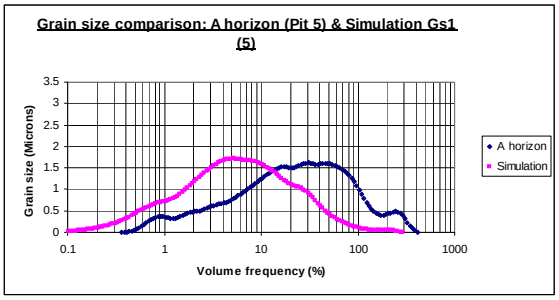

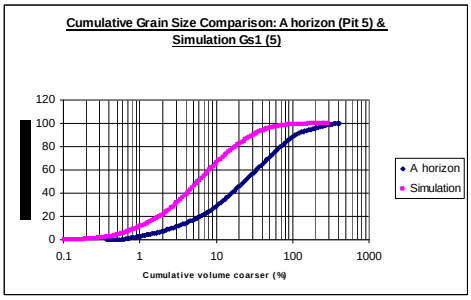

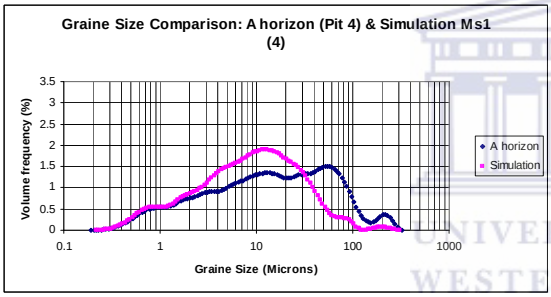

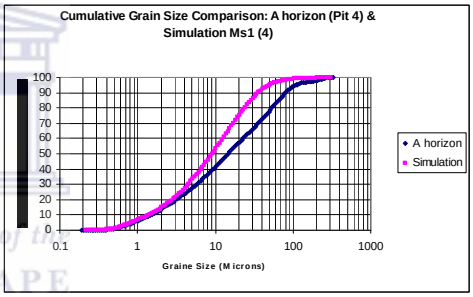

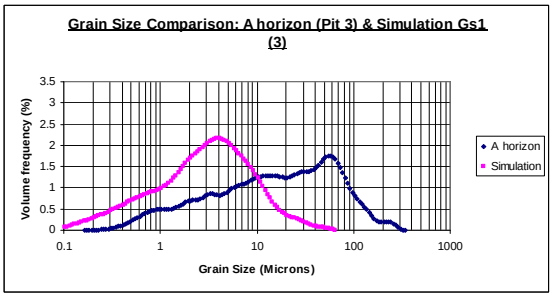

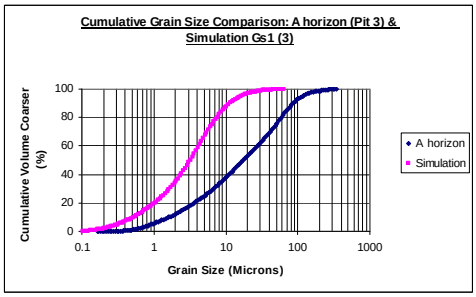

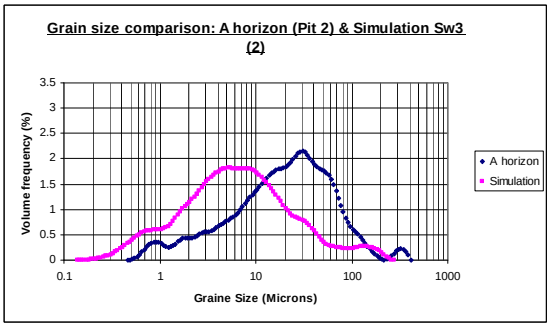

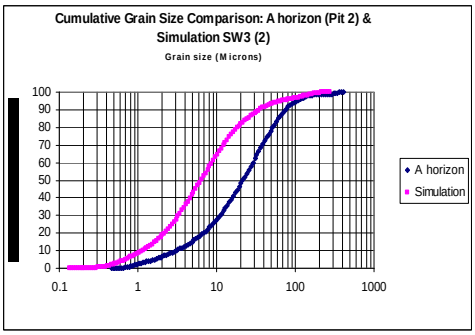

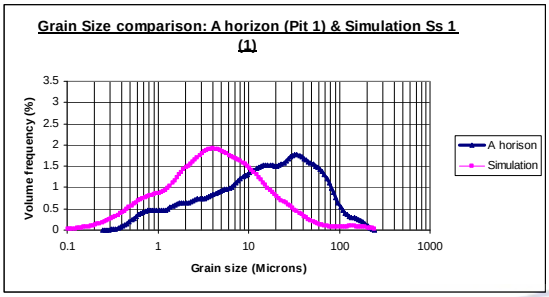

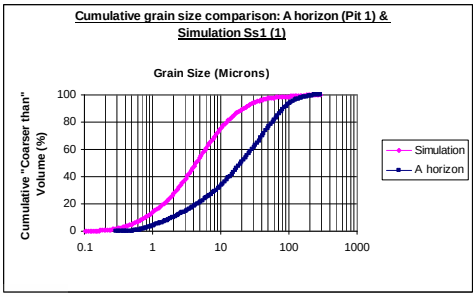

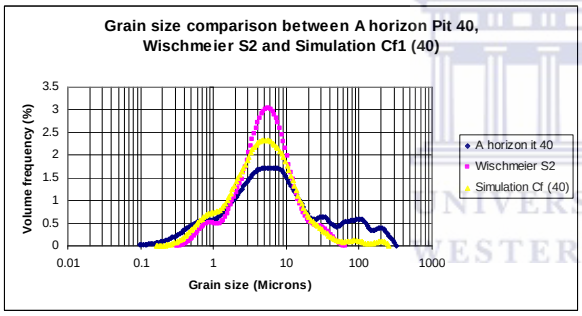

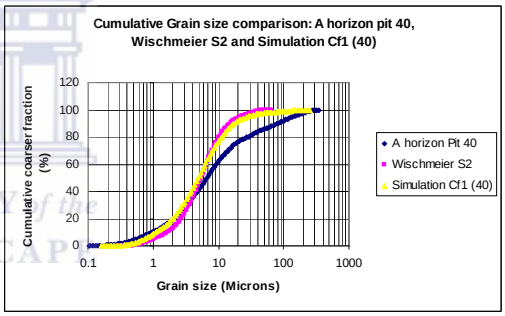

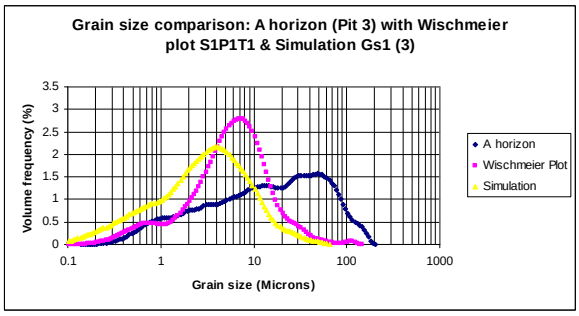

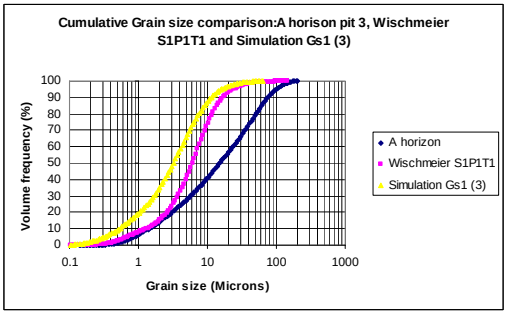

Appendix 6

Materials used during rainfall-simulation processes

Figure 6.1 illustrating crack structure on the soil surface

Figure 6.2 illustrating different equipment used during rainfall simulation, canes containing water and wooden boxes for samples

Figure 6.3 illustrating the occurrence of the first run-off

Figure 6.4 illustrating the timer that was used during the simulations

Figure 6.5 illustrating sample bottles, cylinder to measure the run-off, metal container to collect run-off, paper form for recording the data, wooden box to keep the samples

Figure 6.6 illustrating the collection of run-off